Nicotinic acetylcholine receptor signaling maintains epithelial barrier integrity

Nadja S. Katheder[1], Kristen C. Browder[1], Diana Chang[2], Ann De Mazière[3], Pekka Kujala[3], Suzanne van Dijk[3], Judith Klumperman[3], Tzu-Chiao Lu[4], Hongjie Li[4,5], Zijuan Lai[6], Dewakar Sangaraju[6], Heinrich Jasper[1*]

[1]Regenerative Medicine, Genentech, South San Francisco, United States
[2]Human Genetics, Genentech, South San Francisco, United States
[3]Center for Molecular Medicine, Cell Biology, University Medical Center Utrecht, The Netherlands
[4]Huffington Center on Aging, Baylor College of Medicine, Houston, United States
[5]Department of Molecular and Human Genetics, Baylor College of Medicine, Houston, United States
[6]Drug Metabolism & Pharmacokinetics, Genentech, South San Francisco, United States

* corresponding author: jasperh@gene.com

Abstract

Disruption of epithelial barriers is a common disease manifestation in chronic degenerative diseases of the airways, lung and intestine. Extensive human genetic studies have identified risk loci in such diseases, including in chronic obstructive pulmonary disease (COPD) and inflammatory bowel diseases (IBD). The genes associated with these loci have not fully been determined, and functional characterization of such genes requires extensive studies in model organisms. Here, we report the results of a screen in *Drosophila melanogaster* that allowed for rapid identification, validation and prioritization of COPD risk genes that were selected based on risk loci identified in human genome-wide

association studies (GWAS) studies. Using intestinal barrier dysfunction in flies as a readout, our results validate the impact of candidate gene perturbations on epithelial barrier function in 56% of the cases, resulting in a prioritized target gene list. We further report the functional characterization in flies of one family of these genes, encoding for nicotinic acetylcholine receptor subunits (nAchR). We find that nAchR signaling in enterocytes of the fly gut promotes epithelial barrier function and epithelial homeostasis by regulating the production of the peritrophic matrix. Our findings identify COPD associated genes critical for epithelial barrier maintenance, and provide insight into the role of epithelial nAchR signaling for homeostasis.

Introduction

Barrier epithelia such as the skin, linings of the gastrointestinal and urogenital tracts and the airways play a critical role in maintaining a strict separation of external and internal environments, yet also enable the exchange of gases, water, nutrients and immune mediators. They serve as a first layer of defense against external insults and possess remarkable regenerative capacity that declines with age (Jasper, 2020). In *Drosophila*, loss of intestinal barrier function is accompanied by commensal dysbiosis and inflammation and reliably predicts impending organismal death (Rera et al., 2012). Similarly, increased barrier permeability and changes in microbiome composition and abundance have been reported in various human diseases, such as inflammatory bowel disease and chronic obstructive pulmonary disease (COPD) (Raftery et al., 2020).

COPD is a major contributor to global morbidity and mortality and is characterized by an obstructed airflow resulting in shortness of breath upon exertion. At the tissue level, lungs of COPD patients display chronic inflammation, extensive cellular remodeling and barrier dysfunction (Aghapour et al., 2018; Barnes, 2019; Carlier et al., 2021).

While smoking or exposure to environmental air pollutants remain major risk factors, many COPD patients are non-smokers, suggesting a genetic component contributing to disease susceptibility (Aghapour et al., 2022; Barnes, 2019). Several GWAS studies have been performed in which risk loci for incidence of COPD have been identified

(Hobbs, de Jong, Lamontagne, Bossé, et al., 2017; Pillai et al., 2009; Sakornsakolpat, Prokopenko, Lamontagne, Reeve, Guyatt, Jackson, Shrine, Qiao, Bartz, Kim, Lee, Latourelle, Li, Morrow, Obeidat, Wyss, Bakke, Barr, Beaty, Belinsky, Brusselle, Crapo, de Jong, DeMeo, Fingerlin, Gharib, Gulsvik, Hall, Hokanson, Kim, Lomas, London, Meyers, O'Connor, Rennard, Schwartz, Sliwinski, Sparrow, Strachan, Tal-Singer, Tesfaigzi, Vestbo, Vonk, Yim, Zhou, Bossé, et al., 2019). One of the most well-known risk loci is located near the nicotinic acetylcholine receptor CHRNA3/5 genes and has also been associated with increased nicotine dependence and smoking behavior, and lung cancer (Amos et al., 2008; Carlier et al., 2021; Cui et al., 2014; Hobbs, de Jong, Lamontagne, Bossé, et al., 2017; Hung et al., 2008; Pillai et al., 2009; Wilk et al., 2012). Recent work has demonstrated a role for CHRNA5 in the formation of COPD-like lesions in the respiratory epithelium independently of cigarette smoke, suggesting a direct involvement of nicotinic acetylcholine receptors (nAchRs) in shaping epithelial integrity (Routhier et al., 2021). The endogenous ligand of nAchR, acetylcholine (Ach), is a classic neurotransmitter synthesized by Choline Acetyltransferase (ChAT) in cholinergic neurons, as well as in immune cells and epithelial cells, such as brush/tuft cells (Kummer & Krasteva-Christ, 2014; Wessler & Kirkpatrick, 2008). Such cells orchestrate type 2 inflammatory responses (O'Leary et al., 2019; Sell et al., 2021), mucociliary clearance (Perniss et al., 2020) and limit biliary inflammation (O'Leary et al., 2022; O'Leary et al., 2019). How Ach influences homeostasis of barrier epithelia and how disease-associated nAchR variants perturb epithelial function remains mostly unclear.

Overall, experimental evidence for the involvement of specific genes associated with the COPD risk loci identified in these studies is mostly lacking, and will be essential for the development of therapeutic strategies targeting novel pathways. The use of genetically accessible model systems with enough physiological complexity to model cell and tissue interactions in barrier epithelia may help accelerate the evaluation of potential disease-causing genes identified in COPD GWAS studies. To test this idea, we have here used the *Drosophila* midgut as a genetically accessible model for epithelial barrier homeostasis to interrogate genes predicted to be involved in COPD based on GWAS studies. The *Drosophila* intestine is lined by a pseudostratified epithelium consisting of

enterocytes (ECs) and enteroendocrine cells (EEs) that are regenerated from a basal population of intestinal stem cells (ISCs) (Miguel-Aliaga et al., 2018). In its structure, cell composition and molecular regulation of regenerative processes, the fly intestinal epithelium resembles mammalian airway epithelia (Biteau et al., 2011).

Under stress conditions, in response to enteropathogen infection, as well as during normal aging, the fly intestinal epithelium loses its barrier function and exhibits stem cell hyperplasia and commensal dysbiosis (Jasper, 2020). These phenotypes recapitulate changes observed in airway epithelia of COPD patients and can thus be used as a model for pathophysiological changes occurring in this disease (Carlier et al., 2021; Raftery et al., 2020).

To assess the role of candidate genes associated with risk alleles in COPD GWAS studies in the maintenance of barrier epithelia integrity, we performed an RNA interference screen perturbing their *Drosophila* orthologues systemically and quantifying the impact of these perturbations on intestinal barrier function. Several of the candidate genes identified in this screen as required for barrier integrity encode for subunits of the nicotinic acetylcholine receptor (nAchR).

In the fly intestine, we find that ChAT is expressed by a subset of enteroendocrine cells and that enterocyte-specific expression of nAchR is required for barrier integrity by stimulating chitin release and ensuring maintenance of the peritrophic matrix (PM), a chitinous structure protecting the epithelium from luminal insults. In ECs, Ach is required for the expression of Syt4, a critical regulator of exocytosis (Yoshihara et al., 2005; Zhang et al., 2011) which is required for the maintenance of PM structure and epithelial barrier function. Our data illustrate the usefulness of *Drosophila* as a model for prioritization of potential disease genes identified in GWAS studies, and identify nAchR signaling as a critical mediator of epithelial homeostasis in barrier epithelia.

Results

A genetic screen assessing the role of COPD candidate genes in barrier function

To obtain a curated candidate gene list for COPD, we assigned candidate genes to COPD risk loci (Hobbs, de Jong, Lamontagne, Bossé, et al., 2017) using a combination of expression quantitative trait loci, coding annotation and distance-based metrics (see Methods, Supplementary File 1). *Drosophila* orthologs were identified with the DRSC integrative ortholog prediction tool (DIOPT (Hu et al., 2011)) and corresponding hits with the highest DIOPT score were selected, resulting in a total of 33 *Drosophila* genes screened initially (Fig. 1A).

We perturbed these genes systemically by RNA interference (RNAi) in an inducible fashion using the ubiquitous RU486-inducible Gal4 driver da-GeneSwitch (da-GS) and scored epithelial barrier dysfunction in homeostatic and stress conditions using the "smurf assay" (Rera et al., 2011). In this approach flies are fed food containing a non-absorbable blue food dye. If the intestinal epithelial barrier is compromised, the dye leaks into the open circulatory system and gives the fly a blue appearance reminiscent of the popular blue cartoon characters. Where available, a minimum of 2 different RNAi lines per gene were included (Supplementary File 2). Female flies carrying the da-GS driver and RNAi construct were allowed to mature and mate for 10-12 days before being placed on blue food with RU486 to induce knockdown for 24h. Since COPD is strongly associated with environmental stress, we then challenged flies with Paraquat (N, N'-dimethyl-4,4'-bipyridinium dichloride), a herbicide known to inflict oxidative stress and damage to the fly gut comparable to the effects of cigarette smoke on the lung epithelium (Biteau et al., 2008; Caliri et al., 2021). After 16h Paraquat challenge the flies were moved back to blue food containing RU486 and smurf numbers were recorded over the span of about a week (Fig 1B). We generated a "barrier dysfunction index" for every RNAi line by calculating the natural logarithm (ln) of the ratio of peak smurf percentage between RNAi line and control knockdown and plotted individual RNAi lines accordingly. A positive index implies an enhancement of barrier dysfunction after depletion, while a negative index suggests rescue of barrier integrity after depletion (Fig. 1C). Based on the outcomes of individual RNAi knockdowns, we assigned an overall rating for each candidate gene (Supplementary File 2). We found that disruption of 17 genes (~52%) resulted in enhancement (e.g. these genes were necessary for barrier integrity), while disruption of 4 genes (12%) resulted in suppression of the barrier

dysfunction. The remaining 12 genes did not display any effect on barrier function (Fig. 1D). Out of the 16 of *Drosophila* hits where eqtl data was available for the corresponding human gene, 9 were consistent with the direction of the effect inferred from the association of the COPD risk allele with gene expression (56%, Fig. 1A, Supplementary File 2).

nAchR subunit expression in ECs is required for barrier function

Our initial screen identified disruption of 5 nAchR subunits as a strong enhancers of barrier dysfunction. Ubiquitous knockdown of various nAchR subunits with da-GS lead to mild barrier dysfunction under homeostatic conditions, and greatly enhanced barrier dysfunction after Paraquat challenge (Fig. 2A, Fig. 2 – figure supplement 1B), suggesting a sensitization of the epithelium to stress. To account for different genetic backgrounds of RNAi lines, we tested a range of control lines and did not observe any significant differences between them (Fig. 2 – figure supplement 1A).

Acetylcholine (Ach) is the physiological ligand for nAchRs and is produced by ChAT, an enzyme that catalyzes the transfer of an acetyl group from coenzyme acetyl-CoA to choline (Taylor P., 1999). Modulation of total organismal Ach levels by RNAi-mediated silencing of ChAT under control of da-GS also resulted in increased barrier dysfunction after Paraquat exposure (Fig. 2B, Fig. 2 – figure supplement 1C), further supporting the role of Ach/nAChR signaling in maintaining intestinal epithelial homeostasis.

To investigate a possible direct intestinal role for nAchR, and to identify the requirement for individual subunits, we used the drivers NP1-Gal4 and 5966-GS to separately deplete nAchR subunits. The former induces expression of UAS-linked transgenes in enterocytes, while the latter targets enteroblasts and enterocytes. (Jiang et al., 2009; Zeng & Hou, 2015). While 5966-GS is inducible using RU486, we combined NP1-Gal4 with tubG80^{ts} (NP1^{ts}) to allow for temperature-mediated induction (TARGET system (McGuire et al., 2004)) before subjecting the flies to Paraquat. Knockdown of nAchR α4

or β3 with both drivers increased the numbers of smurf flies, indicating a defective epithelial barrier (Fig. 2C, 2D, Fig. 2 – figure supplement 1D, E).

Knockdown of nAchR in ECs resulted in various hallmarks of epithelial stress. These include induction of intestinal stem cell (ISC) proliferation (Fig. 2E), presumably due to stress signals released by ECs (Biteau et al., 2011), as well as activation of JAK/STAT signaling (measured using the 2xSTAT::GFP reporter (Bach et al., 2007)) and ER stress signaling (measured using an Xbp1-eGFP reporter (Sone et al., 2013) (Fig. 2F, G). Interestingly, organization of epithelial junctions in ECs remained mostly unaltered, as visualized by staining for the septate junction marker Dlg and Coracle as well as localization of arm-GFP, suggesting that barrier dysfunction may be caused by a separate mechanism (Fig. 2H, 2I, Fig. 2 – figure supplement 2A).

To further confirm and characterize the role for nAchR subunits in epithelial homeostasis, we specifically depleted nAchR subunits in stem cells using esg-Gal4, UAS-2xEYFP; Su(H)GBE-Gal80, tub-Gal80^{ts} (ISC^{ts}). Individual knockdown of nAchR α2, α4, β1 or β3 resulted in increased barrier dysfunction after Paraquat challenge as well as decreased survival after *Pseudomonas entomophila* (PE) infection (Fig. 2 – figure supplement 2B, C). When challenged with PE, stem cells depleted for various nAchR subunits underwent mitosis at a similar rate as their control counterparts (Fig. 2 – figure supplement 2D), suggesting that barrier dysfunction is not caused by an inability of stem cells to regenerate the epithelium. We generated MARCM mutant clones (Lee & Luo, 2001) lacking *nAChRα2* using the null allele *nAChRα2^{attP}* generated by CRISPR/Cas9 based homologous recombination resulting in the introduction of an attP site, 3xP3-RFP and a loxP site (Deng et al., 2019; Lu et al., 2022). Clone formation, growth, and cell composition also provide insight into a possible role of *nAChRα2* in ISC proliferation and differentiation. Consistent with the results of the ISC-specific knockdown, *nAChR α2^{attP}* clones grew to similar cell numbers as their control counterparts. Interestingly, however, they failed to produce normal numbers of EEs, as only 32% of *nAChR α2* clones contained at least 1 EE compared to 72% of clones in the control samples (Fig. 2J). Similar results (although the reduction of EE numbers was not significant) were also observed in loss of function MARCM clones for a separate

subunit, *nAchR α1* (Fig. 2 – figure supplement 2E). In addition to a broader role for *nAchR* in maintaining barrier integrity, *nAchR* may thus also be required for the proper differentiation of EEs. We also knocked down additional subunits, generating clones depleted for these subunits via RNAi using the esgF/O approach (Jiang et al., 2009). Depletion of nAchR α4 and β3 slightly reduced overall size of the clones compared to control, and we detected a non-significant trend towards fewer EEs after nAchR depletion (Fig. 2 – figure supplement 2F, the weak phenotypes observed in these RNAi experiments may be a consequence of incomplete knockdown efficiency).

Acetylcholine promotes barrier function

We sought to identify the source of Ach activating these receptors in the gut epithelium next. Because of its well understood role as a neurotransmitter, we initially focused on the innervation of the fly gut, which has been described previously (Cognigni et al., 2011). Expression of UAS-GFP under the control of two independently established ChAT-Gal4 drivers confirmed that some of these neurons are indeed cholinergic (Fig. 3A, 3B', Fig. 3 – figure supplement 1A). Upon closer examination of the epithelium, we also noticed a subset of prospero-positive EEs expressing GFP, predominantly located in the R4 and R5 regions of the midgut (Fig. 3B, 3C, Fig. 3 – figure supplement 1A). In addition, labeling of guts expressing GFP under the control of prospero-Gal4 or ChAT-Gal4 combined with tubGal80^{ts} (pros^{ts} and ChAT^{ts}) with a ChAT antibody confirmed ChAT expression in a subset of EEs (Fig. 3D, Fig. 3 – figure supplement 1B). ChAT antibody staining labeled more cells than ChAT-Gal4 (Mi{Trojan-GAL4.0}ChAT[MI04508-TG4.0] CG7715[MI04508-TG4.0-X]), suggesting that this driver may not fully capture all EEs expressing ChAT. Depletion of nAchR subunits in ECs did not affect the number of EEs (Fig. 3 – figure supplement 1C).

To address the role of Ach production in barrier integrity, we depleted ChAT with pros^{ts}, as well as with ChAT^{ts}. Reduction of ChAT levels with both drivers rendered flies more susceptible to barrier dysfunction after Paraquat exposure (Fig. 3E, F). Prospero is a known neuronal driver (Balakireva et al., 1998) and is also expressed in enteric neurons

(Fig. 3 – figure supplement 1D). We screened additional drivers in order to separate the neuronal and epithelial contribution of Ach to barrier function, such as CG32547-Gal4 (Guo et al., 2019), which also presented expression in enteric neurons (Fig. 3 – figure supplement 2A) and Orcokinin-Gal, a driver identified through the publicly available scRNA data from the fly cell atlas (Li et al., 2022) While Orcokinin transcript levels were low in body neurons and high in EEs, this driver is also partially expressed in ECs, thus preventing a clean separation of Ach sources and their contributions to barrier function (Fig. 3 – figure supplement 2A). Further attempts to leverage previously identified neuropeptide- drivers or a split-Gal4 approach did not yield a clean separation of neuronal and EE-labeling, either (Fig. 3 – figure supplement 2B and figure supplement 3).

Combined, these data support the notion that Ach signaling is critical to maintain barrier integrity and stress resilience in the intestinal epithelium of the fly. While cholinergic innervation is a likely source of the ligand in this response, local production of Ach by enteroendocrine cells may also play a role in maintaining homeostasis.

Transcriptional changes after disruption of Ach signaling in the intestinal epithelium

As we observed barrier dysfunction without obvious deregulation of epithelial junctions after nAChR loss in ECs, we decided to profile changes in gene expression elicited in the gut by nAchR depletion. We performed RNAseq on whole guts depleted for nAchR β1 or β3 for 3 days under the control of $NP1^{ts}$. PCA analysis suggested that the transcriptomes from intestines with nAchR knockdown were clearly distinct from transcriptomes of intestines with a control RNAi construct (mCherry RNAi; Fig. 4A). Overall, we observed 240 upregulated and 215 downregulated genes (Fig. 4B; FDR<= 0.1; log2(fold change) < -1 or > 1; 100% of samples have >= 1 reads), of which 171 were differentially expressed in both nAchR β1 and β3 knockdowns, supporting the idea that these subunits have partially overlapping functions (Fig. 4B, Fig. 4 – figure supplement 1A, F). Synaptotagmin 4 (Syt4) was the most significantly downregulated gene in both knockdowns (Fig. 4D). RT-qPCR analysis confirmed a reduction of Syt4

levels after nAchR depletion (Fig. 4 – figure supplement 1B). GO term enrichment analysis revealed increased expression of glucosidases and hydrolases after nAchR knockdown (Fig. 4 – figure supplement 1C, F), and downregulation of genes involved in immune responses such as lysozymes (Fig. 4C, Fig. 4 – figure supplement 1D) and genes related to chitin binding and metabolism (Fig. 4C).

In parallel, we analyzed the transcriptome of whole guts depleted of ChAT using pros^{ts} for 3 days. While the knockdown samples also separated clearly from the control, they displayed fewer differentially regulated genes than guts depleted of nAchR (Fig. 4E, F, Fig. 4 – figure supplement 1G). However, Syt4 remained the most significantly downregulated gene (Fig. 4H) and enriched GO terms overlapped significantly with the previous experiment, especially with regards to immune responses (Fig. 4G). Chitin-related GO terms were also trending towards enrichment among downregulated genes (Fig. 4G), and the genes associated with these terms partially overlapped with the ones identified after nAchR knockdown (Fig. 4C). We also detected an enrichment of chitin-related gene sets among upregulated genes after ChAT depletion in EEs (Fig. 4 – figure supplement 1E), however the genes associated with these terms were different from the ones previously identified. Direct comparison of differentially regulated genes revealed an overlap of 56 genes between guts depleted for nAchR in ECs and guts where ChAT was silenced using pros^{ts} (Fig. 4I).

We referenced scRNAseq data recently reported by us in the Aging Fly Cell Atlas (Lu et al., 2023) to characterize expression patterns of nAchR signaling components more closely across the different intestinal cell types (Fig. 4 – figure supplement 2A, B). Overall, all nAchR subunits as well as the Ach-producing enzyme ChAT are lowly expressed in the gut epithelium of 5-day old animals, with nAchR α4 showing the highest expression levels across all cell types. All subunits are expressed in ECs and EEs, while expression in ISCs and EBs is more variable. Subunit α5 shows an enrichment in EEs. ChAT is preferentially expressed in EEs, but also shows some residual EC expression. The Ach-degrading enzyme Ace on the other hand is more widely expressed and shows an enrichment in ECs, potentially suggesting a local modulation of Ach levels in the gut epithelium. Finally, Syt4 is expressed at low levels among all intestinal epithelial cell types.

nAchR depletion disrupts PM integrity

The enrichment of chitin GO terms in our RNAseq experiments prompted us to examine the peritrophic matrix (PM). The PM is a protective structure lining the gut of many insects, consisting of crosslinked glycoproteins, proteoglycans and chitin (Erlandson et al., 2019; Hegedus et al., 2009; Hegedus et al., 2019). It surrounds the food bolus and forms a selectively permeable physical barrier preventing direct contact between abrasive food particles and bacteria with the epithelium, thus helping to compartmentalize digestive processes as well as protecting the animal from ingested toxins and pathogens (Erlandson et al., 2019; Hegedus et al., 2019). In flies, it was shown that the PM protects against pathogenic bacteria and their pore-forming toxins, such as *Pseudomonas entomophilia* and *Serratia marcescens* (Kuraishi et al., 2011). Dipteran insects such as *Drosophila* are thought to continuously produce a type II PM originating in the cardia at the anterior end of the midgut (Hegedus et al., 2019). There is evidence suggesting remodeling activity along the posterior midgut, as transcripts for PM components were found enriched in the R4 region of the midgut (Buchon et al., 2013). Moreover, intestinal IMD signaling as well as a subset of enteric neurons have been implicated in modulating the composition and permeability of the PM, however the underlying molecular mechanisms of PM remodeling remain poorly understood (Buchon, Broderick, Poidevin, et al., 2009; Kenmoku et al., 2016).

Transcript levels of a putative component of the PM, CG32302, were noticeably reduced in guts depleted of nAchR subunits (Fig. 5 – figure supplement 1A). Earlier studies highlighted the importance of the PM in protecting the animal against lethal pathogenic bacterial infection with *Pseudomonas entomophila* (PE) (Kuraishi et al., 2011). Indeed, depletion of nAchR subunits in ECs significantly reduced survival after PE infection (Fig. 5A). Overnight (16h) PE infection led to a significant upregulation of nAchR β3 subunit transcript levels, while Acetylcholine esterase (Ace) levels were significantly reduced (Fig. 5 – figure supplement 1B), indicating a possible activation of the pathway in response to infection. ChAT transcript levels as well as numbers of

ChAT-expressing cells in the gut epithelium remained unaffected by pathogenic infection (Fig. 5 – figure supplement 1B, C).

Defects in the PM can be visualized with confocal light microscopy by feeding animals fluorescently labeled latex beads that are retained in the food bolus and stay separated from the epithelium if the PM sleeve is intact (Kenmoku et al., 2016). The surface of the bead-containing ingested food appeared relatively smooth in control animals. In contrast, silencing of nAchR β1 or β3 led to spiny protrusions of the fluorescent matter, indicating a damaged PM (Fig. 5 – figure supplement 1D). We further modified this assay by crossing in the brush border marker A142-GFP (Buchon et al., 2013) and visualizing the PM with fluorescently labeled wheat germ agglutinin (WGA), a lectin that recognizes chitin (Carlini & Grossi-de-Sá, 2002), in addition to feeding the latex beads. Guts depleted of nAchR α4 displayed fluorescent signal scattered throughout the lumen and making contact with the brush border while the beads stayed confined to the PM sleeve and separated from the epithelium in control guts (Fig. 5B).

Electron microscopy has been successfully applied to detect subtle defects in PM morphology (Kuraishi et al., 2011). We therefore performed an ultrastructural analysis of the R4 compartment of guts depleted of nAchR β1. The PM was visible as a continuous folded ring in the lumen of control flies, consisting of electron-dense membranous material of roughly 100-200 nm thickness. Additionally, a second, much thinner (15-20nm) membranous ring-shaped layer was observed between the PM and the apical surface of the epithelial cells (Fig. 5C, Fig. 5 – figure supplement 1E).

In the majority of the 18 examined nAchR β1 knockdown midguts the thick PM layer was not compromised (Fig. 5 – figure supplement 1F). However, in 56% of samples the thin layer was clearly disrupted or missing altogether (Fig. 5C). Notably, none of the guts presented an intact thin layer in the absence of the thick layer. In all examined control and knockdown guts, the septate junctions connecting adjacent cells appeared normal, consistent with our Dlg and coracle staining (Fig. 2H, Fig. 2 – figure supplement 2A), as well as the fact that no changes in junctional protein expression was observed in our RNAseq experiments.

Defects in Ach signaling disturb gut compartmentalization and cause dysbiosis and JAK-STAT-mediated inflammation

Since the PM has been connected to regulation of the microbiome in mosquitos (Rodgers et al., 2017), we hypothesized that nAchR silencing also deregulates the microbial community inhabiting the fly gut. To test this assumption, we measured microbial load by plating pooled guts of control or nAchR knockdown animals on selective media supporting the growth of commensals such as Lactobacilli, Acetobacteriaceae or Enterobacteriaceae. The amount of CFUs after 8 days of nAchR β1, β3 or α4 silencing exceeded control levels significantly, indicating that these flies struggle to maintain appropriate commensal numbers (Fig. 5D). The fly midgut is functionally compartmentalized and contains a stomach-like region of acid-producing copper cells (Dubreuil, 2004). A previous study has highlighted the importance of gut compartmentalization in controlling microbiome abundance and distribution. As flies age, this spatial organization is progressively lost due to chronic JAK-STAT activation leading to metaplasia of copper cells in the acidic gastric region, ultimately resulting in dysbiosis and death of the animal (Li et al., 2016). Gut compartmentalization can be visualized by feeding flies the pH indicator Bromophenol blue, which labels the acidic copper cell region in yellow, while the rest of gut remains blue, indicative of a more basic pH (Li et al., 2016). Reduction of nAchR levels lead to an increase of disturbed acidity patterns, ranging from completely blue guts to samples with weak staining and white patches, which has been attributed to expansion of acid-producing commensals like Lactobacillus along the whole gut (Li et al., 2016) (Fig. 5E).

Dysbiosis can be a consequence of IMD pathway disruption, but at the same time triggers chronic IMD pathway activation (Buchon, Broderick, Chakrabarti, et al., 2009; Guo et al., 2014) Surprisingly, we did not observe an upregulation of antimicrobial peptides (AMP) transcripts classically associated with an IMD response (De Gregorio et al., 2002; Imler & Bulet, 2005), which is in line with the enrichment of immune-related terms among downregulated genes in our bulk RNAseq data sets (Fig. 4C and 4G).

Furthermore, depletion of ChAT in EEs with pros^{ts} also caused increased susceptibility to PE infection (Fig. 5F) as well as dysbiosis (Fig. 5G). Conversely, overexpression of ChAT promoted survival after bacterial infection (Fig. 5 – figure supplement 1G).

Together these results suggest that Ach signaling is required to maintain a healthy microbiome and protect the animals against pathogenic infections.

Syt4 is a transcriptional target of nAchR regulating PM function

One of the most significantly downregulated genes identified in our RNAseq data sets is Synaptotagmin 4, a vesicular Ca^{2+}-binding protein promoting retrograde signaling at synapses (Yoshihara et al., 2005). RNAi-meditated silencing of Syt4 under control of NP1^{ts} reduced survival after challenge with PE (Fig. 6A, Fig. 6 – figure supplement 1A) and caused PM defects visualized with the bead feeding assay (Fig. 6B). Moreover, Syt4 depletion increased commensal numbers (Fig. 6 – figure supplement 1B), disrupted gut compartmentalization (Fig. 6 – figure supplement 1C) as well as the morphology of the gastric region: Acid-producing copper cells usually form deep invaginations of the apical membrane (Dubreuil, 2004), giving rise to a gastric unit that can be visualized with anti-cut staining (Li et al., 2016). Syt4-depletion resulted in a disorganized morphology and a marked flattening of these units (Fig. 6 – figure supplement 1D). Combined knockdown of Syt4 and nAchR subunits did not have an additive effect on survival after PE infection, consistent with an epistatic relationship between these genes (Fig. 6 – figure supplement 1E).

We generated a new Syt4 null mutant (Syt4$^{\Delta}$) with CRISPR/Cas9 technology to further substantiate these findings. While these mutant animals were homozygous viable, they displayed enhanced susceptibility to PE challenge (Fig. 6C) and a fragmented PM, often accompanied by enlarged WGA-positive structures within the epithelium (Fig. 6D). To control for potential off target effects of the CRISPR/Cas9 technology, we outcrossed Syt4$^{\Delta}$ to a deficiency covering the Syt4 locus and found that the resulting offspring were also highly sensitive to PE infection (Fig. 6C) and displayed barrier dysfunction after bacterial challenge (Fig. 6 – figure supplement 1F). The response of these mutants to Paraquat stress was less robust: Syt4 mutant animals were slightly (but not

significantly) more sensitive to Paraquat than wild-type controls (Fig. 6 – figure supplement 1G). Accordingly, RNAi-mediated knockdown of Syt4 in enterocytes resulted in overall mild and experimentally inconsistent increases in barrier dysfunction after Paraquat treatment (Fig. 6 – figure supplement 1H).

To characterize the localization of Syt4 in the gut epithelium we utilized a 3xFLAG-mCherry-labeled protein trap line under UAS control (Singari et al., 2014). Overexpression of this construct with $NP1^{ts}$ had a protective effect on animal survival after PE challenge (Fig. 6E), but was not able to rescue PE sensitivity when nAchR subunits were knocked down simultaneously, suggesting that Syt4 expression is not sufficient for barrier protection in a nAchR loss of function context (Fig. 6 – figure supplement 1I). Immunofluorescence analysis of the overexpressed construct yielded a vesicular staining pattern that overlapped with Golgi and lysosomal markers (Fig. 6 – figure supplement 1J). Interestingly, we noticed a significant colocalization of Syt4-mCherry-positive structures and WGA staining in immunofluorescence experiments, suggesting that Syt4 vesicles contain chitin (Fig. 6F). Immunogold electron microscopy confirmed the colocalization of mCherry-Syt4 and WGA in vesicular structures containing highly folded membrane swirls and amorphous cargo (Fig. 6G). These vesicles also stained positive for the late endosomal/lysosomal marker Lamp1 (Fig. 6 – figure supplement 1K). Similar WGA or Lamp1 carrying structures were observed in wild-type (OreR) guts (Fig. 6G and Fig. 6 – figure supplement 1K).

Discussion

Our study identified 22 candidate COPD genes that modulate barrier integrity in the fly and demonstrates the utility of the genetically accessible fly to screen candidate disease genes from human GWAS studies to provide mechanistic insight into their role in tissue homeostasis and pathophysiology. In particular, our results provide a role for nAchR signaling in maintaining intestinal barrier function. Since depletion of several nAchR subunits in enterocytes, or of ChAT in neurons and EEs leads to loss of barrier integrity and decreased survival after chemical or bacterial challenge, we propose that acetylcholine-mediated crosstalk between cholinergic neurons and/or EEs with ECs is critical to maintain intestinal epithelial homeostasis. This role of nAchR signaling is mediated by transcriptional regulation of Syt4 in ECs, which in turn maintains secretion of chitin vesicles to maintain the peritrophic matrix (Fig. 6H).

The exact source of acetylcholine in this regulation remains unclear due to the lack of specific drivers that would allow separating cholinergic neurons and EEs. Recent work suggests a vital role of neuronally-derived Ach during regeneration (Petsakou et al., 2023). While neuronal Ach seems to be the main driver regulating return to homeostasis after injury, it is possible that acetylcholine secreted by both cell types may contribute to the maintenance of the epithelium under homeostatic conditions and it will be of interest to explore these contributions in future studies.

Of further interest for future studies is to assess the regulation of nAchR signaling activity in the context of stress and infection. Our transcriptome analysis, which shows that nAchRβ3 is induced and Ace is repressed after PE infection is in line with previous findings and suggests that the pathway is dynamically regulated in response to enteropathogen infection. In addition to regulating tissue recovery, Ca^{2+} signaling in ECs may also strengthen PM integrity through promoting Syt4-mediated vesicle fusion (Wang & Chapman, 2010)

Our data using nAChR subunit loss of function clones suggest that nAchR signaling only mildly impacts regenerative processes, influencing the balance between EEs and ECs in newly formed cell populations. It is possible that perturbing other subunits may have a stronger impact on ISC proliferation and / or differentiation and an exhaustive

loss of function study evaluating the role of specific subunits will be of interest. We do observe a strong proliferative response of ISCs to nAchR subunit knock down in ECs, on the other hand, and this response is consistent with previously described proliferative responses of ISCs to EC stress and damage (Jiang et al., 2009).

A role for acetylcholine signaling in human barrier epithelia is supported by previous studies: muscarinic acetylcholine receptors have been successfully targeted in the clinic to relieve bronchoconstriction and mucus hypersecretion in COPD and asthma (Calzetta et al., 2021), although nicotinic AchRs remain more elusive from a therapeutic perspective (Hollenhorst & Krasteva-Christ, 2021). While Ach is a classic neurotransmitter, a growing body of work has uncovered an important role of Ach beyond the context of the nervous system: various non-neuronal cell types express the machinery for Ach synthesis and secretion, ranging from diverse immune cells to epithelial cells, such as brush/tuft cells (Kummer & Krasteva-Christ, 2014; Wessler & Kirkpatrick, 2008). Airway tuft cells have been implicated in orchestrating type 2 inflammatory responses (O'Leary et al., 2019; Sell et al., 2021) and mucociliary clearance (Perniss et al., 2020), whereas their intestinal counterparts participate in defense against helminths and protists and limit biliary inflammation (O'Leary et al., 2022; O'Leary et al., 2019). With a wide range of cell types able to produce or sense Ach, non-neuronal Ach serves as a versatile signaling molecule eliciting complex intercellular crosstalk with diverse outcomes; depending on the context, Ach may promote inflammation or conversely exert anti-inflammatory functions (Hollenhorst & Krasteva-Christ, 2021; Kummer & Krasteva-Christ, 2014; Sell et al., 2021). Accordingly, it was recently reported that expression of a COPD risk allele of CHRNA5 in epithelial cells leads to airway remodeling *in vivo*, increased proliferation and production of pro-inflammatory cytokines through decreased calcium entry and increased adenylyl-cyclase activity (Routhier et al., 2021).

Previous work has further shown a downregulation of junctional proteins such as ZO-1 and p120 after depletion of CHRNA5 in A549 cells lung cancer cells (Krais et al., 2011). While we observed a mildly disorganized pattern of junctional markers such as Dlg after nAchR subunit knockdown in the fly intestinal epithelium, junctional architecture appeared normal when analyzed by electron microscopy. Furthermore, transcriptome

analysis revealed little to no changes in the expression of proteins involved in polarity or cellular junction formation, suggesting that nAchR signaling regulates barrier function through other mechanisms. A role for the Syt4-mediated secretion of PM protein components and chitin in maintaining barrier integrity is supported by the observation that mCherry-tagged Syt4 partially overlaps with chitin-binding wheat germ agglutinin staining.

While the *Drosophila* PM is thought to be produced mostly in the anterior most portion of the gut (Hegedus et al., 2019), the existence of WGA-positive vesicles throughout the entire midgut suggests continuous remodeling along the length of the tissue. This finding is consistent with the previously reported expression of PM-related transcripts in the R4 compartment of the midgut (Buchon et al., 2013). PM integrity can be modulated by enteric neurons, although a role for cholinergic signaling was not tested in this context (Kenmoku et al., 2016).

Our study highlights the evolutionary conservation of mechanisms maintaining epithelial barrier function. The PM is functionally analogous to mucus and surfactant layers in mammalian airways, and it remains to be explored whether COPD risk alleles in nAchR subunits also cause a dysfunction in the secretion of such barrier components. The elevated inflammation and airway remodeling in mice expressing the CHRNA5 risk allele suggest that such a mechanism may be conserved as well (Routhier et al., 2021) . It is critical to note that the epithelial dysfunction observed in these animals, as well as part of the association of COPD risk with specific CHRNA loci, emerge independently of cigarette smoke (Parker et al., 2019; Routhier et al., 2021; Siedlinski et al., 2013), indicating that nAchR signaling is critical to maintain homeostasis not only in the context of oxidative stress, but under homeostatic conditions. Supporting this view, our data show that knockdown of nAchR subunits in fly ECs also results in epithelial stress signaling in the absence of Paraquat exposure.

These consistencies further validate the approach of prioritizing candidate genes associated with COPD risk loci using the *Drosophila* intestine as a model system. Characterization of the epithelial role of other identified candidate orthologues from our screen will likely provide further insight into the biology and pathophysiology of barrier

dysfunction and epithelial homeostasis. Such studies will be critical for target identification and validation for therapeutic intervention in COPD.

Material and methods

Drosophila stocks and husbandry

Flies were raised and kept on standard fly food prepared according to the following recipe: 1 l distilled water, 13.8 g agar, 22 g molasses, 75 g malt extract, 18 g inactivated dry yeast, 80 g corn flour, 10 g soy flour, 6.26 ml propionic acid, 2 g methyl 4-hydroxybenzoate in 7.2 ml of ethanol. Flies were reared at 25°C with 65% humidity on a 12 h light/dark cycle. All animals used in this study were mated females matured for 4-6 days.

The TARGET system was used to conditionally express UAS-linked transgenes in specific cell populations in combination with indicated Gal drivers (McGuire et al., 2004).

Crosses containing tub::Gal80^{ts} were reared at 18°C to avoid premature gene expression. Transgene expression was induced by shifting the flies to 29°C for 1-8 days, as indicated in the figure legends.

For experiments using a GeneSwitch driver, flies were reared on normal food before being shifted to food containing 200mM Mifepristone (RU486); for barrier function experiments (smurf assay). FD&C blue dye (Neta Scientific, SPCM-FD110-04) was added to the food at final concentration of 2.5% (w/v).

Formation of MARCM clones was induced with heat shock for 1h at 37°C and clones were analyzed after 7 days at 25°C. EsgF/O clones were analyzed after 8 days at 29°C.

RNAi lines used in the barrier dysfunction screen are listed in Suppl Fig. 1B.

The following additional lines were obtained from the Bloomington *Drosophila* Stock Center: w^{1118} (3605), Oregon-R (5), UAS-mCherry^{RNAi} (35785), UAS-ChAT^{RNAi} (60028), FRT82B (2051), TI{TI}nAChRα2^{attP} (84540), Mi{Trojan-GAL4.0}ChAT[MI04508-TG4.0] CG7715[MI04508-TG4.0-X]/TM6B (60317), TI{2A-GAL4}ChAT[2A-GAL4] (84618), Orcokinin-Gal4 (92253), arm-GFP (8555), Df(3R)BSC423/TM6C (24927), CG32547-Gal4/FM7a (84614), UAS-Luciferase^{RNAi}(31603), nAChRalpha1^{attP}/TM6B (84539), UAS-Syt4^{RNAi} (39016), Mi{Hto-WP}GldGYB Syt4GYB/TM6B (56539), UAS-2xEGFP (6874), dimm-Gal4 (25373), CCAP-Gal4 (25686), CCAP-Gal4 (25685), Burs-Gal4 (51980),

Dsk[2A]-Gal4 (84630), Dsk-Gal4 (51981), Nplp4[2A]-Gal4 (84674), R57F07-p65.AD; UAS-DSCP-6XEGFP (91402), UAS-DSCP-6XEGFP; R57F07-Gal4.DBD (91403), R33A12-Gal4.DBD (68537), R61H08-Gal4.DBD (69158), Mi{Trojan-Gal4.DBD.0}ChAT[MI04508-TG4DBD.0] CG7715[MI04508-TG4DBD.0-X] (60318)

The following additional lines were obtained from the Vienna *Drosophila* Stock Center: UAS-nAchRβ1^{RNAi} (33825, pruned), UAS-nAchRβ3^{RNAi} (42742, pruned), UAS-ChAT^{RNAi} (20183), UAS-Syt4^{RNAi} (v33317)

The following lines were gifts: 5966-GeneSwitch (B. Ohlstein), 2xSTAT::GFP (E. Bach), NP1-Gal4 (D. Ferrandon), A142-GFP (N. Buchon), Mex1-Gal4;tubGal80^{ts} (L. O'Brien), MARCM82 (hsFlp; tubGal4, UAS-GFP; FRT82, tubGal80, N. Perrimon), ProsV1-Gal4 (J-F.Ferveur), da-GeneSwitch (V. Monnier), UAS-Xbp1-eGFP (H. D. Ryoo), esg-Gal4, UAS-GFP, tubGal80^{ts} ; UAS-Flp, Actin>CD2>Gal4 (esgF/O, B.Edgar)

Generation of UAS-ChAT

DNA encoding the sequence of Choline O-acetyltransferase (Uniprot identifier P07668, amino acid residues 1-721), was synthesized and subcloned into pUASTattB under the control of the hsp70 promoter. Transgenic lines were established by WellGenetics, Taiwan. In brief, pUASTattB plasmid containing the ChAT sequence was microinjected into embryos of y[1] M{vas-int.Dm}ZH-2A w[*]; P{y[+t7.7]=CaryP}attP40 or y[1] M{vas-int.Dm}ZH-2A w[*]; P{y[+t7.7]=CaryP}attP2. Transgenic F1 flies were screened for the selection marker white+ (orange colored eyes).

Syt4 CRISPR mutant

CRISPR mediated mutagenesis was performed by WellGenetics, Inc. (Taiwan) using modified methods of Kondo and Ueda (Kondo & Ueda, 2013). In brief, the upstream gRNA sequences TTTCCACTCGATGTTCCTGG[CGG] and downstream gRNA sequences CGCAGGCGCCCCTTAATGAG[GGG] were cloned into U6 promoter plasmids separately. Cassette 3xP3 RFP, which contains a floxed 3xP3 RFP and two

homology arms, were cloned into pUC57 Kan as donor template for repair. Syt4/CG10047- targeting gRNAs and hs Cas9 were supplied in DNA plasmids, together with donor plasmid for microinjection into embryos of control strain w[1118]. F1 flies carrying the selection marker 3xP3 RFP were further validated by genomic PCR and sequencing. This CRISPR editing generates a 2,603 bp deletion allele of Syt4, deleting the entire CDS and replacing it with a 3xP3 RFP cassette.

Gene assignment to COPD genome-wide association study (GWAS) loci

Publicly available summary statistics for the discovery stage of the COPD GWAS reported by Hobbs *et al.,* 2017 were obtained from dbGaP (accession: phs000179). Forty-eight candidate genes were assigned to the 22 loci reported in Hobbs *et al.,* 2017 based upon expression quantitative trait loci (eQTL), coding variation level support or physical distance if a gene could not be assigned via the former criteria. First, candidate genes were assigned to loci if the index variant was an eQTL in any tissue for any gene within 250 kilobases of the variant in GTEx (Battle et al., 2017) (V6p). We further applied colocalization (via the coloc package in R) (Giambartolomei et al., 2014) to estimate the probability the eQTL and COPD risk association signal share a casual variant. Of the 40 genes with eQTL support, 24 had a colocalization probability > 0.6. Candidate genes were also assigned to loci if the index variant was in linkage disequilibrium (LD) (r^2>0.6) with coding variants for the gene. LD was estimated using individuals of European ancestry from 1000 Genomes (Auton et al., 2015). Eight candidate genes were assigned to five loci, six of which overlapped genes with eQTL level support.

Since we first obtained this candidate gene list, a larger COPD risk GWAS was published (Sakornsakolpat, Prokopenko, Lamontagne, Reeve, Guyatt, Jackson, Shrine, Qiao, Bartz, Kim, Lee, Latourelle, Li, Morrow, Obeidat, Wyss, Bakke, Barr, Beaty, Belinsky, Brusselle, Crapo, de Jong, DeMeo, Fingerlin, Gharib, Gulsvik, Hall, Hokanson, Kim, Lomas, London, Meyers, O'Connor, Rennard, Schwartz, Sliwinski, Sparrow, Strachan, Tal-Singer, Tesfaigzi, Vestbo, Vonk, Yim, Zhou, Bossé, et al., 2019) that made use of not only lung eQTL and coding variant data, but also epigenetic and gene-

set similarity approaches to assign candidate genes to COPD risk loci (see Supplementary Table 7 in Sakornsakolpat *et al*., 2019). We found our assigned candidate genes overlapped with candidate genes from this newer study at 13/22 loci reported in the Hobbs et al., 2017 study, including CHRNA3/5. Overall 20/48 candidate genes were also listed as candidate genes in the Sakornsakolpat et al. study.

Barrier Dysfunction Screen

For the barrier dysfunction assay, males from candidate RNAi lines were crossed at a 1:1 ratio with virgin *daughterless*-GeneSwitch driver line females in Bloomington-modified food (standard medium) bottles. Crosses were raised at 25°C and brooded every 2-3 days. Progeny were collected and females were sorted after mating for 2-3 days (discarding males). This yielded about 200 females per genotype depending on the RNAi line. Sorted females were aged in standard medium at 25°C for 10-12 days. Aged females (~25 per vial; exact number recorded per vial for assay read-out) were then exposed to standard medium prepared with 200mM Mifepristone (RU486) from Sigma Aldrich (cat# 856177) and 2.5% w/v FD&C Blue Dye no 1 from Spectrum (cat# FD110) for 24 hours at 25°C or 29°C. Prior to Paraquat exposure, flies were dry starved for 2-3 hours at the experimental temperature. 25mM Paraquat solution (5% sucrose and 2.5% w/v FD&C Blue Dye in sterile water) or mock solution (sucrose and blue dye only) was freshly prepared for each experiment.. Starved flies were placed in empty vials with a Whatman filter paper (VWR, 89013-946) on top of a foam biopsy pad (Neta Sciences, BPLS-6110) and 1.25mL of Paraquat or mock solution for 16 hours at 25°C or 29°C and then shifted back to medium with 200mM Mifepristone (RU486) and 2.5% w/v FD&C Blue Dye no 1. Entirely Blue (Smurf) flies were counted starting post-16-hour exposure. Smurf flies were counted daily or every-other day. About 8-12 candidate RNAi lines were tested in sets with Luciferase RNAi always included as a control.

The average proportion of smurf flies across technical replicates per time point were calculated and graphed. The natural log (LN) ratio was calculated for each candidate RNAi by dividing the candidate RNAi proportion average from the final time point by the luciferase RNAi proportion average for the same time point (=LN(Candidate

RNAi/Luciferase RNAi)). Candidate RNAi results were ranked by establishing a scale with arbitrary LN ratio ranges to define: strong enhancers (≥ 1), enhancers (≥ 0.43 to ≤ 0.99), weak enhancers (≥ 0.20 to ≤ 0.42), no effect (≥ -0.30 to ≤ 0.19), weak suppressors (≥ -0.70 to ≤ -0.31), suppressors (≥ -1.10 to ≤ -0.71), and strong suppressors (≤ -1.11).

Paraquat feeding

20-25 flies per vial were kept on food containing FD&C blue for 1-3 days and dry starved in empty vials for 2-3h prior to Paraquat exposure. Methyl viologen dichloride hydrate (Paraquat, 856177, Sigma Aldrich) solution was prepared freshly for each experiment in 5% (w/v) sucrose in water with 2% (w/v) FD&C blue. Paraquat concentration was 12.5mM unless indicated otherwise. Starved flies were transferred to vials containing 600µl of Paraquat solution or 5% sucrose (mock treatment) as well as a circular Whatman filter paper (VWR, 89013-946) on top of a foam biopsy pad (Neta Sciences, BPLS-6110). Flies were treated for 16h overnight and then transferred back to fly food with FD&C blue dye. The number of smurf flies was recorded 24h after the start of the Paraquat challenge and subsequently monitored over the course of 7-10 days.

***Pseudomonas entomophila* infection**

Pseudomonas entomophila (PE, gift from B. Lemaitre), was cultured in LB medium at 29 °C overnight for 16-18h (15ml/sample to be infected). Bacteria were centrifuged at 4000g for 10 min at RT and resuspended in 5% sucrose (OD_{600}=100). 500µl of concentrated bacterial suspension or 5% (w/v) sucrose solution (mock treatment) was added to empty fly vials containing a circular Whatman filter paper (VWR, 89013-946) on top of a foam biopsy pad (Neta Sciences, BPLS-6110). For assessment of barrier function, bacteria were suspended in 5% sucrose + 2% w/v FD&C Blue Dye no 1. 20-25 flies per vial were starved in empty vials for 2–3 h before infection. Survival was

monitored over the course of 7-10 days and 100µl of 5% sucrose or 5% sucrose+2% w/v FD&C Blue Dye no 1 solution was added daily.

Gut compartmentalization

Gut compartmentalization was assessed as described in Li et al., 2016: 100µl of 2% w/v Bromphenol blue solution (Sigma Aldrich, B5525) was dispensed in a food vial, the surface was broken up with a pipette tip to allow full absorption of the dye before flies were transferred onto food. Flies were fed overnight and guts were dissected in small groups and immediately scored visually under a stereomicroscope to avoid prolonged exposure to CO_2.

Immunofluorescence microscopy

Guts from adult female flies were dissected in PBS, fixed for 45mins at room temperature (RT) in fixative solution (4% formaldehyde, 100 mM glutamic acid, 25 mM KCl, 20 mM $MgSO_4$, 4 mM Na_2HPO_4, 1 mM $MgCl_2$, pH 7.5), washed twice in wash buffer (1× PBS, 0.5% bovine serum albumin and 0.1% Triton X-100, 0.005% NaN_3) for 30 min at RT. Primary and secondary antibodies were diluted in wash buffer. Samples were incubated overnight at 4°C with primary antibody, washed twice for 30min with wash buffer before incubating 4-6h at RT with secondary antibody. Hoechst33342 (Invitrogen, H3570, 1:10’000) or wheat germ agglutinin-AlexaFluor647 (Invitrogen, W32466, 1:500) were added to the secondary antibody cocktail to visualize DNA or the peritrophic matrix (PM) respectively. Samples were washed again twice for 30mins before mounting in Prolong Glass antifade mounting media (Invitrogen, P36982).

To assess the integrity of the PM, flies were dry starved for 2h and then fed Fluoresbrite microspheres (Polysciences, 17149 (0.05µm, green) or 195075 (0.5µm, red), diluted 1:50 in 5% sucrose solution on Whatman filter paper for 16h overnight. Guts were dissected, fixed and processed for immunofluorescence microscopy analysis as described above.

For lysotracker staining, freshly dissected guts were incubated for 5mins in 1× PBS with Lysotracker Deep Red (Invitrogen, L12492, 1:500) before fixation. Samples were washed twice for 10mins before and after 1h incubation with Hoechst, mounted and analyzed within one day.

Primary antibodies used in this study: chicken anti-GFP (Abcam, ab13970, 1:1000), mouse anti-armadillo (DSHB, N2 7A1, 1:100), mouse anti-Delta (DSHB, C594.9B, 1:50), mouse anti-Dlg (DSHB, 4F3 anti-discs large, 1:20), mouse anti-ChAT (DSHB, ChAT4B1, 1:100), rabbit anti-phospho Histone H3 (Millipore, 06-570, 1:2000), mouse anti-prospero (DSHB, MR1A, 1:250), mouse anti-cut (DSHB, 2B10, 1:100), mouse anti-Golgin84 (DSHB, Golgin 84 12-1, neat), mouse anti-Coracle heavy isoform (DSHB, C615.16, 1:20)

Secondary antibodies were from Jackson ImmunoResearch Laboratories and diluted 1:1000. donkey anti-mouse Cy3 (Jackson ImmunoResearch Laboratories, 715-165-150, 1:1000), donkey anti-mouse Alexa-647 (Invitrogen, A31571, 1:1000), donkey anti-chicken Alexa-488 (Jackson ImmunoResearch Laboratories, 703-545-155, 1:1000), donkey anti-rabbit Cy3 (Jackson ImmunoResearch Laboratories, 711-165-152, 1:1000), donkey anti-rabbit Alexa 647 (Jackson ImmunoResearch Laboratories, 711-605-152, 1:1000)

All Images were taken on a Leica SP8 confocal microscope and processed using FIJI(Schindelin et al., 2012) and Adobe Illustrator.

CFU counting

Commensal bacteria were cultured as described in (Guo et al., 2014):. In brief, intact flies were sanitized in 70% ethanol for 1min and rinsed 3x in sterile PBS. 5 guts per sample were dissected and homogenized in 250µl sterile PBS. Serial dilutions were plated on selective media, plates were incubated for 48-72h at 29°C and colonies counted.

Selective plates were prepared according to the following recipes: *Acetobacteriaceae*: 25 g/l D-mannitol, 5 g/l yeast extract, 3 g/l peptone, and 15 g/l agar. *Enterobacteriaceae*: 10 g/l Tryptone, 1.5 g/l yeast extract, 10 g/l glucose, 5 g/l sodium chloride, 12 g/l agar. *Lactobacilli* MRS agar: 70 g/l BD Difco Lactobacilli MRS agar. *Nutrient Rich Broth*: 23 g/l BD Difco Nutrient agar. All media were autoclaved at 121 degrees Celsius for 15 min.

Electron microscopy (EM)

For the localization of Syt4, flies were allowed to express UAS-3xFLAG-mCherry-Syt4 in enterocytes under control of NP1ts for 2 days before dissection in PBS at room temperature. The dissected gut was cut with a sharp blade at the R3-R4 border and the R4-hindgut segment was immediately immersed in either one of 2 fixative solutions, to obtain samples for immuno-EM and for conventional EM in Epon-embedded material. For immuno-EM (Slot & Geuze, 2007), the fixation was performed with 4% paraformaldehyde (PFA), 0.1% glutaraldehyde (GA) in PHEM buffer (60mM PIPES, 25 mM HEPES, 2 mM $MgCl_2$, 10 mM EGTA), pH 6.9, for 1h at room temperature. Subsequently, fixation was continued in 0.6 % PFA in PHEM buffer at 4 ºC for several days. The samples were then rinsed in PBS, blocked with 0.15 % glycine in PBS, and gradually embedded in gelatin, from 2% (30 min) over 6% (30 min) to 12 % gelatin. Small blocks of solidified gelatin each containing 1 gut segment were cryoprotected overnight with 2.3 M sucrose. They were mounted on aluminum pins in a direction to expose the transversal cut at the R4 segment for cryo-ultramicrotomy and frozen in liquid N2. Syt4 was localized on ultrathin cryosections with polyclonal rabbit anti-RFP antibody (600-401-379, Rockland). Chitin was localized with biotinylated wheat germ agglutinin (B-1025-5, Vector laboratories) followed by polyclonal rabbit anti-biotin antibody (100-4198, Rockland). *Drosophila*-specific rabbit anti-Lamp1 antibody was a gift from Andreas Jenny (Chaudhry et al., 2022). Antibodies were detected with protein A -conjugated with 15 or 10 nm gold particles in a JEOL JEM-1011 electron microscope.

For conventional EM the fixation was performed in 2.5 % GA in 0.1 M Sorensen's phosphate buffer (PB), pH 7.4, for 4 h at room temperature, then overnight at 4 ºC. Subsequently, fixation was continued in 0.6 % PFA in 0.1 M PB at 4 ºC for several days. After rinsing in 0.1 M PB, the guts were postfixed with 1 % OsO_4 and 1.5 % $K_3[Fe(CN)_6]$ in 0.07 M PB, stained en bloc in aqueous 0.5 % uranyl acetate, dehydrated in acetone and embedded in Epon. Transverse sections of the R4 gut segments were stained with uranyl acetate and lead citrate and examined in a JEOL JEM-1011 electron microscope.

Bulk RNAseq

For bulk RNAseq analysis 4 independent biological replicates per sample consisting of 20-25 guts each were dissected and collected on dry ice. RNA was extracted using the Qiagen RNeasy Mini kit.

Total RNA was quantified with Qubit RNA HS Assay Kit (Thermo Fisher Scientific) and quality was assessed using RNA ScreenTape on 4200 TapeStation (Agilent Technologies). For sequencing library generation, the Truseq Stranded mRNA kit (Illumina) was used with an input of 100 nanograms of total RNA. Libraries were quantified with Qubit dsDNA HS Assay Kit (Thermo Fisher Scientific) and the average library size was determined using D1000 ScreenTape on 4200 TapeStation (Agilent Technologies). Libraries were pooled and sequenced on NovaSeq 6000 (Illumina) to generate 30 millions single-end 50-base pair reads for each sample. Reads were aligned to the *Drosophila* genome, version BDGP6, using the GSNAP aligner as part of the HTSeqGenie R package (version 4.2). Reads that uniquely aligned within exonic boundaries of genes were used to derive expression estimates. nRPKM values, in which total library sizes were normalized using the median ratio method as previously described (Anders & Huber, 2010), were generated for each gene. Partek Flow was used to perform differential gene expression and PCA analysis, gene ontology term enrichment as well as creation of illustrative graphs.

Aging Fly Cell Atlas scRNAseq analysis

The analysis of snRNA-seq data relies on the Aging Fly Cell Atlas (AFCA) dataset (Lu et al., 2023). We specifically focus on the gut cell types, such as intestinal stem cell,

enteroblast, adult differentiating enterocyte, enterocyte, and enteroendocrine cell, which were selected from the 5-day AFCA data and further subclustered. Before generating the Uniform Manifold Approximation and Projection (UMAP) plots, we took into account sex and tissue differences by employing the hormony correction method to adjust the principal components. (Korsunsky et al., 2019)

RT-qPCR

3-5 independent biological replicates consisting of 20-25 guts per sample were dissected and collected on dry ice. RNA was extracted using the Qiagen RNeasy Mini kit. 25ng RNA were used as input for the TaqMan RNA-to-CT 1-Step Kit (Applied Biosciences) in a 384-well format. Assays were run on a QuantStudio 6 real-time PCR system according to the kit instructions and analyzed using the ΔΔCT method (normalized to GAPDH).

Taqman FAM-MGB probes used in this study (Thermo Fisher): Syt4 (Dm02135118_g1), ChAT (Dm02134803_m1), Ace (Dm02134758_g1), nAchR α1(Dm02151345_m1), nAchR α2(Dm02150710_m1), nAchR α3(Dm01843751_m1), nAchR α4(Dm01843901_m1), nAchR α5(Dm01808491_g1), nAchR α6(Dm01803895_m1), nAchR α7(Dm01799687_m1), nAchR β1(Dm01822104_m1), nAchR β2(Dm02150716_g1), nAchR β3(Dm01843796_g1), GADPH (Dm01843827_s1).

Statistical analyses

Generation of graphs and statistical analyses were performed with Graphpad Prism 9.

Experiments with two conditions were compared with a two-tailed parametric Student's T-test or Fischer's exact test, as appropriate. Experiments with multiple conditions were evaluated either by ordinary one-way ANOVA followed by Dunnett's post-hoc test to compare a control group with experimental conditions or a Chi square test for categorical data. Barrier dysfunction curves were analyzed with 2-way repeated measures ANOVA. Survival curves were compared with the Mantel-Cox method.

No statistical methods were used to predetermine sample sizes; sample sizes were determined based on variation observed in pilot experiments and previously published literature. Exact numbers are listed in figure legends. All animals were randomly allocated to treatment groups. The experimenter was blinded for image analysis and other quantifications. The number of repeats for each experiment is listed in figure legends, all attempts at replication were successful. The initial screen as well as electron microscopy and RNAseq experiments were performed once for data gathering and hypothesis generation; the data was later validated by other methods. No data points were excluded from analyses.

Data availability

All data generated and analyzed are included in the manuscript, figures and figure supplements. All sequencing data generated in this study has been deposited in GEO under accession code GSE236071.

Illustrative model

Illustrative model summarizing results was created with BioRender.com

Material availability

Fly lines generated in this study (UAS-ChAT and Syt4 CRISPR mutant) are available without restriction upon an agreement with a material transfer agreement (MTA).

Adherence to community standards

This study and manuscript were prepared in accordance with ARRIVE and ICMJE guidelines.

Acknowledgements

We thank Dr Andreas Jenny (Albert Einstein College of Medicine) for the *Drosophila*-specific rabbit anti-Lamp1 antibody.
We thank Dr Aniek Janssen and Dr Lucie van Leeuwen (UMC Utrecht) for the Oregon R flies for EM.

Funding

The microscopy infrastructure in this work is subsidized by the Roadmap for Large-Scale Research Infrastructure (NEMI) of Netherlands Organization for Scientific Research (grant number 184.034.014 to J.K.).

H.L. is a CPRIT Scholar in Cancer Research (RR200063) and supported by NIH (R00AG062746), the Longevity Impetus Grant, the Welch Foundation, and Ted Nash Long Life Foundation.

References

Aghapour, M., Raee, P., Moghaddam, S. J., Hiemstra, P. S., & Heijink, I. H. (2018). Airway Epithelial Barrier Dysfunction in Chronic Obstructive Pulmonary Disease: Role of Cigarette Smoke Exposure. *Am J Respir Cell Mol Biol*, *58*(2), 157-169. https://doi.org/10.1165/rcmb.2017-0200TR

Aghapour, M., Ubags, N. D., Bruder, D., Hiemstra, P. S., Sidhaye, V., Rezaee, F., & Heijink, I. H. (2022). Role of air pollutants in airway epithelial barrier dysfunction in asthma and COPD. *Eur Respir Rev*, *31*(163). https://doi.org/10.1183/16000617.0112-2021

Amos, C. I., Wu, X., Broderick, P., Gorlov, I. P., Gu, J., Eisen, T., Dong, Q., Zhang, Q., Gu, X., Vijayakrishnan, J., Sullivan, K., Matakidou, A., Wang, Y., Mills, G., Doheny, K., Tsai, Y. Y., Chen, W. V., Shete, S., Spitz, M. R., & Houlston, R. S. (2008). Genome-wide association scan of tag SNPs identifies a susceptibility locus for lung cancer at 15q25.1. *Nat Genet*, *40*(5), 616-622. https://doi.org/10.1038/ng.109

Anders, S., & Huber, W. (2010). Differential expression analysis for sequence count data. *Genome Biol*, *11*(10), R106. https://doi.org/10.1186/gb-2010-11-10-r106

Auton, A., Brooks, L. D., Durbin, R. M., Garrison, E. P., Kang, H. M., Korbel, J. O., Marchini, J. L., McCarthy, S., McVean, G. A., & Abecasis, G. R. (2015). A global reference for human genetic variation. *Nature*, *526*(7571), 68-74. https://doi.org/10.1038/nature15393

Bach, E. A., Ekas, L. A., Ayala-Camargo, A., Flaherty, M. S., Lee, H., Perrimon, N., & Baeg, G. H. (2007). GFP reporters detect the activation of the Drosophila JAK/STAT pathway in vivo. *Gene Expr Patterns*, *7*(3), 323-331. https://doi.org/10.1016/j.modgep.2006.08.003

Balakireva, M., Stocker, R. F., Gendre, N., & Ferveur, J. F. (1998). Voila, a new Drosophila courtship variant that affects the nervous system: behavioral, neural, and genetic characterization. *J Neurosci*, *18*(11), 4335-4343. https://doi.org/10.1523/JNEUROSCI.18-11-04335.1998

Barnes, P. J. (2019). Inflammatory endotypes in COPD. *Allergy*, *74*(7), 1249-1256. https://doi.org/10.1111/all.13760

Battle, A., Brown, C. D., Engelhardt, B. E., & Montgomery, S. B. (2017). Genetic effects on gene expression across human tissues. *Nature*, *550*(7675), 204-213. https://doi.org/10.1038/nature24277

Beebe, K., Park, D., Taghert, P. H., & Micchelli, C. A. (2015). The Drosophila Prosecretory Transcription Factor dimmed Is Dynamically Regulated in Adult Enteroendocrine Cells and Protects Against Gram-Negative Infection. *G3 (Bethesda)*, *5*(7), 1517-1524. https://doi.org/10.1534/g3.115.019117

Biteau, B., Hochmuth, C. E., & Jasper, H. (2008). JNK activity in somatic stem cells causes loss of tissue homeostasis in the aging Drosophila gut. *Cell Stem Cell*, *3*(4), 442-455. https://doi.org/10.1016/j.stem.2008.07.024

Biteau, B., Hochmuth, C. E., & Jasper, H. (2011). Maintaining tissue homeostasis: dynamic control of somatic stem cell activity. *Cell Stem Cell*, *9*(5), 402-411. https://doi.org/10.1016/j.stem.2011.10.004

Buchon, N., Broderick, N. A., Chakrabarti, S., & Lemaitre, B. (2009). Invasive and indigenous microbiota impact intestinal stem cell activity through multiple pathways in Drosophila. *Genes Dev*, *23*(19), 2333-2344. https://doi.org/10.1101/gad.1827009

Buchon, N., Broderick, N. A., Poidevin, M., Pradervand, S., & Lemaitre, B. (2009). Drosophila intestinal response to bacterial infection: activation of host defense and stem cell proliferation. *Cell Host Microbe*, *5*(2), 200-211. https://doi.org/10.1016/j.chom.2009.01.003

Buchon, N., Osman, D., David, F. P., Fang, H. Y., Boquete, J. P., Deplancke, B., & Lemaitre, B. (2013). Morphological and molecular characterization of adult midgut compartmentalization in Drosophila. *Cell Rep*, *3*(5), 1725-1738. https://doi.org/10.1016/j.celrep.2013.04.001

Caliri, A. W., Tommasi, S., & Besaratinia, A. (2021). Relationships among smoking, oxidative stress, inflammation, macromolecular damage, and cancer. *Mutat Res Rev Mutat Res*, *787*, 108365. https://doi.org/10.1016/j.mrrev.2021.108365

Calzetta, L., Coppola, A., Ritondo, B. L., Matino, M., Chetta, A., & Rogliani, P. (2021). The Impact of Muscarinic Receptor Antagonists on Airway Inflammation: A Systematic Review. *Int J Chron Obstruct Pulmon Dis*, *16*, 257-279. https://doi.org/10.2147/COPD.S285867

Carlier, F. M., de Fays, C., & Pilette, C. (2021). Epithelial Barrier Dysfunction in Chronic Respiratory Diseases. *Front Physiol*, *12*, 691227. https://doi.org/10.3389/fphys.2021.691227

Carlini, C. R., & Grossi-de-Sá, M. F. (2002). Plant toxic proteins with insecticidal properties. A review on their potentialities as bioinsecticides. *Toxicon*, *40*(11), 1515-1539. https://doi.org/10.1016/s0041-0101(02)00240-4

Chaudhry, N., Sica, M., Surabhi, S., Hernandez, D. S., Mesquita, A., Selimovic, A., Riaz, A., Lescat, L., Bai, H., MacIntosh, G. C., & Jenny, A. (2022). Lamp1 mediates lipid transport, but is dispensable for autophagy in Drosophila. *Autophagy*, *18*(10), 2443-2458. https://doi.org/10.1080/15548627.2022.2038999

Chen, J., Kim, S. M., & Kwon, J. Y. (2016). A Systematic Analysis of Drosophila Regulatory Peptide Expression in Enteroendocrine Cells. *Mol Cells*, *39*(4), 358-366. https://doi.org/10.14348/molcells.2016.0014

Cognigni, P., Bailey, A. P., & Miguel-Aliaga, I. (2011). Enteric neurons and systemic signals couple nutritional and reproductive status with intestinal homeostasis. *Cell Metab*, *13*(1), 92-104. https://doi.org/10.1016/j.cmet.2010.12.010

Cui, K., Ge, X., & Ma, H. (2014). Four SNPs in the CHRNA3/5 alpha-neuronal nicotinic acetylcholine receptor subunit locus are associated with COPD risk based on meta-analyses. *PLoS One*, *9*(7), e102324. https://doi.org/10.1371/journal.pone.0102324

Davie, K., Janssens, J., Koldere, D., De Waegeneer, M., Pech, U., Kreft, L., Aibar, S., Makhzami, S., Christiaens, V., Bravo Gonzalez-Blas, C., Poovathingal, S., Hulselmans, G., Spanier, K. I., Moerman, T., Vanspauwen, B., Geurs, S., Voet, T., Lammertyn, J., Thienpont, B., . . . Aerts, S. (2018). A Single-Cell Transcriptome Atlas of the Aging Drosophila Brain. *Cell*, *174*(4), 982-998 e920. https://doi.org/10.1016/j.cell.2018.05.057

De Gregorio, E., Spellman, P. T., Tzou, P., Rubin, G. M., & Lemaitre, B. (2002). The Toll and Imd pathways are the major regulators of the immune response in Drosophila. *Embo j*, *21*(11), 2568-2579. https://doi.org/10.1093/emboj/21.11.2568

Deng, B., Li, Q., Liu, X., Cao, Y., Li, B., Qian, Y., Xu, R., Mao, R., Zhou, E., Zhang, W., Huang, J., & Rao, Y. (2019). Chemoconnectomics: Mapping Chemical Transmission in Drosophila. *Neuron*, *101*(5), 876-893.e874. https://doi.org/10.1016/j.neuron.2019.01.045

Dubreuil, R. R. (2004). Copper cells and stomach acid secretion in the Drosophila midgut. *Int J Biochem Cell Biol*, *36*(5), 745-752. https://doi.org/10.1016/j.biocel.2003.07.004

Erlandson, M. A., Toprak, U., & Hegedus, D. D. (2019). Role of the peritrophic matrix in insect-pathogen interactions. *J Insect Physiol*, *117*, 103894. https://doi.org/10.1016/j.jinsphys.2019.103894

Giambartolomei, C., Vukcevic, D., Schadt, E. E., Franke, L., Hingorani, A. D., Wallace, C., & Plagnol, V. (2014). Bayesian test for colocalisation between pairs of genetic association studies using summary statistics. *PLoS Genet*, *10*(5), e1004383. https://doi.org/10.1371/journal.pgen.1004383

Guo, L., Karpac, J., Tran, S. L., & Jasper, H. (2014). PGRP-SC2 promotes gut immune homeostasis to limit commensal dysbiosis and extend lifespan. *Cell*, *156*(1-2), 109-122. https://doi.org/10.1016/j.cell.2013.12.018

Guo, X., Yin, C., Yang, F., Zhang, Y., Huang, H., Wang, J., Deng, B., Cai, T., Rao, Y., & Xi, R. (2019). The Cellular Diversity and Transcription Factor Code of Drosophila Enteroendocrine Cells. *Cell Rep*, *29*(12), 4172-4185 e4175. https://doi.org/10.1016/j.celrep.2019.11.048

Hegedus, D., Erlandson, M., Gillott, C., & Toprak, U. (2009). New insights into peritrophic matrix synthesis, architecture, and function. *Annu Rev Entomol*, *54*, 285-302. https://doi.org/10.1146/annurev.ento.54.110807.090559

Hegedus, D. D., Toprak, U., & Erlandson, M. (2019). Peritrophic matrix formation. *J Insect Physiol*, *117*, 103898. https://doi.org/10.1016/j.jinsphys.2019.103898

Hobbs, B. D., de Jong, K., Lamontagne, M., Bossé, Y., Shrine, N., Artigas, M. S., Wain, L. V., Hall, I. P., Jackson, V. E., Wyss, A. B., London, S. J., North, K. E., Franceschini, N., Strachan, D. P., Beaty, T. H., Hokanson, J. E., Crapo, J. D., Castaldi, P. J., Chase, R. P., . . . Cho, M. H. (2017). Genetic loci associated with chronic obstructive pulmonary disease overlap with loci for lung function and pulmonary fibrosis. *Nat Genet*, *49*(3), 426-432. https://doi.org/10.1038/ng.3752

Hobbs, B. D., de Jong, K., Lamontagne, M., Bosse, Y., Shrine, N., Artigas, M. S., Wain, L. V., Hall, I. P., Jackson, V. E., Wyss, A. B., London, S. J., North, K. E., Franceschini, N., Strachan, D. P., Beaty, T. H., Hokanson, J. E., Crapo, J. D., Castaldi, P. J., Chase, R. P., . . . International, C. G. C. (2017). Genetic loci associated with chronic obstructive pulmonary disease overlap with loci for lung function and pulmonary fibrosis. *Nat Genet*, *49*(3), 426-432. https://doi.org/10.1038/ng.3752

Hollenhorst, M. I., & Krasteva-Christ, G. (2021). Nicotinic Acetylcholine Receptors in the Respiratory Tract. *Molecules*, *26*(20). https://doi.org/10.3390/molecules26206097

Holsopple, J. M., Cook, K. R., & Popodi, E. M. (2022). Identification of novel split-GAL4 drivers for the characterization of enteroendocrine cells in the Drosophila melanogaster midgut. *G3 (Bethesda)*, *12*(6). https://doi.org/10.1093/g3journal/jkac102

Hu, Y., Flockhart, I., Vinayagam, A., Bergwitz, C., Berger, B., Perrimon, N., & Mohr, S. E. (2011). An integrative approach to ortholog prediction for disease-focused and other functional studies. *BMC Bioinformatics*, *12*, 357. https://doi.org/10.1186/1471-2105-12-357

Hung, R. J., McKay, J. D., Gaborieau, V., Boffetta, P., Hashibe, M., Zaridze, D., Mukeria, A., Szeszenia-Dabrowska, N., Lissowska, J., Rudnai, P., Fabianova, E., Mates, D., Bencko, V., Foretova, L., Janout, V., Chen, C., Goodman, G., Field, J. K., Liloglou, T., . . . Brennan, P. (2008). A susceptibility locus for lung cancer maps to nicotinic acetylcholine receptor subunit genes on 15q25. *Nature*, *452*(7187), 633-637. https://doi.org/10.1038/nature06885

Imler, J. L., & Bulet, P. (2005). Antimicrobial peptides in Drosophila: structures, activities and gene regulation. *Chem Immunol Allergy*, *86*, 1-21. https://doi.org/10.1159/000086648

Jasper, H. (2020). Intestinal Stem Cell Aging: Origins and Interventions. *Annu Rev Physiol*, *82*, 203-226. https://doi.org/10.1146/annurev-physiol-021119-034359

Jiang, H., Patel, P. H., Kohlmaier, A., Grenley, M. O., McEwen, D. G., & Edgar, B. A. (2009). Cytokine/Jak/Stat signaling mediates regeneration and homeostasis in the Drosophila midgut. *Cell*, *137*(7), 1343-1355. https://doi.org/10.1016/j.cell.2009.05.014

Kenmoku, H., Ishikawa, H., Ote, M., Kuraishi, T., & Kurata, S. (2016). A subset of neurons controls the permeability of the peritrophic matrix and midgut structure in Drosophila adults. *J Exp Biol*, *219*(Pt 15), 2331-2339. https://doi.org/10.1242/jeb.122960

Kondo, S., & Ueda, R. (2013). Highly improved gene targeting by germline-specific Cas9 expression in Drosophila. *Genetics*, *195*(3), 715-721. https://doi.org/10.1534/genetics.113.156737

Korsunsky, I., Millard, N., Fan, J., Slowikowski, K., Zhang, F., Wei, K., Baglaenko, Y., Brenner, M., Loh, P. R., & Raychaudhuri, S. (2019). Fast, sensitive and accurate integration of

single-cell data with Harmony. *Nat Methods*, *16*(12), 1289-1296. https://doi.org/10.1038/s41592-019-0619-0

Krais, A. M., Hautefeuille, A. H., Cros, M. P., Krutovskikh, V., Tournier, J. M., Birembaut, P., Thépot, A., Paliwal, A., Herceg, Z., Boffetta, P., Brennan, P., & Hainaut, P. L. (2011). CHRNA5 as negative regulator of nicotine signaling in normal and cancer bronchial cells: effects on motility, migration and p63 expression. *Carcinogenesis*, *32*(9), 1388-1395. https://doi.org/10.1093/carcin/bgr090

Kummer, W., & Krasteva-Christ, G. (2014). Non-neuronal cholinergic airway epithelium biology. *Curr Opin Pharmacol*, *16*, 43-49. https://doi.org/10.1016/j.coph.2014.03.001

Kuraishi, T., Binggeli, O., Opota, O., Buchon, N., & Lemaitre, B. (2011). Genetic evidence for a protective role of the peritrophic matrix against intestinal bacterial infection in Drosophila melanogaster. *Proc Natl Acad Sci U S A*, *108*(38), 15966-15971. https://doi.org/10.1073/pnas.1105994108

Lee, T., & Luo, L. (2001). Mosaic analysis with a repressible cell marker (MARCM) for Drosophila neural development. *Trends Neurosci*, *24*(5), 251-254. https://doi.org/10.1016/s0166-2236(00)01791-4

Li, H., Janssens, J., De Waegeneer, M., Kolluru, S. S., Davie, K., Gardeux, V., Saelens, W., David, F. P. A., Brbic, M., Spanier, K., Leskovec, J., McLaughlin, C. N., Xie, Q., Jones, R. C., Brueckner, K., Shim, J., Tattikota, S. G., Schnorrer, F., Rust, K., . . . Zinzen, R. P. (2022). Fly Cell Atlas: A single-nucleus transcriptomic atlas of the adult fruit fly. *Science*, *375*(6584), eabk2432. https://doi.org/10.1126/science.abk2432

Li, H., Qi, Y., & Jasper, H. (2016). Preventing Age-Related Decline of Gut Compartmentalization Limits Microbiota Dysbiosis and Extends Lifespan. *Cell Host Microbe*, *19*(2), 240-253. https://doi.org/10.1016/j.chom.2016.01.008

Lu, T. C., Brbic, M., Park, Y. J., Jackson, T., Chen, J., Kolluru, S. S., Qi, Y., Katheder, N. S., Cai, X. T., Lee, S., Chen, Y. C., Auld, N., Liang, C. Y., Ding, S. H., Welsch, D., D'Souza, S., Pisco, A. O., Jones, R. C., Leskovec, J., . . . Li, H. (2023). Aging Fly Cell Atlas identifies exhaustive aging features at cellular resolution. *Science*, *380*(6650), eadg0934. https://doi.org/10.1126/science.adg0934

Lu, W., Liu, Z., Fan, X., Zhang, X., Qiao, X., & Huang, J. (2022). Nicotinic acetylcholine receptor modulator insecticides act on diverse receptor subtypes with distinct subunit

compositions. *PLoS Genet*, *18*(1), e1009920. https://doi.org/10.1371/journal.pgen.1009920

McGuire, S. E., Mao, Z., & Davis, R. L. (2004). Spatiotemporal gene expression targeting with the TARGET and gene-switch systems in Drosophila. *Sci STKE*, *2004*(220), pl6. https://doi.org/10.1126/stke.2202004pl6

Miguel-Aliaga, I., Jasper, H., & Lemaitre, B. (2018). Anatomy and Physiology of the Digestive Tract of Drosophila melanogaster. *Genetics*, *210*(2), 357-396. https://doi.org/10.1534/genetics.118.300224

O'Leary, C. E., Sbierski-Kind, J., Kotas, M. E., Wagner, J. C., Liang, H. E., Schroeder, A. W., de Tenorio, J. C., von Moltke, J., Ricardo-Gonzalez, R. R., Eckalbar, W. L., Molofsky, A. B., Schneider, C., & Locksley, R. M. (2022). Bile acid-sensitive tuft cells regulate biliary neutrophil influx. *Sci Immunol*, *7*(69), eabj1080. https://doi.org/10.1126/sciimmunol.abj1080

O'Leary, C. E., Schneider, C., & Locksley, R. M. (2019). Tuft Cells-Systemically Dispersed Sensory Epithelia Integrating Immune and Neural Circuitry. *Annu Rev Immunol*, *37*, 47-72. https://doi.org/10.1146/annurev-immunol-042718-041505

Parker, M. M., Lutz, S. M., Hobbs, B. D., Busch, R., McDonald, M. N., Castaldi, P. J., Beaty, T. H., Hokanson, J. E., Silverman, E. K., & Cho, M. H. (2019). Assessing pleiotropy and mediation in genetic loci associated with chronic obstructive pulmonary disease. *Genet Epidemiol*, *43*(3), 318-329. https://doi.org/10.1002/gepi.22192

Perniss, A., Liu, S., Boonen, B., Keshavarz, M., Ruppert, A. L., Timm, T., Pfeil, U., Soultanova, A., Kusumakshi, S., Delventhal, L., Aydin, Ö., Pyrski, M., Deckmann, K., Hain, T., Schmidt, N., Ewers, C., Günther, A., Lochnit, G., Chubanov, V., . . . Kummer, W. (2020). Chemosensory Cell-Derived Acetylcholine Drives Tracheal Mucociliary Clearance in Response to Virulence-Associated Formyl Peptides. *Immunity*, *52*(4), 683-699.e611. https://doi.org/10.1016/j.immuni.2020.03.005

Petsakou, A., Liu, Y., Liu, Y., Comjean, A., Hu, Y., & Perrimon, N. (2023). Cholinergic neurons trigger epithelial Ca(2+) currents to heal the gut. *Nature*, *623*(7985), 122-131. https://doi.org/10.1038/s41586-023-06627-y

Pillai, S. G., Ge, D., Zhu, G., Kong, X., Shianna, K. V., Need, A. C., Feng, S., Hersh, C. P., Bakke, P., Gulsvik, A., Ruppert, A., Lødrup Carlsen, K. C., Roses, A., Anderson, W.,

Rennard, S. I., Lomas, D. A., Silverman, E. K., & Goldstein, D. B. (2009). A genome-wide association study in chronic obstructive pulmonary disease (COPD): identification of two major susceptibility loci. *PLoS Genet*, *5*(3), e1000421. https://doi.org/10.1371/journal.pgen.1000421

Raftery, A. L., Tsantikos, E., Harris, N. L., & Hibbs, M. L. (2020). Links Between Inflammatory Bowel Disease and Chronic Obstructive Pulmonary Disease. *Front Immunol*, *11*, 2144. https://doi.org/10.3389/fimmu.2020.02144

Rera, M., Bahadorani, S., Cho, J., Koehler, C. L., Ulgherait, M., Hur, J. H., Ansari, W. S., Lo, T., Jr., Jones, D. L., & Walker, D. W. (2011). Modulation of longevity and tissue homeostasis by the Drosophila PGC-1 homolog. *Cell Metab*, *14*(5), 623-634. https://doi.org/10.1016/j.cmet.2011.09.013

Rera, M., Clark, R. I., & Walker, D. W. (2012). Intestinal barrier dysfunction links metabolic and inflammatory markers of aging to death in Drosophila. *Proc Natl Acad Sci U S A*, *109*(52), 21528-21533. https://doi.org/10.1073/pnas.1215849110

Rodgers, F. H., Gendrin, M., Wyer, C. A. S., & Christophides, G. K. (2017). Microbiota-induced peritrophic matrix regulates midgut homeostasis and prevents systemic infection of malaria vector mosquitoes. *PLoS Pathog*, *13*(5), e1006391. https://doi.org/10.1371/journal.ppat.1006391

Routhier, J., Pons, S., Freidja, M. L., Dalstein, V., Cutrona, J., Jonquet, A., Lalun, N., Merol, J. C., Lathrop, M., Stitzel, J. A., Kervoaze, G., Pichavant, M., Gosset, P., Tournier, J. M., Birembaut, P., Dormoy, V., & Maskos, U. (2021). An innate contribution of human nicotinic receptor polymorphisms to COPD-like lesions. *Nat Commun*, *12*(1), 6384. https://doi.org/10.1038/s41467-021-26637-6

Sakornsakolpat, P., Prokopenko, D., Lamontagne, M., Reeve, N. F., Guyatt, A. L., Jackson, V. E., Shrine, N., Qiao, D., Bartz, T. M., Kim, D. K., Lee, M. K., Latourelle, J. C., Li, X., Morrow, J. D., Obeidat, M., Wyss, A. B., Bakke, P., Barr, R. G., Beaty, T. H., . . . Cho, M. H. (2019). Genetic landscape of chronic obstructive pulmonary disease identifies heterogeneous cell-type and phenotype associations. *Nat Genet*, *51*(3), 494-505. https://doi.org/10.1038/s41588-018-0342-2

Sakornsakolpat, P., Prokopenko, D., Lamontagne, M., Reeve, N. F., Guyatt, A. L., Jackson, V. E., Shrine, N., Qiao, D., Bartz, T. M., Kim, D. K., Lee, M. K., Latourelle, J. C., Li, X.,

Morrow, J. D., Obeidat, M., Wyss, A. B., Bakke, P., Barr, R. G., Beaty, T. H., . . . International, C. G. C. (2019). Genetic landscape of chronic obstructive pulmonary disease identifies heterogeneous cell-type and phenotype associations. *Nat Genet*, *51*(3), 494-505. https://doi.org/10.1038/s41588-018-0342-2

Schindelin, J., Arganda-Carreras, I., Frise, E., Kaynig, V., Longair, M., Pietzsch, T., Preibisch, S., Rueden, C., Saalfeld, S., Schmid, B., Tinevez, J. Y., White, D. J., Hartenstein, V., Eliceiri, K., Tomancak, P., & Cardona, A. (2012). Fiji: an open-source platform for biological-image analysis. *Nat Methods*, *9*(7), 676-682. https://doi.org/10.1038/nmeth.2019

Sell, E. A., Ortiz-Carpena, J. F., Herbert, D. R., & Cohen, N. A. (2021). Tuft cells in the pathogenesis of chronic rhinosinusitis with nasal polyps and asthma. *Ann Allergy Asthma Immunol*, *126*(2), 143-151. https://doi.org/10.1016/j.anai.2020.10.011

Siedlinski, M., Tingley, D., Lipman, P. J., Cho, M. H., Litonjua, A. A., Sparrow, D., Bakke, P., Gulsvik, A., Lomas, D. A., Anderson, W., Kong, X., Rennard, S. I., Beaty, T. H., Hokanson, J. E., Crapo, J. D., Lange, C., & Silverman, E. K. (2013). Dissecting direct and indirect genetic effects on chronic obstructive pulmonary disease (COPD) susceptibility. *Hum Genet*, *132*(4), 431-441. https://doi.org/10.1007/s00439-012-1262-3

Singari, S., Javeed, N., Tardi, N. J., Marada, S., Carlson, J. C., Kirk, S., Thorn, J. M., & Edwards, K. A. (2014). Inducible protein traps with dominant phenotypes for functional analysis of the Drosophila genome. *Genetics*, *196*(1), 91-105. https://doi.org/10.1534/genetics.113.157529

Slot, J. W., & Geuze, H. J. (2007). Cryosectioning and immunolabeling. *Nat Protoc*, *2*(10), 2480-2491. https://doi.org/10.1038/nprot.2007.365

Sone, M., Zeng, X., Larese, J., & Ryoo, H. D. (2013). A modified UPR stress sensing system reveals a novel tissue distribution of IRE1/XBP1 activity during normal Drosophila development. *Cell Stress Chaperones*, *18*(3), 307-319. https://doi.org/10.1007/s12192-012-0383-x

Taylor P., B. J. (1999). Synthesis, Storage and Release of Acetylcholine. In A. B. Siegel GJ, Albers RW, et al., editors (Ed.), *Basic Neurochemistry: Molecular, Cellular and Medical Aspects* (6th ed.). Lippincott-Raven. https://www.ncbi.nlm.nih.gov/books/NBK28051/

Wang, Z., & Chapman, E. R. (2010). Rat and Drosophila synaptotagmin 4 have opposite effects during SNARE-catalyzed membrane fusion. *J Biol Chem*, *285*(40), 30759-30766. https://doi.org/10.1074/jbc.M110.137745

Wessler, I., & Kirkpatrick, C. J. (2008). Acetylcholine beyond neurons: the non-neuronal cholinergic system in humans. *Br J Pharmacol*, *154*(8), 1558-1571. https://doi.org/10.1038/bjp.2008.185

Wilk, J. B., Shrine, N. R., Loehr, L. R., Zhao, J. H., Manichaikul, A., Lopez, L. M., Smith, A. V., Heckbert, S. R., Smolonska, J., Tang, W., Loth, D. W., Curjuric, I., Hui, J., Cho, M. H., Latourelle, J. C., Henry, A. P., Aldrich, M., Bakke, P., Beaty, T. H., . . . Stricker, B. H. (2012). Genome-wide association studies identify CHRNA5/3 and HTR4 in the development of airflow obstruction. *Am J Respir Crit Care Med*, *186*(7), 622-632. https://doi.org/10.1164/rccm.201202-0366OC

Yoshihara, M., Adolfsen, B., Galle, K. T., & Littleton, J. T. (2005). Retrograde signaling by Syt 4 induces presynaptic release and synapse-specific growth. *Science*, *310*(5749), 858-863. https://doi.org/10.1126/science.1117541

Zeng, X., & Hou, S. X. (2015). Enteroendocrine cells are generated from stem cells through a distinct progenitor in the adult Drosophila posterior midgut. *Development*, *142*(4), 644-653. https://doi.org/10.1242/dev.113357

Zhang, G., Bai, H., Zhang, H., Dean, C., Wu, Q., Li, J., Guariglia, S., Meng, Q., & Cai, D. (2011). Neuropeptide exocytosis involving synaptotagmin-4 and oxytocin in hypothalamic programming of body weight and energy balance. *Neuron*, *69*(3), 523-535. https://doi.org/10.1016/j.neuron.2010.12.036

Figure Legends

Figure 1: A *Drosophila* screen for COPD-associated candidate genes

A) List of human candidate genes for genetic loci associated with COPD risk and their *Drosophila* orthologs. An overall rating was assigned to the *Drosophila* genes based on the detailed results of the individual RNAi lines included in the screen: Genes exacerbating barrier dysfunction upon depletion were categorized as enhancers, while genes whose depletion improved barrier function were rated as suppressors of barrier dysfunction (Supplementary File 2). When available, the human risk allele expression data is compared to the results of the *Drosophila* screen (agreement column).

(SNP, Single nucleotide polymorphism; CHR, chromosome; BP, base pair number; eqtl, expression quantitative trait loci).

B) Experimental design of intestinal barrier function screen. Flies carrying the ubiquitous driver da-GS were crossed to RNAi lines targeting candidate genes. The female offspring were aged for 10-12 days before induction of RNAi expression by RU486 for 24h on blue food. Flies were challenged with sucrose alone (mock) or 25mM Paraquat (PQ) for 16h overnight and then placed back on blue food with RU486. Blue flies with a defective intestinal barrier ("smurfs") were counted daily for 5-7 days.

C) Ranking of screened RNAi lines based on the natural logarithm (ln) of the ratio between the proportion of smurfs after candidate gene knockdown and luciferase RNAi control. Each number corresponds to an RNAi line listed in Supplementary File 2. Cut offs for the different categories are indicated.

D) Summary of screen results based on broad categorization as enhancer, suppressor or no effect. If several RNAi lines targeting the same gene unanimously had no effect, the gene was rated "no effect, conclusive", while inconsistent results were rated "no effect, inconclusive". For details see Supplementary File 2.

Figure 2: nAchR genes are required for barrier function in enterocytes (ECs) and enteroendocrine (EEs) cell differentiation

A) Barrier dysfunction assay after Luciferase (control) or nAchR α4 subunit depletion for 24h with ubiquitous driver da-GS. nAchR α4: n=100 for Luciferase RNAi (control) on sucrose; n=125 animals for Luciferase RNAi on sucrose+Paraquat; n=150 for nAchR α4 RNAi on sucrose; n=175 animals for nAchR α4 on sucrose+Paraquat. Paraquat concentration 25mM. N=1. Two-way repeated measures (RM) ANOVA (significance stated next to "genotypes").

B) Barrier dysfunction assay after mCherry (control) or ChAT depletion for 24h with ubiquitous driver da-GS. n=75 animals per genotype and condition; N=3. Paraquat concentration 15mM. Two-way RM ANOVA.

C) Barrier dysfunction assay after mCherry (control) or nAchR α4 depletion for 24h with enterocyte-specific driver NP1-Gal4, tubGal80^{ts} (NP1^{ts}). n=125 animals per genotype and condition; N=3. Two-way RM ANOVA.

D) Barrier dysfunction assay after mCherry (control) or nAchR α4 depletion for 24h with enterocyte and enteroblast-specific driver 5966-GS. n=175 animals per genotype and condition; N=3. Two-way RM ANOVA.

E) Quantification of ISC mitoses in guts depleted of nAchR β3 and α4 subunits in ECs for 8 days.

Mitotically active ISCs are labeled with anti-pH3 antibody; n=12;10;13 guts for mCherry (control), nAchR α4 RNAi and nAchR β1 RNAi, respectively. N=3. Ordinary one-way ANOVA followed by Dunnett's multiple comparisons test.

F) Confocal microscopy images of guts expressing a 2xSTAT::GFP reporter (green) depleted of mCherry (control) or nAchR α4 for 8 days in ECs with Mex-Gal4, tubGal80^{ts}. n=10 guts per genotype. N=3. Scale bar 50μm.

G) Confocal immunofluorescence image of posterior midguts expressing the UPR-reporter UAS-Xbp1-eGFP (green) after 8 days of nAchR subunit knockdown by RNAi. The EGFP tag is only in frame with the Xbp1(s) coding sequence after splicing using the unconventional splice site, which occurs under stress conditions. DNA (blue) is labeled with Hoechst. n=8 guts per genotype. N=3. Scale bar 25μm.

H) Confocal immunofluorescence images examining epithelial organization of septate junctions stained with anti-Dlg antibody (white), DNA (blue) is labeled with Hoechst. Yellow boxed insets are shown enlarged in bottom row. n=8 guts per genotype. N=3. Scale bars 10μm.

I) Confocal microscopy images of guts expressing GFP-tagged armadillo (arm-GFP, green) depleted of mCherry (control) or nAchR α4 for 8 days in ECs with NP1-Gal4, tubGal80^{ts}. n=8 guts per genotype. N=3. Scale bar 10μm.

J) Confocal immunofluorescence images of wildtype and nAchR α2 MARCM clones (green) 7 days after heat shock. Stem cells and enteroblasts are stained with anti-armadillo antibody (white); EEs are labeled with anti-prospero antibody (white, nuclear signal highlighted with yellow arrowheads) and DNA (blue) is labeled with Hoechst. Scale bars 15μm. Quantification of EE numbers within clones: n=32;38 clones for wildtype or nAchR α2, respectively from 3 pooled experiments. Fisher's exact test. Quantification of cell numbers/clone: n=32;38 clones for wildtype or nAchR α2, respectively from 3 pooled experiments. Unpaired two-tailed t-test.

Data presented as mean ± SEM. ns, not significant, $P > 0.05$; *$P \leq 0.05$; **$P \leq 0.01$; ***$P \leq 0.001$; ****$P \leq 0.0001$. n: number of animals or midguts analyzed; N: number of independent experiments performed with similar results and a similar n.

Figure 2 – figure supplement 1

A) Barrier dysfunction assay using various RNAi background control lines or nAchR α4 (positive control) depletion for 24h with enterocyte-specific driver NP1-Gal4, tubGal80ts (NP1^{ts}) before 15mM Paraquat (PQ) exposure. n=75 animals per genotype and condition; N=2. Gray background panel highlights the Paraquat exposed controls.

Analysis: comparing all control lines exposed to Paraquat to each other (not including nAchR α4). Two-way repeated measures ANOVA.

Details for control lines:

BL35785: Expresses dsRNA for RNAi of mCherry under UAS control in the VALIUM20 vector; attP2.

BL31603: Expresses dsRNA for RNAi of Ppyr\LUC (FBgn0014448) under UAS control in the VALIUM1 vector; attP2.

BL35789: Expresses firefly Luciferase under the control of UAS in the VALIUM1 vector; attP2.

BL35788: Expresses firefly Luciferase under the control of UAS in the VALIUM10 vector.

Can be used as a control for VALIUM10 or VALIUM20; attP2.

BL35786: Expresses GFP under the control of UAS in the VALIUM10 vector.

Can be used as a control for VALIUM10 or VALIUM20; attP2.

BL36304: 2nd chromosome attP docking site for phiC31 integrase-mediated transformation.

Note that the attP40 docking site is located within Msp300 and it may disrupt gene function.

BL36303: 3rd chromosome attP docking site for phiC31 integrase-mediated transformation.

B) Barrier dysfunction assay after mCherry (control) or indicated nAchR subunit depletion for 24h with ubiquitous driver da-GS. N=1. Two-way RM ANOVA.

nAchR α4 (v12441GD): n=100 for Luciferase RNAi (control) on sucrose; n=125 animals for Luciferase RNAi on sucrose+Paraquat; n=125 for nAchR α4 RNAi on sucrose; n=150 animals for nAchR α4 RNAi on sucrose+Paraquat.

nAchR β2(v1200GD): n=100 for Luciferase RNAi (control) on sucrose; n=125 animals for Luciferase RNAi on sucrose+Paraquat; n=75 for nAchR β2 RNAi on sucrose; n=150 animals for nAchR β2 RNAi on sucrose+Paraquat

nAchR β2(v109450KK): n=100 for Luciferase RNAi (control) on sucrose; n=125 animals for Luciferase RNAi on sucrose+Paraquat; n=125 for nAchR β2 RNAi on sucrose; n=150 animals for nAchR β2 RNAi on sucrose+Paraquat

nAchR α2 (v1194GD): n=100 for Luciferase RNAi (control) on sucrose; n=125 animals for Luciferase RNAi on sucrose+Paraquat; n=125 for nAchR α2 RNAi on sucrose; n=150 animals for nAchR α2 RNAi on sucrose+Paraquat.

nAchR α2 (v1195GD): n=100 for Luciferase RNAi (control) on sucrose; n=125 animals for Luciferase RNAi on sucrose+Paraquat; n=125 for nAchR α2 RNAi on sucrose; n=150 animals for nAchR α2 RNAi on sucrose+Paraquat.

nAchR α2 (BL27493): n=100 for Luciferase RNAi (control) on sucrose; n=125 animals for Luciferase RNAi on sucrose+Paraquat; n=125 for nAchR α2 RNAi on sucrose; n=125 animals for nAchR α2 RNAi on sucrose+Paraquat.

nAchR α1 (v1189GD): n=175 for Luciferase RNAi (control) on sucrose; n=175 animals for Luciferase RNAi on sucrose+Paraquat; n=175 for nAchR α1 RNAi on sucrose; n=175 animals for nAchR α1 RNAi on sucrose+Paraquat.

nAchR α1 (v48159GD): n=150 for Luciferase RNAi (control) on sucrose; n=150 animals for Luciferase RNAi on sucrose+Paraquat; n=125 for nAchR α1 RNAi on sucrose; n=150 animals for nAchR α1 RNAi on sucrose+Paraquat.

nAchR α1 (v48162GD): n=1075 for Luciferase RNAi (control) on sucrose; n=175 animals for Luciferase RNAi on sucrose+Paraquat; n=150 for nAchR α1 RNAi on sucrose; n=150 animals for nAchR α1 RNAi on sucrose+Paraquat.

nAchR α3 (BL61225): n=100 for Luciferase RNAi (control) on sucrose; n=125 animals for Luciferase RNAi on sucrose+Paraquat; n=50 for nAchR α3 RNAi on sucrose; n=75 animals for nAchR α3 RNAi on sucrose+Paraquat.

nAchR α3 (v101806KK): n=175 for Luciferase RNAi (control) on sucrose; n=175 animals for Luciferase RNAi on sucrose+Paraquat; n=175 for nAchR α3 RNAi on sucrose; n=175 animals for nAchR α3 RNAi on sucrose+Paraquat.

nAchR β2: n=100 for Luciferase RNAi (control) on sucrose; n=125 animals for Luciferase RNAi on sucrose+Paraquat; n=75 for nAchR β2 RNAi on sucrose; n=100 animals for nAchR β2 RNAi on sucrose+Paraquat.

C) Barrier dysfunction assay after mCherry (control) or ChAT depletion for 24h with ubiquitous driver da-GS. n=75 animals per genotype and condition; N=3. Two-way RM ANOVA.

D) Barrier dysfunction assay after mCherry (control) or nAchR β3 depletion for 24h with enterocyte-specific driver 5966-GS. Paraquat concentration 7.5mM. nAchR β3: n=175 for mCherry RNAi (control) on sucrose; n=175 animals for mCherry RNAi on sucrose+Paraquat; n=150 for nAchR β3 RNAi on sucrose; n=150 animals for nAchR β3 RNAi on sucrose+Paraquat. N=3. Two-way ANOVA.

E) Barrier dysfunction assay after mCherry (control) or nAchR β3 depletion for 24h with enterocyte-specific driver NP1-Gal4, tubGal80^{ts} (NP1^{ts}). Paraquat concentration 7.5mM. n=200 animals per genotype and condition; N=3. Two-way RM ANOVA.

Figure 2 – figure supplement 2

A) Confocal immunofluorescence images depicting sideviews of guts depleted of indicated nAchR subunits in ECs for 8 days with 5966-GS. Septate junctions are stained with anti-Coracle or anti-Dlg antibody (white), DNA (blue) is labeled with Hoechst, cell outline is visualized with phalloidin staining of actin (red). Scale bars 5μm.

B) Barrier dysfunction (smurf) assay after Paraquat challenge following depletion of nAchR subunits specifically in stem cells with esg-Gal4, UAS-2xEYFP; Su(H)GBE-Gal80, tubGal80^{ts} (ISC^{ts}). n=75 animals per genotype and conditions, expect for nAchR β1, where n= 50 animals per condition. N=2. Two-way RM ANOVA.

C) Survival after *Pseudomonas entomophila* (PE) infection following depletion of nAchR subunits in intestinal stem cells. n=75 animals per genotype and condition, N=2. Log Rank (Mantel-Cox) test.

D) Quantification of ISC mitoses in guts depleted of nAchR subunits in ECs for 3 days before 16h of PE infection. Mitotically active ISCs are labeled with anti-pH3 antibody. n=8 guts per genotype, N=2. Ordinary one-way ANOVA followed by Dunnett's multiple comparisons test.

E) Quantification of EE number and total cell numbers in nAchR α1 MARCM clones 7 days after heat shock. EE numbers: n= 22 clones for control and n=13 clones for nAchR α1; two independent pooled experiments are shown. Fischer's exact test. Total cell numbers per clone: n= 22 clones for control and n=13 clones for nAchR α1; two independent pooled experiments are shown. Unpaired two-tailed t-test.

F) Confocal immunofluorescence images of esg-Gal4, UAS-GFP, tubGal80ts ; UAS-Flp, Actin>CD2>Gal4 (esgF/O) clones (green) after 8 days of mCherry^{RNAi}, w^{1118} (controls) or nAchR α2^{RNAi} at 29°C. Stem cells are stained with anti-Delta antibody (white); EEs are labeled with anti-prospero antibody (white) and DNA (blue) is labeled with Hoechst. Scale bars 5μm.

Quantification of EE numbers and total cell numbers within clones after 8 days at 29°C: n=26 clones for mCherry^{RNAi}, n=17 clones for w^{1118}; n=30 clones for nAchR α2^{RNAi}, n=15 clones for nAchR β3^{RNAi}, n=14 clones for nAchR α4^{RNAi} from 2 independent pooled experiments. Chi square test for EE numbers, One-way ANOVA with Dunnett's multiple comparisons test for total cell numbers.

Data presented as mean ± SEM. ns, not significant, P > 0.05; *P ≤ 0.05; **P ≤ 0.01; ***P ≤ 0.001; ****P ≤ 0.0001. n: number of animals or midguts analyzed; N: number of independent experiments performed with similar results and a similar n.

Figure 3: Acetylcholine produced in EEs and/or neurons promotes barrier function

A) Confocal immunofluorescence image of cholinergic innervation of different intestinal compartments. GFP (green) expression is driven by Mi{Trojan-GAL4.0}ChAT[MI04508-TG4.0] CG7715[MI04508-TG4.0-X] and detected in the anterior (cardia/R1) as well as posterior midgut (R4-R5), at the hindgut boundary and rectal ampulla. DNA (blue) is labeled with Hoechst. n=5 guts. N=3. Scale bars 50μm.

B) Stitched confocal immunofluorescence images of a gut expressing GFP (green) under control of Mi{Trojan-GAL4.0}ChAT[MI04508-TG4.0] CG7715[MI04508-TG4.0-X], stained with anti-cut antibody (white). Yellow arrows indicate GFP-positive cells. Enlarged insert shows GFP-positive cells adjacent to the gastric region labeled with cut (pink arrows). DNA (blue) is labeled with Hoechst. n=5 guts. N=3. Scale bar 50μm.

B') Confocal image of a gut expressing GFP (green) under control of Mi{Trojan-GAL4.0}ChAT[MI04508-TG4.0] CG7715[MI04508-TG4.0-X], stained with Phalloidin (red). Transverse section of the epithelium is shown revealing inter-epithelial axons from ChAT+ neurons. White arrowheads highlight axonal boutons. n=5 guts. N=3

C) Fluorescent immunohistochemistry image of posterior midgut expressing GFP (green) under the control of Mi{Trojan-GAL4.0}ChAT[MI04508-TG4.0] CG7715[MI04508-TG4.0-X], stained with anti-prospero antibody (white). Arrows indicate GFP-positive cells that also label for pros. DNA (blue) is labeled with Hoechst. n=8 guts. N=3. Scale bar 10μm.

D) Confocal immunofluorescence image of ChAT antibody staining of the posterior midgut. EEs are expressing GFP (green) driven by pros-Gal4, yellow arrows indicate the overlap between ChAT staining (white) and pros-positive cells. DNA (blue) is labeled with Hoechst. n=8 guts. N=3. Scale bar 10μm.

E) Barrier dysfunction assay after mCherry (control) or ChAT knockdown in EEs for 3 days with prospero-Gal4. n=100 animals per genotype and condition; N=3. Two-way RM ANOVA.

F) Barrier dysfunction assay after mCherry (control) or ChAT knockdown with Mi{Trojan-GAL4.0}ChAT[MI04508-TG4.0] CG7715[MI04508-TG4.0-X] for 3 days. n=120 animals per genotype and condition; N=3. Two-way RM ANOVA.

Data presented as mean ± SEM. ns, not significant, P > 0.05; *P ≤ 0.05; **P ≤ 0.01; ***P ≤ 0.001; ****P ≤ 0.0001. n: number of animals or midguts analyzed; N: number of independent experiments performed with similar results and a similar n.

Figure 3 – figure supplement 1

A) Stitched confocal immunofluorescence overview as well as detail images of guts expressing GFP (green) under control of TI{2A-GAL4}ChAT[2A-GAL4]. GFP expression is detected a subset of pros-positive cells (yellow arrowheads, pink arrowheads indicate GFP-negative EEs) in the anterior (R1-R2) and posterior midgut (R4-R5), as well as in enteric neurons innervating the cardia (yellow arrowheads). DNA (blue) is labeled with Hoechst. n=5 guts. N=3. Scale bar 100μm (stitched overview) and 25μm, respectively.

B) Confocal image of a gut expressing GFP (green) under control of Mi{Trojan-GAL4.0}ChAT[MI04508-TG4.0] CG7715[MI04508-TG4.0-X], stained with anti-ChAT antibody. Yellow arrowheads highlight GFP-positive cells positive for ChAT staining, while pink arrowheads highlight GFP-negative cells staining positive for ChAT antibody. DNA (blue) is labeled with Hoechst. n=5 guts. N=3. Scale bar 10μm.

C) Quantification of EE numbers after depletion of nAchR subunits in ECs with 5966-GS for 8 days. 2 independent pooled experiments are shown. n=20 guts for mCherry RNAi, n=18 for w^{1118}, n=14 for nAchR β1 RNAi, n=14 for nAchR α2 RNAi, n=20 for nAchR β3 RNAi, n=16 for nAchR α4 RNAi. One-way ANOVA followed by Dunnett's multiple comparisons test.

D) Confocal immunofluorescence images of guts expressing GFP (green) under control of pros-Gal4. Yellow arrowheads highlight enteric innervation in different parts of the organ. DNA (blue) is labeled with Hoechst. n=5 guts. N=3. Scale bar 100μm (stitched overview) and 25μm, respectively.

Data presented as mean ± SEM. ns, not significant, $P > 0.05$; *$P \leq 0.05$; **$P \leq 0.01$; ***$P \leq 0.001$; ****$P \leq 0.0001$. n: number of animals or midguts analyzed; N: number of independent experiments performed with similar results and a similar n.

Figure 3 – figure supplement 2

A) Identification of EE-specific drivers without neuronal expression: First, we compiled top EE markers from FlyCellAtlas (FCA) data ((Li et al., 2022), panel 1). We then compared their expression in EEs (Guo et al., 2019) and neurons (FCA body data set, panel 2) to identify candidate genes that had low neuronal, but high EE expression (panels 3,4,5) . Orcokinin-Gal4 was the only candidate gene with an available Gal4 line, however, while neuronal expression is low (panel 6, yellow arrowheads), the driver is not entirely EE specific, but also sporadically labels ECs (pink arrows). CG32547-Gal4, an EE-specific driver used by Guo, et al., 2019, also drives enteric neuronal expression of GFP (panel 6, yellow arrowheads). DNA (blue) is labeled with Hoechst. n=5 guts. N=3.Scale bars 25μm.

B) Drivers selected based on table from (Chen et al., 2016) and additional literature (Beebe et al., 2015) as well as low expression in the adult brain (adult brain scRNAseq data (Davie et al., 2018)), crossed to UAS-GFP. Dimm displays neuronal expression and is not EE specific, other drivers didn't yield any expression in the epithelium. DNA (blue) is labeled with Hoechst, EEs are labeled with prospero staining (white). n=5 guts. N=2. Scale bars 25μm.

Figure 3 – figure supplement 3

A) Split Gal4 approach to identify EE-specific drivers without neuronal expression: BL91402 is a EE reference stock expressing EGFP used by (Holsopple et al., 2022) that expresses the p65 activation domain (AD) in EEs under control of sequences in/near Dh31. Crossed to its DBD counterpart, it labels pros-positive EEs with GFP (green), but also ECs (pink arrowheads) and

displays neuronal expression (yellow arrowheads). DNA (blue) is labeled with Hoechst, EEs are labeled with prospero staining (white). n=5 guts. N=2. Scale bars 25µm.

B) We used the collection of EE-specific DNA-binding domain (DBD) drivers (https://bdsc.indiana.edu/stocks/gal4/midgut_EEs.html) to identify two drivers that were expressed in all regions of the gut, but did not display expression in the proventriculus or brain. The first driver combination (BL91402xBL68537) showed clear neuronal GFP expression in the cardia (yellow arrowheads) and did not label all pros-positive EEs (pink arrowheads: pros+,GFP-, yellow arrowheads: pros+, GFP+). The second pair (BL91402xBL69158) had low neuronal expression, but labeled only a small subset of EEs (pink arrowheads: pros+,GFP-, yellow arrowheads: pros+, GFP+, yellow arrowheads in stitched overview image). DNA (blue) is labeled with Hoechst, EEs are labeled with prospero staining (white). n=5 guts. N=2.Scale bars 25µm and 100µm, respectively (stiched image).

C) EE reference driver crossed to a ChAT-Gal4 (DBD) stock, which resulted in the absence of GFP expression in the gut epithelium. DNA (blue) is labeled with Hoechst, EEs are labeled with prospero staining (white). n=5 guts. N=2. Scale bar 100µm.

Figure 4: Transcriptional changes after disruption of Ach signaling in the intestinal epithelium

A) PCA plot of samples after 3 days of nAchR subunit depletion by RNAi in enterocytes with $NP1^{ts}$. n=4 samples. N=1.

B) Volcano plot showing significantly differentially regulated genes after short-term nAchR β1 or β3 knockdown in enterocytes. (FDR<= 0.1; log2(fold change) < -1 or > 1; 100% of samples have >= 1 reads)

C) Gene set enrichment analysis of significantly downregulated genes after nAchR β1 and β3 knockdown in ECs. Genes included in data set associated with chitinase activity, chitin binding and chitin metabolic processes are listed to the right.

D) Top 10 most down- or upregulated genes after 3 days of nAchR subunit depletion by RNAi in enterocytes with $NP1^{ts}$.

E) PCA analysis after 3 days of ChAT depletion with RNAi in EEs under control of $pros^{ts}$. n=4 samples. N=1.

F) Volcano plot of significantly differently regulated genes after 3 days of ChAT knockdown in EEs. (FDR<= 0.1; log2(fold change) < -1 or > 1; 100% of samples have >= 1 reads)

G) Gene set enrichment analysis of significantly downregulated genes after ChAT depletion in EEs. Chitin-related terms show a trend towards enrichment. Genes associated with chitin-related terms are listed to the right.

H) Top 10 most down- or upregulated genes after 3 days of ChAT knockdown by RNAi in EEs with $pros^{ts}$.

I) overlap between differentially regulated genes after 3 days knockdown of ChAT in EEs or nAchR β1 and β3 in ECs.

n: number of samples included; N: number of independent experiments performed with similar results and a similar n.

Figure 4 – figure supplement 1

A) Overlap between differentially regulated genes after 3 days of nAchR β1 or β3 depletion in enterocytes with NP1^{ts}.

B) RT-qPCR analysis of Syt4 expression after nAchR β1 or β3 depletion in enterocytes with NP1^{ts}, normalized to GAPDH levels. n=25 pooled guts per genotype and experiment, N=3.

C) GO term enrichment of significantly upregulated genes after 3 days of nAchR β1 and β3 knockdown with NP1^{ts}.

D) Transcript levels of lysozyme family members in bulk RNAseq data set after 3 days of mCherry (control) or nAchR β1 and β3 subunit depletion in ECs.

E) Gene set enrichment analysis of significantly upregulated genes after ChAT depletion in EEs. Genes included in data set associated with chitin are listed to the right.

F) Heatmap of the top 20 upregulated differentially expressed genes after nAchR β1 and β3 knockdown in ECs for 3 days. (FDR<= 0.1; log2(fold change) > 2.5; 100% of samples have >= 1 reads))

G) Heatmap of top 20 upregulated differentially expressed genes after 3 days of ChAT depletion with RNAi in EEs under control of pros^{ts}. (FDR<= 0.1; log2(fold change) > 1.97; 100% of samples have >= 1 reads)

Data presented as mean ± SEM. ns, not significant, P > 0.05; *P ≤ 0.05; **P ≤ 0.01; ***P ≤ 0.001; ****P ≤ 0.0001. n: number of samples analyzed; N: number of independent experiments performed with similar results and a similar n.

Figure 4 – figure supplement 2

A) UMAP plots showing log-normalized expression of indicated genes using scRNAseq data from the Aging Fly Cell Atlas (Lu et al., 2023).

B) Violin plots of indicated genes showing log-normalized gene expression in intestinal epithelial cell types based on Aging Fly Cell Atlas data (Lu et al., 2023).

Figure 5: nAchR depletion disturbs PM integrity, causes dysbiosis and inflammation

A) Survival of animals depleted for mCherry (control) or nAchR β1, β3 or α4 for 3 days with NP1^{ts} before *Pseudomonas entomophila* infection. n=150 animals per genotype and condition; N=3. Log Rank (Mantel-Cox) test.

B) Confocal immunofluorescence image of posterior midguts depleted for either mCherry (control) or nAchR α4 for 8 days with NP1^{ts}. Animals are expressing a GFP-brush border marker (green) and were fed red fluorescent beads to assess peritrophic matrix (PM) integrity (beads appear yellow/orange due to autofluorescence of beads in GFP channel). PM is labeled with

WGA (white), DNA (blue) is labeled with Hoechst. Pink arrowheads highlight beads no longer contained by the PM sleeve. n=15 guts per genotype. N=3. Scale bar 20μm.

C) Electron microscopy images and quantification of thin PM layer integrity. Thick (yellow arrows) and thin (pink arrows) PM layers are indicated. Asterisks highlight gaps in the thin layer after nAchR β1 depletion. n=16; 18 midguts. N=1. Fisher's exact test.

D) Colony forming units (CFU) of whole guts plated on selective growth media after 8 days of nAchR subunit depletion with 5966-GS. 3 pooled independent experiments are shown. n=5 pooled animals per genotype and experiment. Two-way ANOVA.

E) Gut compartmentalization and acidity after mCherry (control) or nAchR β1, β3 or α4 depletion for 8 days with $NP1^{ts}$. Healthy flies fed with Bromphenol blue pH indicator display an acidic patch (yellow), while loss of gut compartmentalization leads to all blue or white guts. n=87 guts for mCherry RNAi (control), n=93 guts for nAchR β1 RNAi, n=113 guts for nAchR α4 RNAi, n=87 guts for nAchR β3 RNAi and n=90 guts for nAchR α2 RNAi. 4 independent pooled experiments are shown. Chi square test.

F) Survival after 3 days of mCherry (ctrl) or ChAT depletion in EEs followed by *Pseudomonas entomophila* infection. n=80 animals per genotype and condition; N=3. Log Rank (Mantel-Cox) test.

G) Colony forming units (CFU) of whole guts plated on selective growth media after 8 days of ChAT depletion in EEs. 3 pooled independent experiments are shown. n=5 pooled animals per genotype and experiment. Two-way ANOVA.

Data presented as mean ± SEM. ns, not significant, $P > 0.05$; *$P \leq 0.05$; **$P \leq 0.01$; ***$P \leq 0.001$; ****$P \leq 0.0001$. n: number of animals or midguts analyzed; N: number of independent experiments performed with similar results and a similar n.

Figure 5 – figure supplement 1

A) Transcript levels of CG32302, a putative PM component, in bulk RNAseq data set after 3 days of mCherry (control) or nAchR subunit depletion in ECs.

B) RT-qPCR of ChAT, Ace (acetylcholine esterase) and nAchR subunits using 5-day old female wildtype flies after 16h of PE infection. Multiple unpaired two-tailed t-tests followed by multiple comparision correction with Holm- Šídák's method. Separate graph for Ace for better visibility. Unpaired two-tailed t-test. n=25 pooled guts per condition, N=3 (nAchR α1 and nAchR α2), N=5 for all remaining genes.

C) Number of GFP+ cells in guts challenged with PE expressing UAS-GFP under control of Mi{Trojan-GAL4.0}ChAT[MI04508-TG4.0] CG7715[MI04508-TG4.0-X] for 3 days before infection. 3 pooled independent experiments are shown. n=7 animals per condition; N=3. Unpaired two-tailed T-test.

D) Confocal immunofluorescence image of posterior midguts depleted for either mCherry (control), nAchR β1 or β3 for 8 days with $NP1^{ts}$. Animals were fed green fluorescent beads to assess Peritrophic matrix (PM) integrity. DNA (blue) is labeled with Hoechst. n=10 guts. N=3. Scale bar 25μm.

E) Overview of PM layers in posterior midgut (R4) of control animals. (1) The PM lies as an intact ring (black arrowheads) loosely in the gut lumen surrounded by an additional thin layer ring (small arrows). The PM encloses food remnants and short segments of material with a similar ultrastructure as the PM (blue arrows). (2) Detail of the PM layers: Thick layer (black arrowheads) and thin layer ring (small arrows) on top of microvilli of the enterocytes. Septate

junctions (SJ) seal the intercellular spaces between the enterocytes at their apical edges. (3) Detail of the PM ultrastructure. The luminal surface (white arrowhead) is lined by an electron-dense layer of constant thickness. The abluminal surface is less electron-dense and slightly rough (black arrowheads). (4) Detail of the thin layer ring (black arrows)

L, gut lumen. EC, enterocyte. MV, microvilli. N, nucleus. Scale bars: 10 µm (1), 1 µm (2), 200 nm (3), 500 nm (4).

F) Example image of damaged thick PM layer, yellow arrowheads highlight PM fragments in the gut lumen. Quantification of thick PM layer integrity after 8 days of mCherry (control) or nAchR β1 knockdown in ECs. n=16; 18 midguts for mCherry or nAchR β1, respecitvely. N=1. Fisher's exact test.

G) Survival after 3 days of GFP or ChAT overexpression in EEs followed by *Pseudomonas entomophila* infection. n=80 animals for UAS-GFP on sucrose or sucrose+PE; n=40 animals for UAS-ChAT on sucrose or sucrose+PE; N=3. Log Rank (Mantel-Cox) test.

Data presented as mean ± SEM. ns, not significant, P > 0.05; *P ≤ 0.05; **P ≤ 0.01; ***P ≤ 0.001; ****P ≤ 0.0001. n: number of animals or midguts analyzed; N: number of independent experiments performed with similar results and a similar n.

Figure 6: Syt4 knockdown affects PM integrity and phenocopies nAchR depletion

A) Survival after one day of mCherry (ctrl) or Syt4 depletion in ECs followed by *Pseudomonas entomophila* infection. n=175 animals per genotype and condition; N=3. Log Rank (Mantel-Cox) test.

B) Confocal immunofluorescence image of posterior midguts depleted for either mCherry (control) or Syt4 for 8 days. Animals are expressing a GFP-brush border marker (green) and were fed red fluorescent beads to assess peritrophic matrix (PM) integrity (beads appear yellow/orange due to autofluorescence of beads in GFP channel). PM is labeled with WGA (white), DNA (blue) is labeled with Hoechst. Yellow arrowheads indicate beads that leaked out of the PM sleeve. n=10 guts per genotype. N=3. Scale bar 25µm.

C) Survival of w1118 (control), $Syt4^{\Delta}$ CRISPR null mutant flies or $Syt4^{\Delta}$ flies crossed to a deficiency (BL24927) after *Pseudomonas entomophila* infection. n=75 animals per genotype and condition; N=3. Log Rank (Mantel-Cox) test.

D) Confocal immunofluorescence image of posterior midguts of w1118 (control) or $Syt4^{\Delta}$ animals fed with red fluorescent beads to monitor PM integrity. PM is stained with WGA (white), DNA (blue) is labeled with Hoechst in bottom panels. Yellow insets are shown enlarged in bottom row. Yellow arrowheads indicate the presence (w1118) or absence of a clear PM boundary. Cyan arrowheads indicate accumulation of WGA signal within the epithelium. n=10 guts per genotype. N=3. Scale bar 25µm.

E) Survival after overexpression of LacZ-RNAi (control) or LacZ-RNAi together with UAS-FLAG-mCherry-Syt4 for one day before *Pseudomonas entomophila* infection. n=100 animals per genotype and condition; N=3. Log Rank (Mantel-Cox) test.

F) Confocal immunofluorescence image of posterior midguts overexpressing UAS-FLAG-mCherry-Syt4 (red) in enterocytes stained with WGA (white). DNA (blue) is labeled with Hoechst in bottom panels. Yellow arrowheads indicate overlap between Syt4-positive vesicles and WGA staining. n=8 guts. N=3. Scale bar 25μm.

G) Immunogold electron microscopy image of posterior midgut of an Oregon R wildtype animal or an animal overexpressing UAS-FLAG-mCherry-Syt4 in enterocytes with NP1ts. WGA-biotin (10nm gold particles) is detected in multilamellar bodies carrying membranous and amorphous material. Syt4 (stained with anti-mCherry antibody, 15nm gold particles) colocalizes with these structures in animals expressing the UAS-FLAG-mCherry-Syt4, while Oregon R samples are devoid of anti-mCherry antibody labeling. n= 5. N=1. Scale bar 200nm.

H) Model: Neuronal or EE-derived Ach maintains barrier function through Syt4-mediated secretion of PM components such as chitin from ECs. Disrupted Ach signaling leads to barrier dysfunction, peritrophic matrix defects, dysbiosis, as well as loss of gut compartmentalization and inflammation.

Ach, Acetylcholine; nAchR, nicotinic acetylcholine receptor; EC, enterocyte; EE, enteroendocrine cell; Syt4, Synaptotagmin 4

Data presented as mean ± SEM. ns, not significant, $P > 0.05$; *$P \leq 0.05$; **$P \leq 0.01$; ***$P \leq 0.001$; ****$P \leq 0.0001$. n: number of animals or midguts analyzed; N: number of independent experiments performed with similar results and a similar n.

Figure 6 – figure supplement 1

A) Survival after one day of mCherry (ctrl) or Syt4 depletion in ECs followed by *Pseudomonas entomophila* infection. n=175 animals per genotype and condition; N=3. Log Rank (Mantel-Cox) test.

B) CFU of whole guts plated on selective growth media after 8 days of Syt4 depletion in ECs. 2 pooled independent experiments are shown. n=5 pooled animals per genotype and experiment. Two-way ANOVA.

C) Analysis of gut compartmentalization visualized by feeding Bromophenol blue pH indicator (see Fig 5E) after 8 days of Syt4 knockdown in ECs. n=51 guts for mCherry (control), n=43 guts for Syt4 RNAi. 3 independent pooled experiments are shown. Chi square test.

D) Confocal immunofluorescence images of posterior midguts depleted of either mCherry (control) or Syt4 in enterocytes for 8 days, stained with anti-cut antibody (white). Guts are expressing a GFP-brush border marker (green). DNA (blue) is labeled with Hoechst. Yellow arrowheads in side view panels highlight healthy, pocket-like (mCherry) and disrupted gastric units (Syt4-RNAi). n=10 guts. N=3. Scale bar 25μm.

E) Survival after 24h of combined knockdown of Syt4 and nAchR α2 before Pseudomonas entomophila infection. n=75 animals per genotype and condition for both assays; N=3. Log Rank test (Mantel-Cox).

F) Barrier dysfunction assay after *Pseudomonas entomophila* infection of w1118 (control), $Syt4^{\Delta}$ CRISPR null mutant flies or $Syt4^{\Delta}$ flies crossed to a deficiency (BL24927). n=100 animals per genotype and condition; N=2. Two-way RM ANOVA. Both types of Syt4-deficient animals display enhanced barrier dysfunction compared to the control, while not being significantly different from each other (see indicated comparisons).

G) Barrier dysfunction assay after Paraquat challenge of w1118 (control), Syt4$^{\Delta}$ CRISPR null mutant flies or Syt4$^{\Delta}$ flies crossed to a deficiency (BL24927). Paraquat concentration 17.5mM. n=100 animals per genotype and condition; N=3. Two-way RM ANOVA.

H) Barrier dysfunction assay with Paraquat displaying percentage of smurfs at experimental endpoint (8 days chase). 4 individual experiments are shown. n=75 animals per genotype and condition (experiments 1-3), n=50 animals per genotype and condition (experiment 4). Unpaired two-tailed t-test for each experiment.

I,I',I'') Survival after PE infection upon concomitant overexpression of 3xFLAG-mCherry-Syt4 and nAchR knockdown. n=150 animals per genotype and condition, N=1. Log Rank test (Mantel-Cox).

J) Confocal immunofluorescence image of posterior midguts overexpressing UAS-FLAG-mCherry-Syt4 (red) in enterocytes stained with anti-Golgin84 antibody or Lysotracker (white). DNA (blue) is labeled with Hoechst. Yellow arrowheads indicate overlap between Syt4-positive vesicles and Golgin84 or Lysotracker staining. n=10 guts. N=3. Scale bar 5μm.

K) Immunogold electron microscopy image of Syt4 and Lamp1 co-staining in enterocytes of posterior midguts of either wildtype Oregon R flies or animals expressing UAS-FLAG-mCherry-Syt4 under control of NP1^{ts}. Syt4 (detected with mCherry antibody 10nm gold particles) and Lamp1 (15nm gold particles) are colocalizing on multilamellar bodies in animals expressing the Syt4 construct. Oregon R samples are devoid of anti-mCherry antibody staining. n=5 guts. N=1. Scale bar 200nm.

Data presented as mean ± SEM. ns, not significant, $P > 0.05$; *$P \leq 0.05$; **$P \leq 0.01$; ***$P \leq 0.001$; ****$P \leq 0.0001$. n: number of animals or midguts analyzed; N: number of independent experiments performed with similar results and a similar n.

Supplementary File 1

List of candidate genes for genetic variants (human) associated with COPD (Hobbs, de Jong, Lamontagne, Bosse, et al., 2017). Genes highlighted in blue had a clear *Drosophila* ortholog and were included in the screen.

Abbreviations used: SNP, Single nucleotide polymorphism; CHR, chromosome; BP, base pair (GRCh37); eqtl, expression quantitative trait loci; Risk allele, allele associated with increased COPD risk; Alt allele, alternative allele; OR stage1, Odds-ratio of risk allele in stage 1 of P.stage1, P-value in stage 1 of Hobbs et al; P.meta, meta-analysis P-value in Hobbs et al; Evidence.Sakornsakolpat, evidence (if available) from (Sakornsakolpat, Prokopenko, Lamontagne, Reeve, Guyatt, Jackson, Shrine, Qiao, Bartz, Kim, Lee, Latourelle, Li, Morrow, Obeidat, Wyss, Bakke, Barr, Beaty, Belinsky, Brusselle, Crapo, de Jong, DeMeo, Fingerlin, Gharib, Gulsvik, Hall, Hokanson, Kim, Lomas, London, Meyers, O'Connor, Rennard, Schwartz, Sliwinski, Sparrow, Strachan, Tal-Singer, Tesfaigzi, Vestbo, Vonk, Yim, Zhou, Bosse, et al., 2019) (GREx-genetically regulated expression, mQTL-methylation quantitative trait loci, Cod-coding association, Hi-C-chromatin interaction in human lung or IMR90 cell line, DHS-DNase hypersensitivity sites, GSet-genes identified by DEPICT, further details are available in the original publication); colocalization, probability shared causal variant between eQTL (GTEx) and COPD risk association (tissue: probability), only colocalization probability > 0.6 are listed.

Supplementary File 2

List of *Drosophila* genes and RNAi lines included in the screen. RNAi lines were ranked according to the natural logarithm of the ratio between the proportion of smurfs after candidate gene knockdown and luciferase RNAi control. Cutoff scale shown in Fig 1C was used to determine the effect of each RNAi. Based on this fine-grained ranking of individual RNAi lines, an overall rating was assigned to each gene and compared to human eqtl data (see also Fig 1A). Temperature column refers to the temperature the subsets of RNAi lines were screened at.

A

COPD GWAS hits and *Drosophila* candidate orthologues

SNP	CHR	BP	gene	evidence	*Drosophila* ortholog	*Drosophila* rating	eqtl direction risk allele	agreement
rs10429950	1	218624533	TGFB2	nearest	myo, daw	no effect	not available	N/A
rs6837671	4	89873092	FAM13A	nearest	CG6424	suppressor	not available	N/A
rs2806356	6	109266255	ARMC2	nearest	CG32668	no effect	not available	N/A
rs754388	14	93115410	RIN3	coding,eqtl	spri	no effect	higher expression	N/A
rs1441358	15	71612514	THSD4	eqtl	loh	no effect	higher expression	N/A
rs12459249	19	41339896	CYP2A6	nearest	Cyp18a1, Cyp305a1	enhancer	not available	N/A
rs2955083	3	127961178	EEFSEC	eqtl	eEFSec	suppressor	higher expression	Yes
rs2955083	3	127961178	RUVBL1	eqtl	pont	no effect	lower expression	N/A
rs11727735	4	106631870	GSTCD	eqtl	CG10428	enhancer	lower expression	Yes
rs11727735	4	106631870	INTS12	eqtl	IntS12	no effect	higher expression	N/A
rs113897301	5	156929077	ADAM19	eqtl	Meltrin	enhancer	higher expression	No
rs113897301	5	156929077	NIPAL4	eqtl	spict	no effect	higher expression	N/A
rs2076295	6	7563232	DSP	eqtl	shot	suppressor	higher expression	Yes
rs721917	10	81706324	SFTPD	coding,eqtl	lectin-28C	no effect	higher expression	N/A
rs17486278	15	78867482	CHRNA3	eqtl	nAChRβ2, nAChRα4	enhancer	lower expression	Yes
rs17486278	15	78867482	CHRNA5	coding,eqtl	nAChRα1, nAChRα2, nAChRα3	enhancer	inconsistent	N/A
rs17486278	15	78867482	PSMA4	eqtl	Prosα3	no effect	higher expression	N/A
rs17707300	16	28593347	APOBR	coding	Muc11a	enhancer	not available	N/A
rs17707300	16	28593347	EIF3C	eqtl	eIF3c	enhancer	higher expression	No
rs17707300	16	28593347	EIF3CL	eqtl	eIF3c	enhancer	higher expression	No
rs17707300	16	28593347	NFATC2IP	eqtl	Rad60	enhancer	higher expression	No
rs17707300	16	28593347	NUPR1	eqtl	CG6770	enhancer	lower expression	Yes
rs17707300	16	28593347	SH2B1	eqtl	Lnk	enhancer	lower expression	Yes
rs17707300	16	28593347	SPNS1	eqtl	spin	suppressor	higher expression	Yes
rs17707300	16	28593347	SULT1A1	coding,eqtl	St1	enhancer	lower expression	Yes
rs17707300	16	28593347	SULT1A2	coding,eqtl	St1	enhancer	higher expression	No
rs17707300	16	28593347	TUFM	eqtl	mEFTu1	enhancer	higher expression	No
rs7186831	16	75473155	BCAR1	eqtl	p130CAS	no effect	inconsistent	N/A
rs7186831	16	75473155	CFDP1	eqtl	Yeti	no effect	lower expression	N/A
rs7186831	16	75473155	TMEM170A	eqtl	CG12341	enhancer	higher expression	No

B

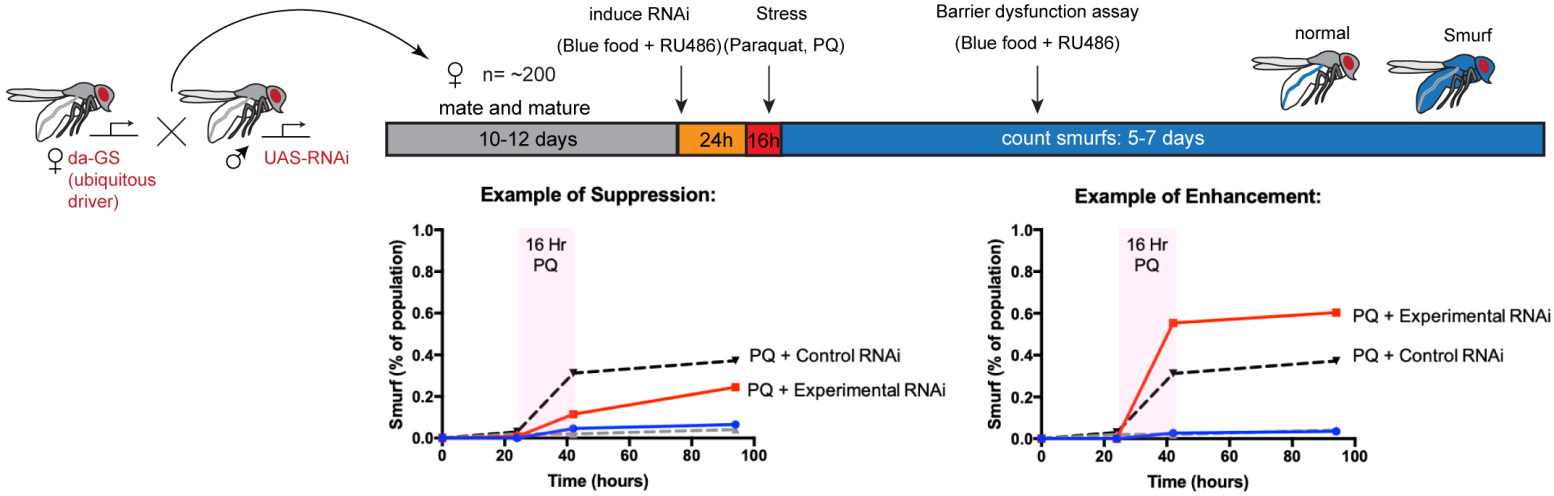

C

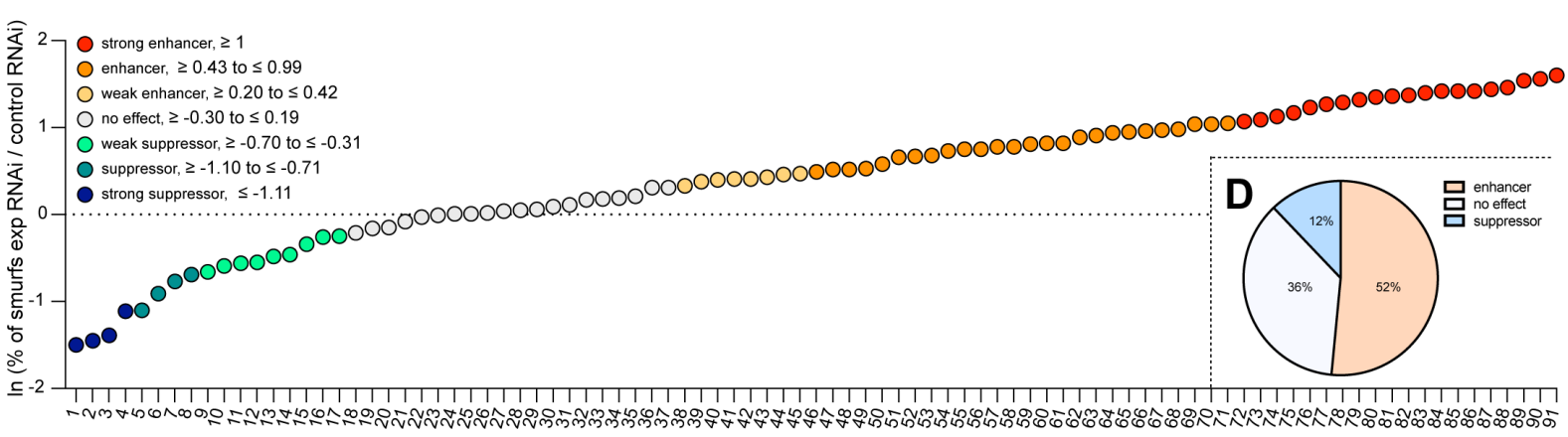

D

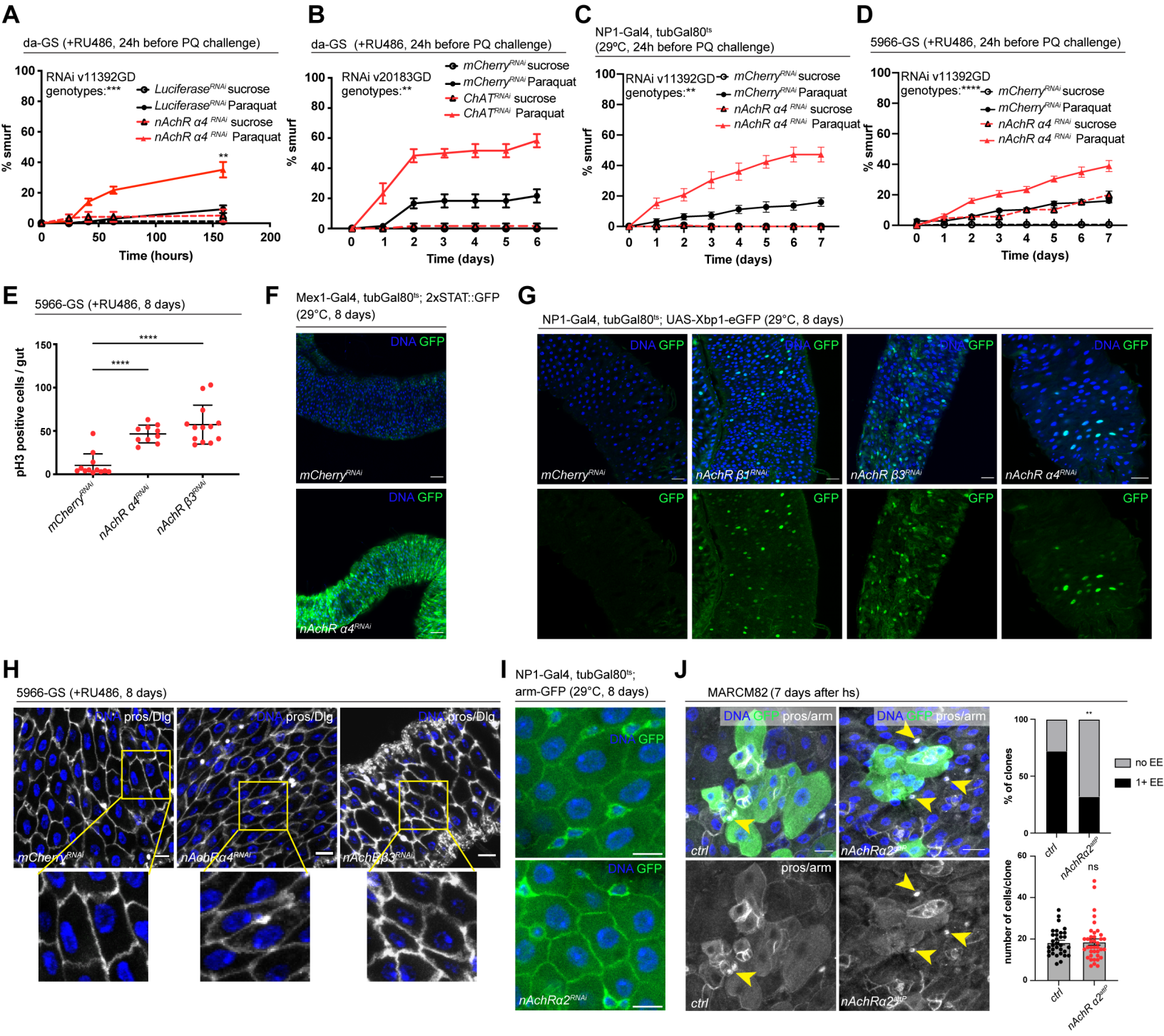
A
da-GS (+RU486, 24h before PQ challenge)
RNAi v11392GD
genotypes:***
Luciferase RNAi sucrose
Luciferase RNAi Paraquat
nAchR α4 RNAi sucrose
nAchR α4 RNAi Paraquat
% smurf
Time (hours)
B
da-GS (+RU486, 24h before PQ challenge)
RNAi v20183GD
genotypes:**
mCherry RNAi sucrose
mCherry RNAi Paraquat
ChAT RNAi sucrose
ChAT RNAi Paraquat
Time (days)
C
NP1-Gal4, tubGal80ts
(29ºC, 24h before PQ challenge)
RNAi v11392GD
genotypes:**
nAchR α4 RNAi sucrose
nAchR α4 RNAi Paraquat
D
5966-GS (+RU486, 24h before PQ challenge)
RNAi v11392GD
genotypes:****
E
5966-GS (+RU486, 8 days)
pH3 positive cells / gut
mCherry RNAi
nAchR α4 RNAi
nAchR β3 RNAi
F
Mex1-Gal4, tubGal80ts; 2xSTAT::GFP
(29°C, 8 days)
DNA GFP
G
NP1-Gal4, tubGal80ts; UAS-Xbp1-eGFP (29°C, 8 days)
nAchR β1 RNAi
nAchR β3 RNAi
H
5966-GS (+RU486, 8 days)
DNA pros/Dlg
I
NP1-Gal4, tubGal80ts;
arm-GFP (29°C, 8 days)
nAchRα2 RNAi
J
MARCM82 (7 days after hs)
DNA GFP pros/arm
ctrl
nAchRα2 3HP
pros/arm
% of clones
no EE
1+ EE
number of cells/clone
ns

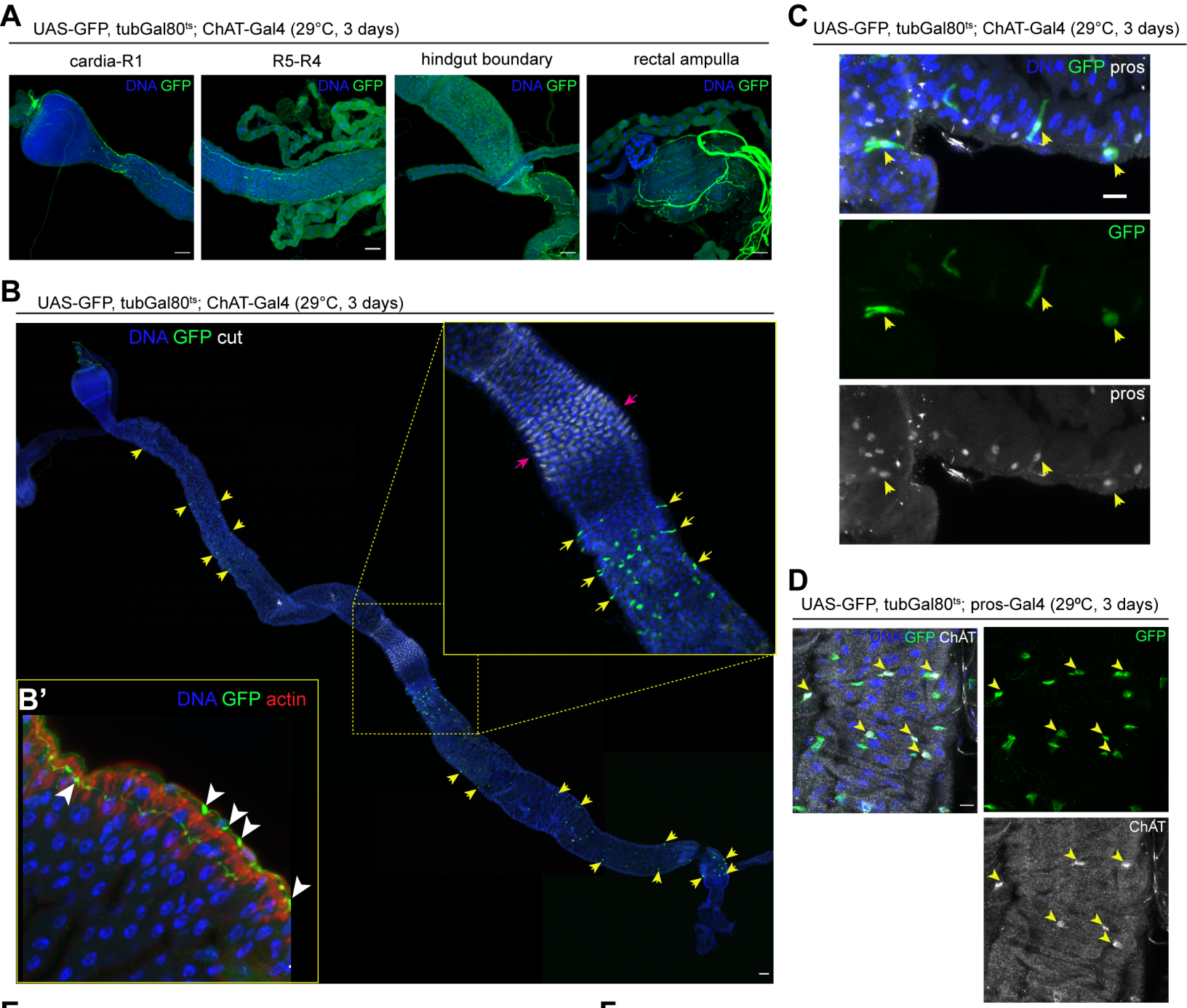
A
UAS-GFP, tubGal80ts; ChAT-Gal4 (29°C, 3 days)
cardia-R1
R5-R4
hindgut boundary
rectal ampulla
DNA GFP
B
UAS-GFP, tubGal80ts; ChAT-Gal4 (29°C, 3 days)
DNA GFP cut
B'
DNA GFP actin
C
UAS-GFP, tubGal80ts; ChAT-Gal4 (29°C, 3 days)
DNA GFP pros
GFP
pros
D
UAS-GFP, tubGal80ts; pros-Gal4 (29ºC, 3 days)
DNA GFP ChAT
GFP
ChAT

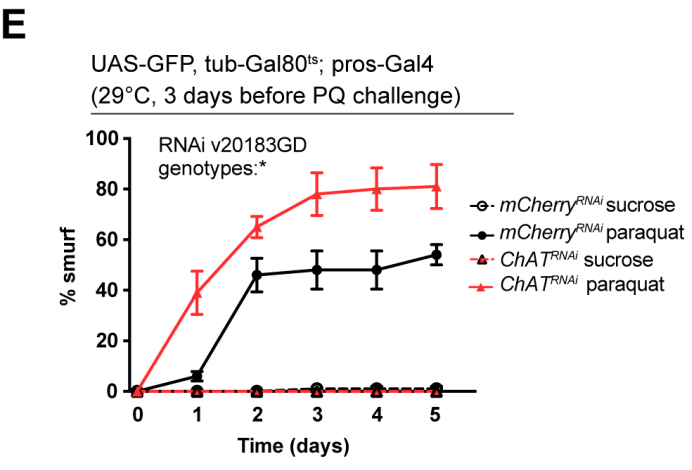
E
UAS-GFP, tub-Gal80ts; pros-Gal4
(29°C, 3 days before PQ challenge)
RNAi v20183GD
genotypes:*
% smurf
Time (days)
mCherryRNAi sucrose
mCherryRNAi paraquat
ChATRNAi sucrose
ChATRNAi paraquat

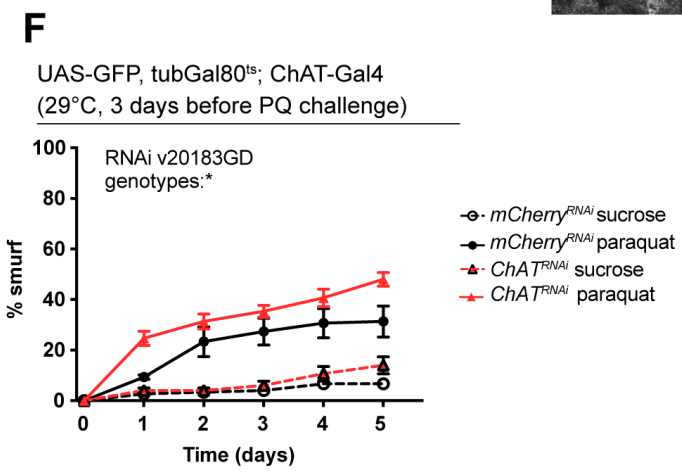
F
UAS-GFP, tubGal80ts; ChAT-Gal4
(29°C, 3 days before PQ challenge)
RNAi v20183GD
genotypes:*
% smurf
Time (days)
mCherryRNAi sucrose
mCherryRNAi paraquat
ChATRNAi sucrose
ChATRNAi paraquat

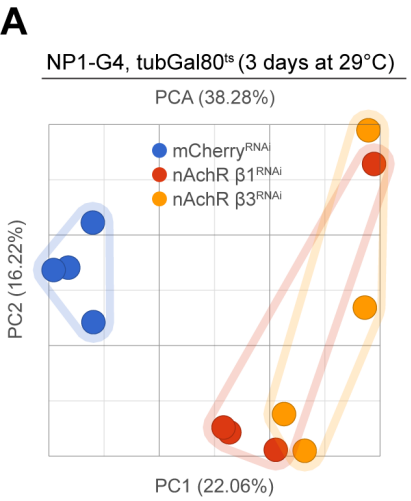

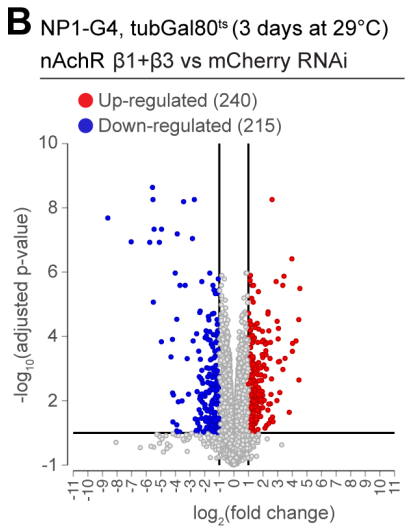

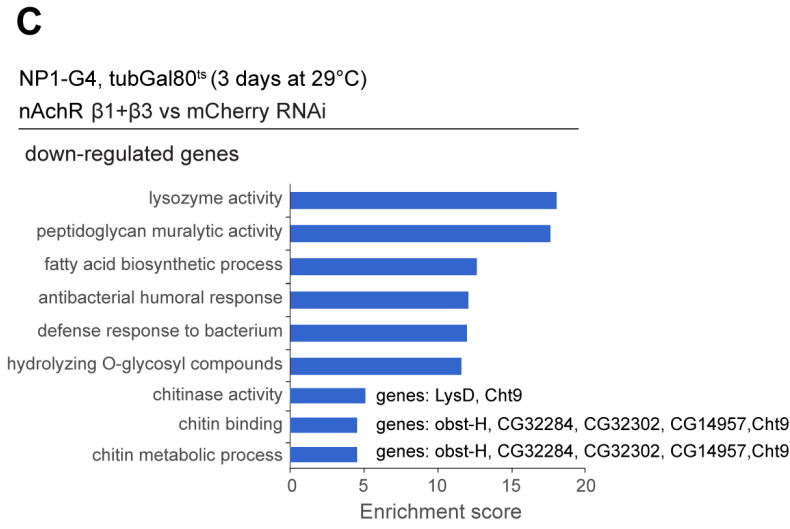

D

Top downregulated genes

Gene symbol	Flybase ID	P-value	FDR	log2(fold change)
Syt4	FBgn0028400	1.29E-11	2.07E-08	-8.63
CG32581	FBgn0052581	1.30E-10	1.14E-07	-7.03
LysD	FBgn0004427	1.48E-10	1.19E-07	-5.76
LysC	FBgn0004426	2.40E-13	2.32E-09	-5.57
CR44383	FBgn0265533	2.30E-12	5.54E-09	-5.54
CG17470	FBgn0032869	4.28E-08	8.59E-06	-5.51
CG9360	FBgn0030332	3.85E-11	4.64E-08	-5.47
LysB	FBgn0004425	1.60E-10	1.19E-07	-5.10
lectin-24A	FBgn0040104	3.54E-11	4.64E-08	-4.95
CG13813	FBgn0036956	1.42E-05	4.33E-04	-4.31

Top upregulated genes

Gene symbol	Flybase ID	P-value	FDR	log2(fold change)
CG3345	FBgn0031240	1.64E-04	2.26E-03	4.46
Ptth	FBgn0013323	2.60E-06	1.38E-04	4.26
CG11570	FBgn0036230	3.51E-06	1.64E-04	4.02
phr	FBgn0003082	5.61E-10	3.87E-07	3.97
CG15263	FBgn0028853	4.86E-03	2.29E-02	3.79
CR45822	FBgn0267472	2.92E-09	1.34E-06	3.43
CG31810	FBgn0051810	8.59E-09	2.58E-06	3.35
CR44628	FBgn0265839	6.46E-04	5.56E-03	3.15
mthl8	FBgn0052475	2.39E-05	5.98E-04	3.13
CG8358	FBgn0037727	6.18E-07	5.63E-05	3.05

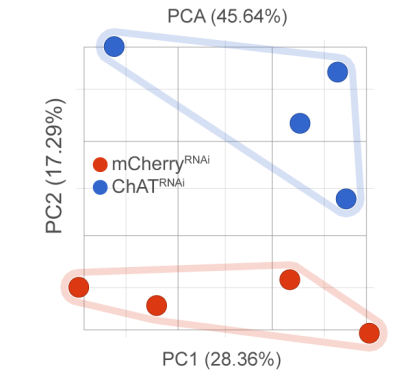

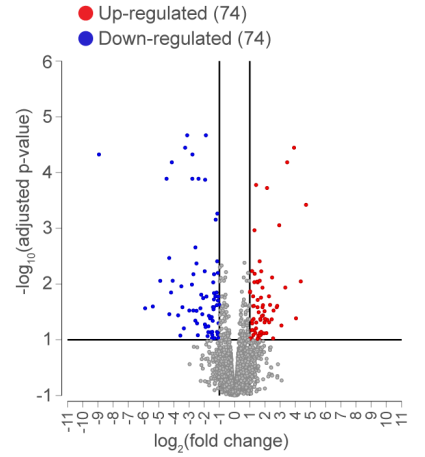

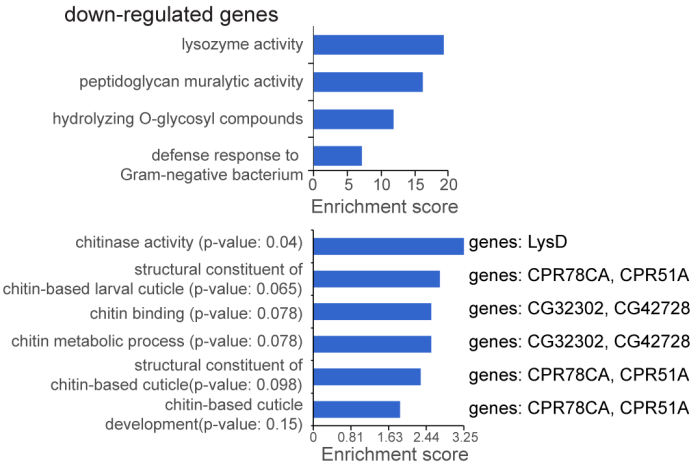

H

Top downregulated genes

Gene symbol	Flybase ID	P-value	FDR	log2(fold change)
Syt4	FBgn0028400	2.90E-08	4.73E-05	-8.93
CG17470	FBgn0032869	2.93E-04	2.73E-02	-5.89
CG32855	FBgn0052855	2.50E-04	2.53E-02	-5.38
CG9360	FBgn0030332	1.36E-07	1.29E-04	-4.48
Cyp4p2	FBgn0033395	8.83E-05	1.42E-02	-4.18
Dscam4	FBgn0263219	4.81E-08	6.54E-05	-4.13
LysC	FBgn0004426	4.91E-04	3.65E-02	-3.72
LysB	FBgn0004425	2.02E-03	8.42E-02	-3.57
CG32187	FBgn0052187	6.06E-05	1.10E-02	-3.51
LysS	FBgn0004430	2.74E-04	2.60E-02	-3.43

Top upregulated genes

Gene symbol	Flybase ID	P-value	FDR	log2(fold change)
Twdlalpha	FBgn0052574	5.80E-07	3.79E-04	4.71
CG32568	FBgn0052568	4.40E-05	8.98E-03	4.36
phr	FBgn0003082	1.13E-08	3.58E-05	3.92
CR45822	FBgn0267472	5.34E-08	6.54E-05	3.47
CR44430	FBgn0265612	6.48E-05	1.16E-02	3.34
Spn88Eb	FBgn0038299	9.97E-04	5.55E-02	3.09
CG9021	FBgn0031747	1.62E-06	8.82E-04	2.94
CG34291	FBgn0085320	2.34E-04	2.46E-02	2.81
CG11570	FBgn0036230	2.68E-04	2.60E-02	2.78
CG7017	FBgn0036951	2.47E-03	9.45E-02	2.54

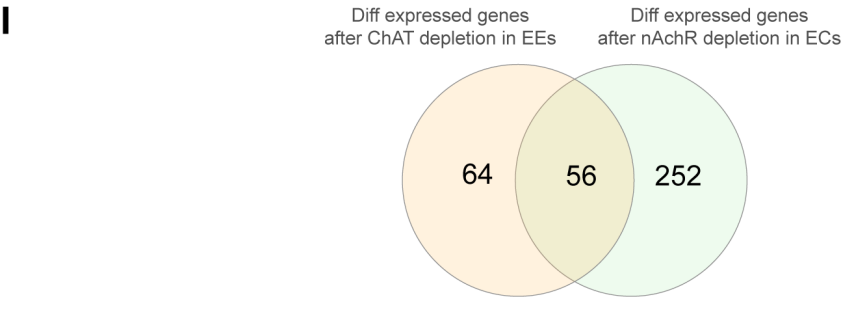

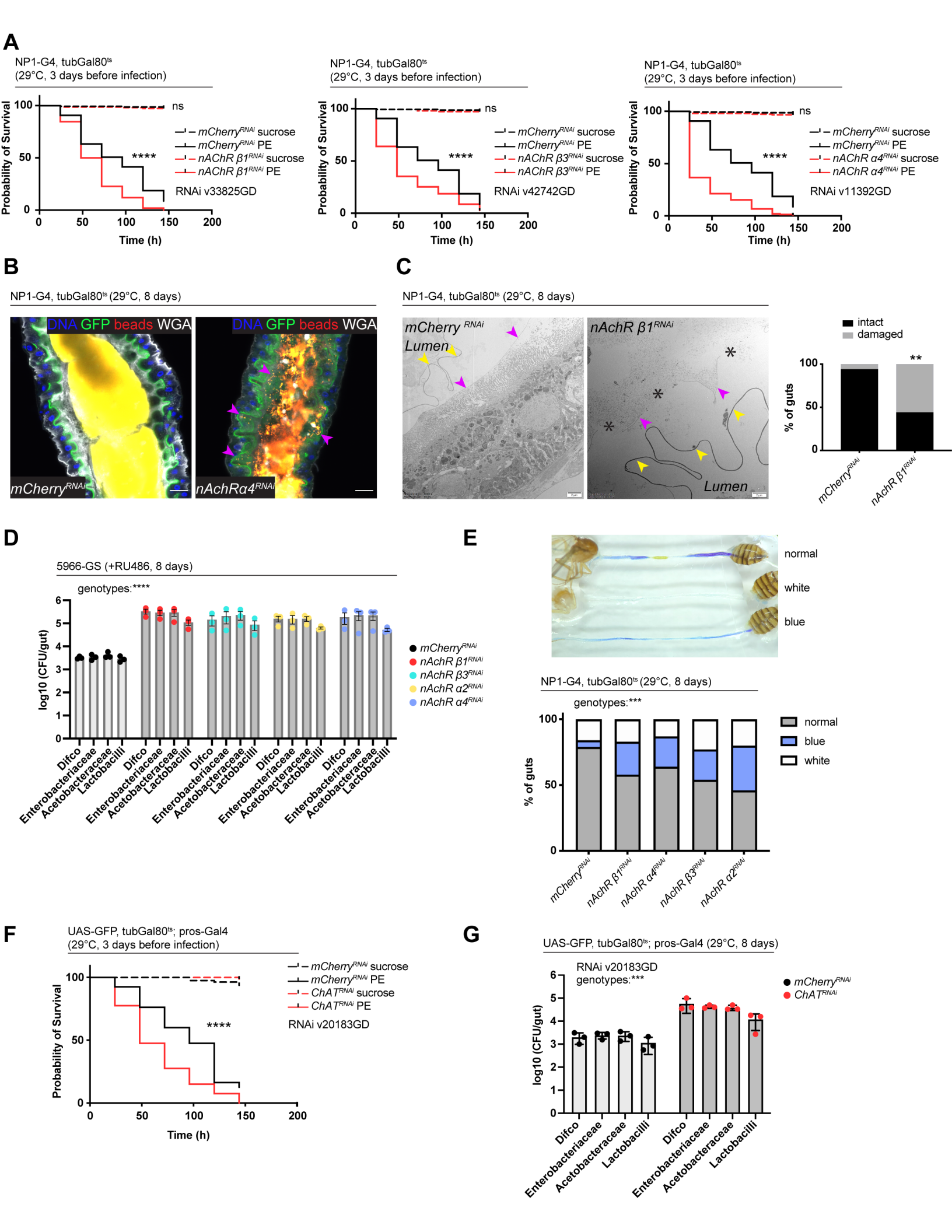
A
NP1-G4, tubGal80ts
(29°C, 3 days before infection)
Probability of Survival
Time (h)
ns
****
mCherryRNAi sucrose
mCherryRNAi PE
nAChR β1RNAi sucrose
nAChR β1RNAi PE
RNAi v33825GD
NP1-G4, tubGal80ts
(29°C, 3 days before infection)
nAChR β3RNAi sucrose
nAChR β3RNAi PE
RNAi v42742GD
NP1-G4, tubGal80ts
(29°C, 3 days before infection)
nAChR α4RNAi sucrose
nAChR α4RNAi PE
RNAi v11392GD
B
NP1-G4, tubGal80ts (29°C, 8 days)
DNA GFP beads WGA
mCherryRNAi
nAchRα4RNAi
C
NP1-G4, tubGal80ts (29°C, 8 days)
mCherry RNAi
Lumen
nAchR β1RNAi
Lumen
intact
damaged
% of guts
**
mCherryRNAi
nAchR β1RNAi
D
5966-GS (+RU486, 8 days)
genotypes:****
log10 (CFU/gut)
mCherryRNAi
nAchR β1RNAi
nAchR β3RNAi
nAchR α2RNAi
nAchR α4RNAi
Difco
Enterobacteriaceae
Acetobacteraceae
Lactobacilli
E
normal
white
blue
NP1-G4, tubGal80ts (29°C, 8 days)
genotypes:***
% of guts
normal
blue
white
mCherryRNAi
nAchR β1RNAi
nAchR α4RNAi
nAchR β3RNAi
nAchR α2RNAi
F
UAS-GFP, tubGal80ts; pros-Gal4
(29°C, 3 days before infection)
Probability of Survival
Time (h)
ns
****
mCherryRNAi sucrose
mCherryRNAi PE
ChATRNAi sucrose
ChATRNAi PE
RNAi v20183GD
G
UAS-GFP, tubGal80ts; pros-Gal4 (29°C, 8 days)
RNAi v20183GD
genotypes:***
log10 (CFU/gut)
mCherryRNAi
ChATRNAi
Difco
Enterobacteriaceae
Acetobacteraceae
Lactobacilli

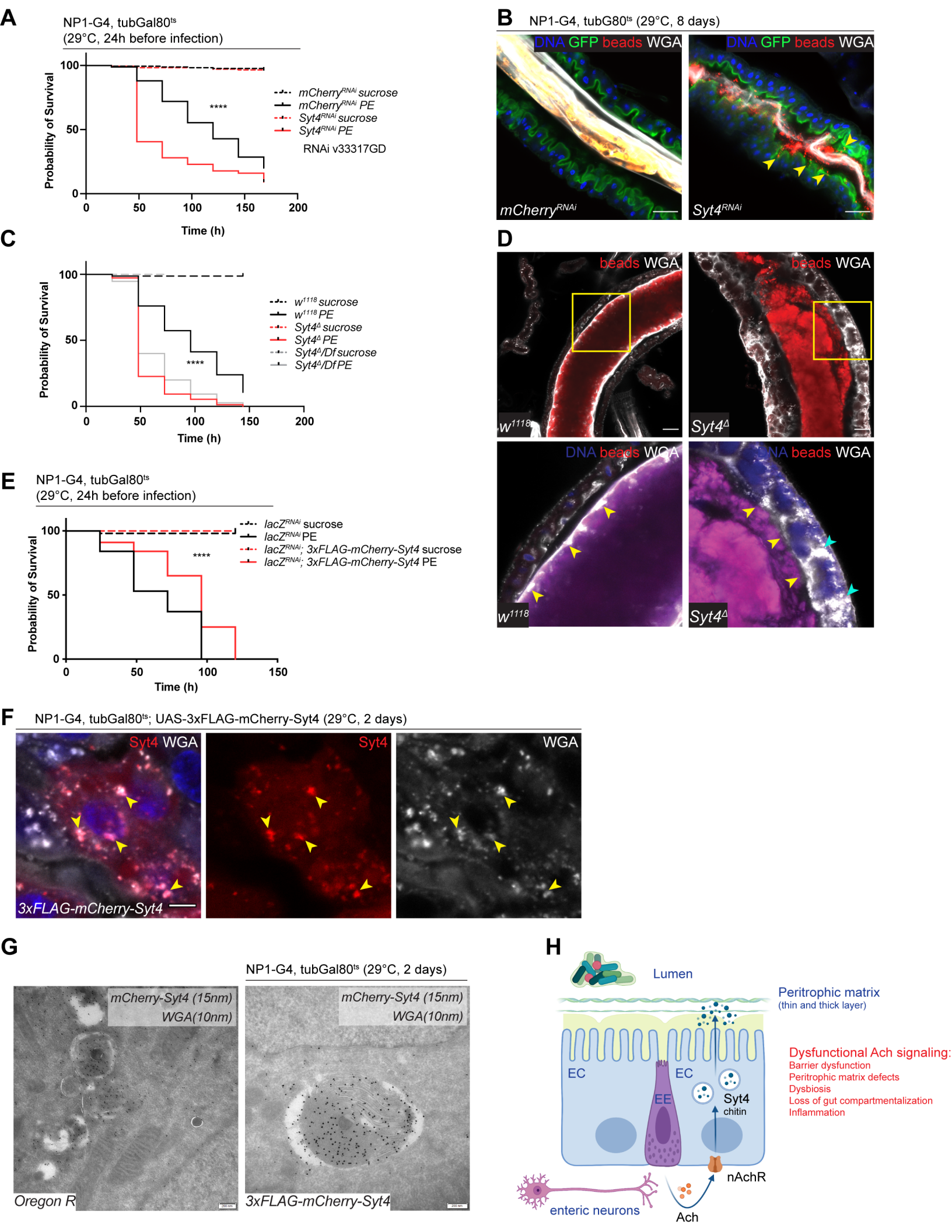
A
NP1-G4, tubGal80ts
(29°C, 24h before infection)
Probability of Survival
Time (h)
mCherryRNAi sucrose
mCherryRNAi PE
Syt4RNAi sucrose
Syt4RNAi PE
RNAi v33317GD
****
B
NP1-G4, tubG80ts (29°C, 8 days)
DNA GFP beads WGA
mCherryRNAi
Syt4RNAi
C
w1118 sucrose
w1118 PE
Syt4Δ sucrose
Syt4Δ PE
Syt4Δ/Df sucrose
Syt4Δ/Df PE
D
beads WGA
DNA beads WGA
w1118
Syt4Δ
E
NP1-G4, tubGal80ts
(29°C, 24h before infection)
lacZRNAi sucrose
lacZRNAi PE
lacZRNAi; 3xFLAG-mCherry-Syt4 sucrose
lacZRNAi; 3xFLAG-mCherry-Syt4 PE
F
NP1-G4, tubGal80ts; UAS-3xFLAG-mCherry-Syt4 (29°C, 2 days)
Syt4 WGA
Syt4
WGA
3xFLAG-mCherry-Syt4
G
NP1-G4, tubGal80ts (29°C, 2 days)
mCherry-Syt4 (15nm)
WGA(10nm)
Oregon R
3xFLAG-mCherry-Syt4
H
Lumen
Peritrophic matrix
(thin and thick layer)
EC
EE
Syt4
chitin
nAchR
enteric neurons
Ach
Dysfunctional Ach signaling:
Barrier dysfunction
Peritrophic matrix defects
Dysbiosis
Loss of gut compartmentalization
Inflammation

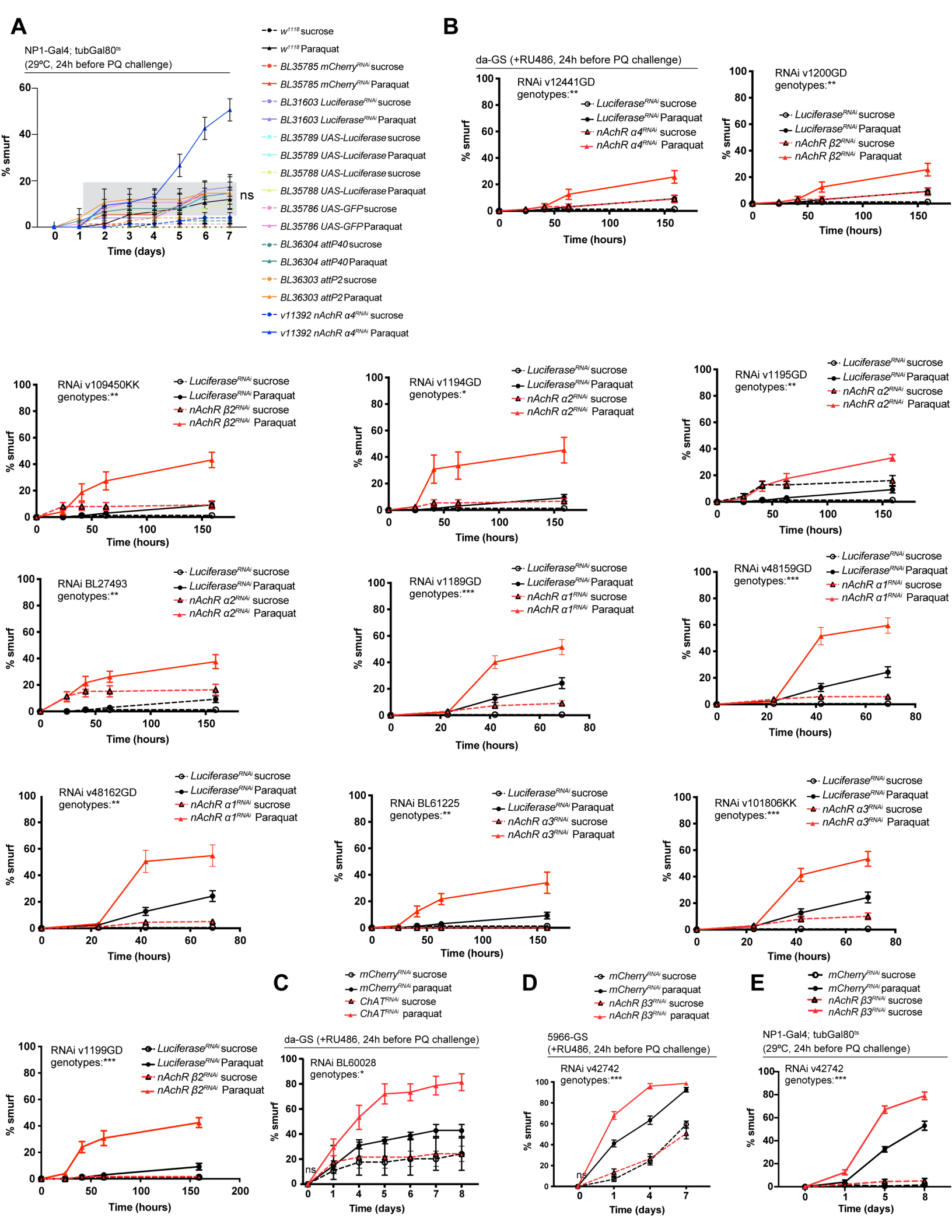
A
NP1-Gal4; tubGal80ts
(29ºC, 24h before PQ challenge)
% smurf
Time (days)
ns
w1118 sucrose
w1118 Paraquat
BL35785 mCherryRNAi sucrose
BL35785 mCherryRNAi Paraquat
BL31603 LuciferaseRNAi sucrose
BL31603 LuciferaseRNAi Paraquat
BL35789 UAS-Luciferase sucrose
BL35789 UAS-Luciferase Paraquat
BL35788 UAS-Luciferase sucrose
BL35788 UAS-Luciferase Paraquat
BL35786 UAS-GFP sucrose
BL35786 UAS-GFP Paraquat
BL36304 attP40 sucrose
BL36304 attP40 Paraquat
BL36303 attP2 sucrose
BL36303 attP2 Paraquat
v11392 nAchR α4RNAi sucrose
v11392 nAchR α4RNAi Paraquat
B
da-GS (+RU486, 24h before PQ challenge)
RNAi v12441GD
genotypes:**
RNAi v1200GD
genotypes:**
LuciferaseRNAi sucrose
LuciferaseRNAi Paraquat
nAchR α4RNAi sucrose
nAchR α4RNAi Paraquat
nAchR β2RNAi sucrose
nAchR β2RNAi Paraquat
% smurf
Time (hours)
RNAi v109450KK
genotypes:**
RNAi v1194GD
genotypes:*
RNAi v1195GD
genotypes:**
nAchR α2RNAi sucrose
nAchR α2RNAi Paraquat
RNAi BL27493
genotypes:**
RNAi v1189GD
genotypes:***
RNAi v48159GD
genotypes:***
nAchR α1RNAi sucrose
nAchR α1RNAi Paraquat
RNAi v48162GD
genotypes:**
RNAi BL61225
genotypes:**
RNAi v101806KK
genotypes:***
nAchR α3RNAi sucrose
nAchR α3RNAi Paraquat
C
mCherryRNAi sucrose
mCherryRNAi paraquat
ChATRNAi sucrose
ChATRNAi paraquat
RNAi v1199GD
genotypes:***
da-GS (+RU486, 24h before PQ challenge)
RNAi BL60028
genotypes:*
Time (days)
D
nAchR β3RNAi sucrose
nAchR β3RNAi paraquat
5966-GS
(+RU486, 24h before PQ challenge)
RNAi v42742
genotypes:***
E
nAchR β3RNAi sucrose
NP1-Gal4; tubGal80ts
(29ºC, 24h before PQ challenge)
RNAi v42742
genotypes:***

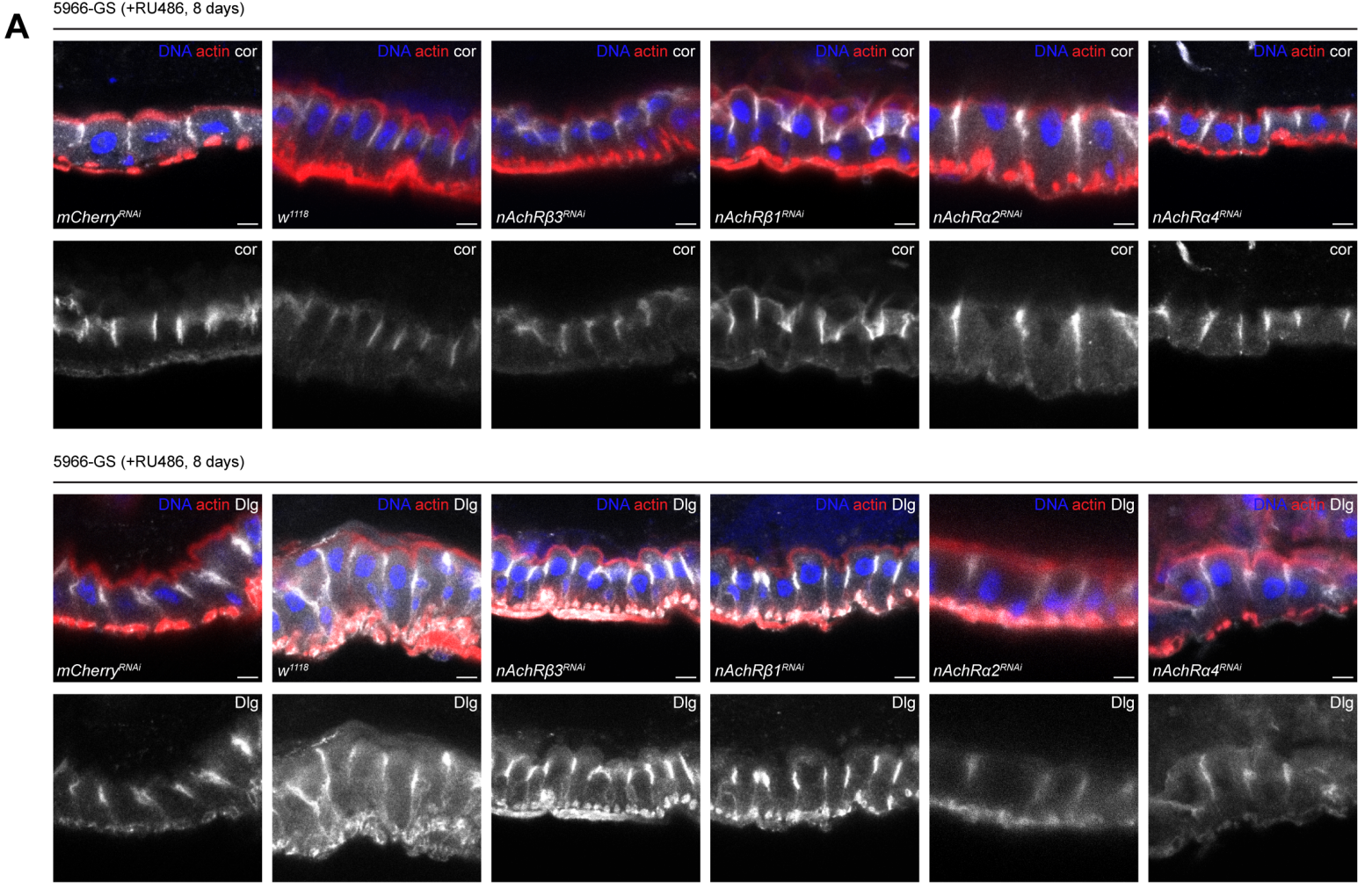
A
5966-GS (+RU486, 8 days)
DNA actin cor
cor
mCherry^RNAi
w^1118
nAchRβ3^RNAi
nAchRβ1^RNAi
nAchRα2^RNAi
nAchRα4^RNAi
5966-GS (+RU486, 8 days)
DNA actin Dlg
Dlg

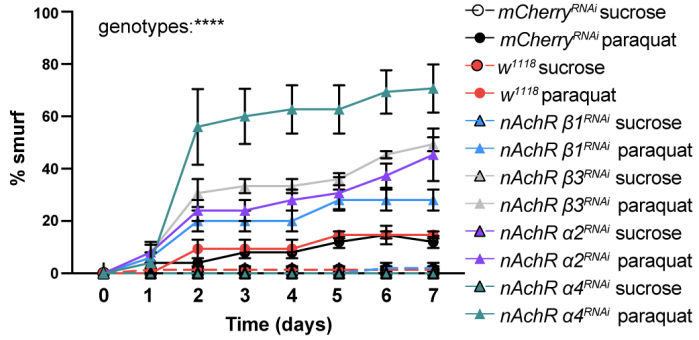
B
esg-Gal4, UAS-2xEYFP; Su(H)GBE-Gal80, tubGal80ts (ISCts)
(29°C, 24h before PQ challenge)
genotypes:****
% smurf
Time (days)
mCherry^RNAi sucrose
mCherry^RNAi paraquat
w^1118 sucrose
w^1118 paraquat
nAchR β1^RNAi sucrose
nAchR β1^RNAi paraquat
nAchR β3^RNAi sucrose
nAchR β3^RNAi paraquat
nAchR α2^RNAi sucrose
nAchR α2^RNAi paraquat
nAchR α4^RNAi sucrose
nAchR α4^RNAi paraquat

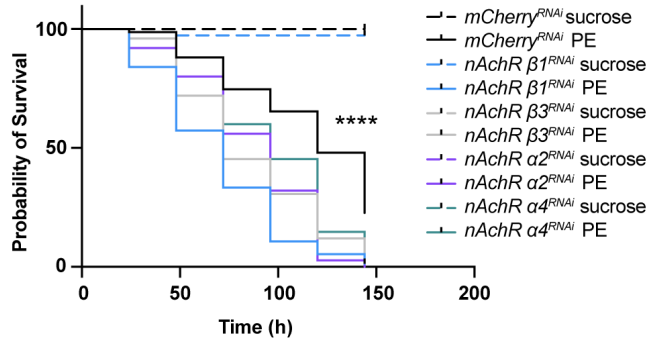
C
esg-Gal4, UAS-2xEYFP; Su(H)GBE-Gal80, tubGal80ts (ISCts)
(29°C, 24h before infection)
Probability of Survival
Time (h)
****
mCherry^RNAi sucrose
mCherry^RNAi PE
nAchR β1^RNAi sucrose
nAchR β1^RNAi PE
nAchR β3^RNAi sucrose
nAchR β3^RNAi PE
nAchR α2^RNAi sucrose
nAchR α2^RNAi PE
nAchR α4^RNAi sucrose
nAchR α4^RNAi PE

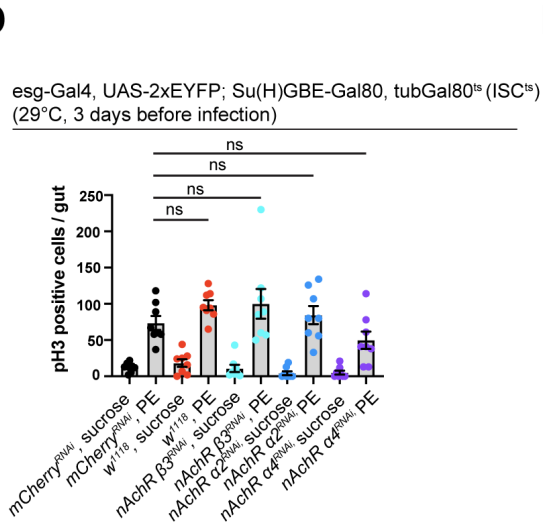
D
esg-Gal4, UAS-2xEYFP; Su(H)GBE-Gal80, tubGal80ts (ISCts)
(29°C, 3 days before infection)
pH3 positive cells / gut
ns
mCherry^RNAi, sucrose
mCherry^RNAi, PE
w^1118, sucrose
w^1118, PE
nAchR β3^RNAi, sucrose
nAchR β3^RNAi, PE
nAchR α2^RNAi, sucrose
nAchR α2^RNAi, PE
nAchR α4^RNAi, sucrose
nAchR α4^RNAi, PE

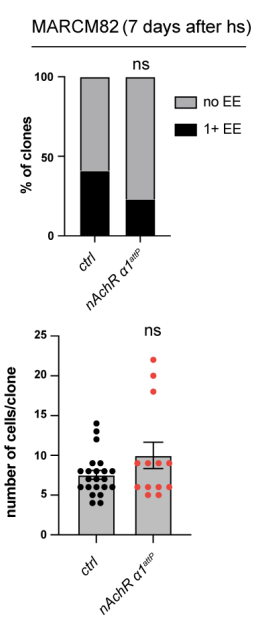
E
MARCM82 (7 days after hs)
% of clones
no EE
1+ EE
ctrl
nAchR α1^RNAi
number of cells/clone
ns

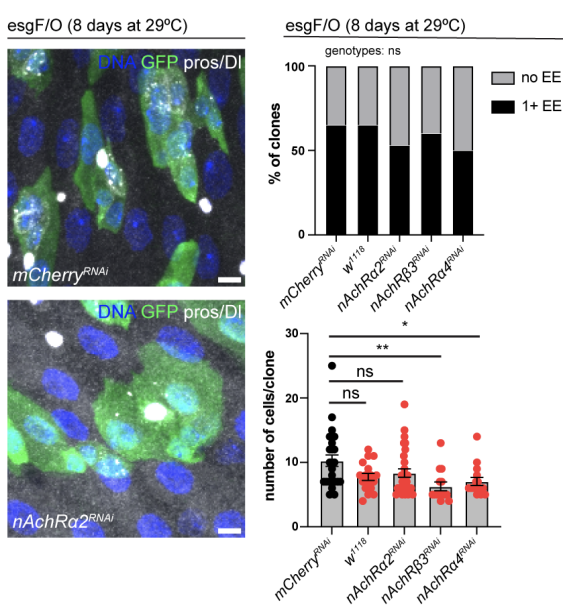
F
esgF/O (8 days at 29ºC)
DNA GFP pros/Dl
mCherry^RNAi
nAchRα2^RNAi
esgF/O (8 days at 29ºC)
genotypes: ns
% of clones
no EE
1+ EE
number of cells/clone
ns
*
**

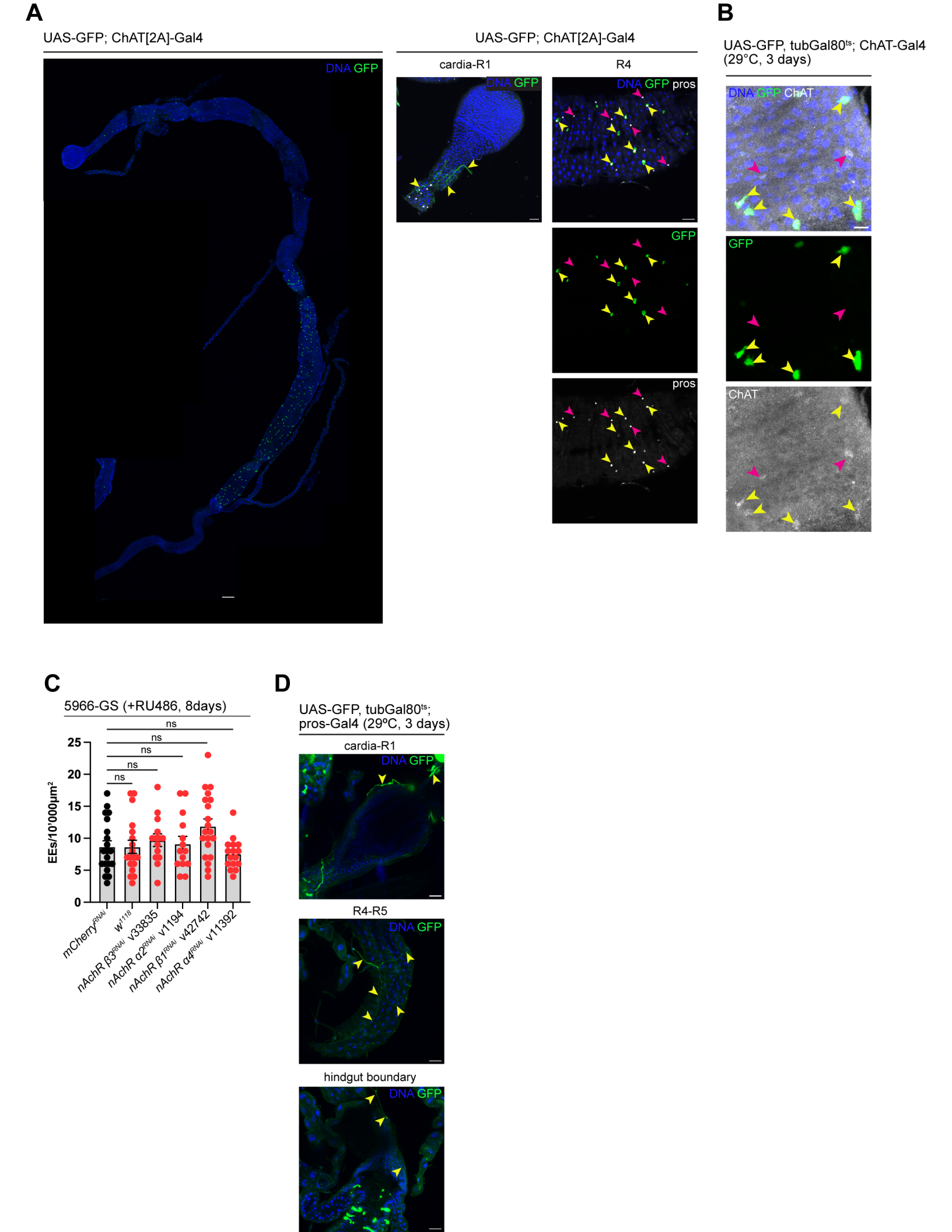
A
UAS-GFP; ChAT[2A]-Gal4
DNA GFP
UAS-GFP; ChAT[2A]-Gal4
cardia-R1
R4
DNA GFP
DNA GFP pros
GFP
pros
B
UAS-GFP, tubGal80ts; ChAT-Gal4
(29°C, 3 days)
DNA GFP ChAT
GFP
ChAT
C
5966-GS (+RU486, 8days)
EEs/10'000µm²
ns
mCherryRNAi
w1118
nAchR β3RNAi v33835
nAchR α2RNAi v1194
nAchR β1RNAi v42742
nAchR α4RNAi v11392
D
UAS-GFP, tubGal80ts;
pros-Gal4 (29ºC, 3 days)
cardia-R1
R4-R5
hindgut boundary
DNA GFP

A

1

Rank by fold-change (EEs/all other cells)

2

Enteroendocrine cells

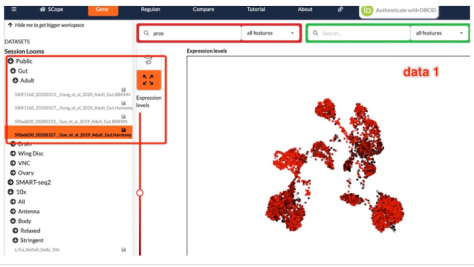

Neurons

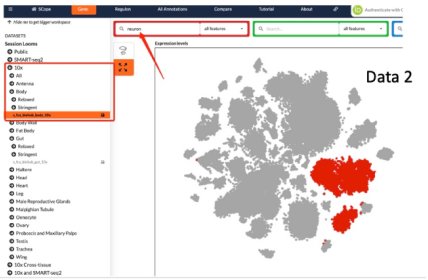

3

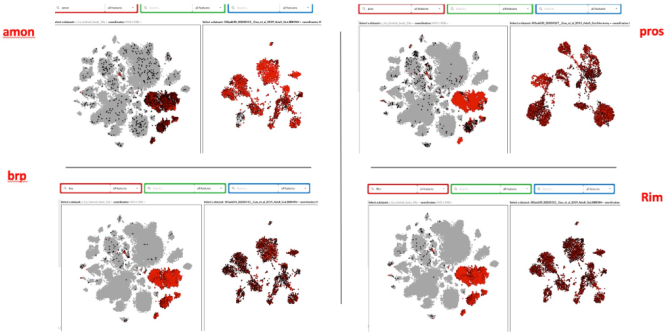

4

Orcokinin expression

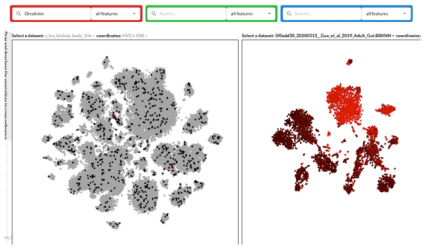

Very low in neurons, high in EEs

BDSC:92253 (FBst0092253) *D. melanogaster* Stock Center 92253

Genotype: y[1] w[*]; TI{CRIMIC.TG4.1}Orcokinin[CR00407-TG4.1]

Collection: Bloomington Drosophila Stock Center

6

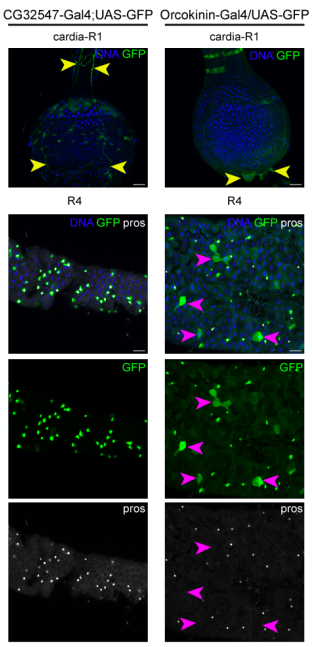

5

additional candidates (7B2 and Pal2), no Gal4 tools available

Low in neurons, high in EEs

Low in neurons, high in half EEs

B

Symbol	Name	Annotation ID	RT-PCT[1]	microarray (midgut)[2]	RNA-seq (4-day)[3]	GAL4 expression[4]
AKH	Adipokinetic hormone	CG1171	+	ND	20	-
AstA	Allatostatin A	CG13633	++	195.2	14	P
AstB; MIP	Myoinhibiting peptide precursor	CG6456	NP	39.6	2	M, P
AstC	Allatostatin C	CG14919	++	1441.9	53	A, M, P
Amn	amnesiac	CG11937	NP	0.4	NA	NA
Apis-ITG-like	Apis-ITG-like	CG8216	-	3.8	0	NA
Burs	bursicon alpha subunit	CG13419	++	113.5	11	-
Pburs	partner of burs	CG15284	-	NA	0	NA
CAPA	capability; CAPA1-2c CAPA-PK1	CG15520	-	4.4	0	-
CCHa1	CCHamide-1	CG14358	++	73.8	13	NA
CCHa2	CCHamide-2; CCHamide	CG14375	++	343.6	73	NA
CRZ	Corazonin	CG3302	-	4.6	0	-
CCAP	Cardioacceleratory peptide	CG4910	+	4.5	0	NA
Dh31	Diuretic hormone 31	CG13094	+	113.6	4	M, P
Dh44	Diuretic hormone 44	CG8348	-	8.4	0	-
ETH	Ecdysis triggering hormone	CG18105	+	2.3	1	-
EH	Eclosion hormone	CG5400	+	2.8	0	NA
FMRFa	FMRFamide	CG2346	NP	0.8	0	-
GPA2	Glycoprotein hormone alpha2	CG17878	-	NA	0	NA
GPB5	Glycoprotein hormone beta5	CG40041	+	NA	0	NA
Hug	Hugin	CG6371	-	4.6	0	-
ITP	ion transport peptide	CG13586	(1) - / (2) ++	40.9	8	-
LK	Insect kinin; Leucokinin	CG13480	NP	ND	0	-
DILP1	Drosophila insulin-like peptide 1	CG14173	NP	1.8	0	NA
DILP2	Drosophila insulin-like peptide 2	CG8167	-	3.7	0	-
DILP3	Drosophila insulin-like peptide 3	CG14167	++	107.4	0	NA
DILP4	Drosophila insulin-like peptide 4	CG6736	-	1.1	0	-
DILP5	Drosophila insulin-like peptide 5	CG33273	-	12	0	NA
DILP6	Drosophila insulin-like peptide 6	CG14049	+	1.1	2	-
DILP7	Drosophila insulin-like peptide 7	CG13317	-	1.6	0	NA
DMS	Dromyosuppressin	CG6440	++	2.3	4	NA
NPF	neuropeptide F	CG10342	++	338.7	26	A, M, P
NPLP1	Neuropeptide-like precursor 1	CG3441	-	3.7	0	-
NPLP2	Neuropeptide-like precursor 2	CG11051	++	126.5	245	NA
NPLP3	Neuropeptide-like precursor 3	CG13061	++	ND	2	NA
NPLP4	Neuropeptide-like precursor 4	CG15361	++	ND	5	NA
Orcokinin	Orcokinin	CG13565	NP	36.3	14	A, M
PDF	Pigment-dispersing factor	CG6496	NP	1.8	0	-
Proctolin	Proctolin	CG7105	-	3	0	-
PTTH	prothoracicotropic hormone	CG13687	+	18.7	1	-
sNPF	short neuropeptide F	CG13968	+	7.4	2	NA
SIFaminde	SIFaminde	CG33527	-	4.5	0	-
DSK	Sulfakinin; Drosulfakinin	CG18090	NP	1.7	0	-
Tk	Tachykinin; Drotachykinin	CG14734	++	356.3	70	NA
SP	Sex peptide Acp70A	CG17673	-	8.8	5	NA

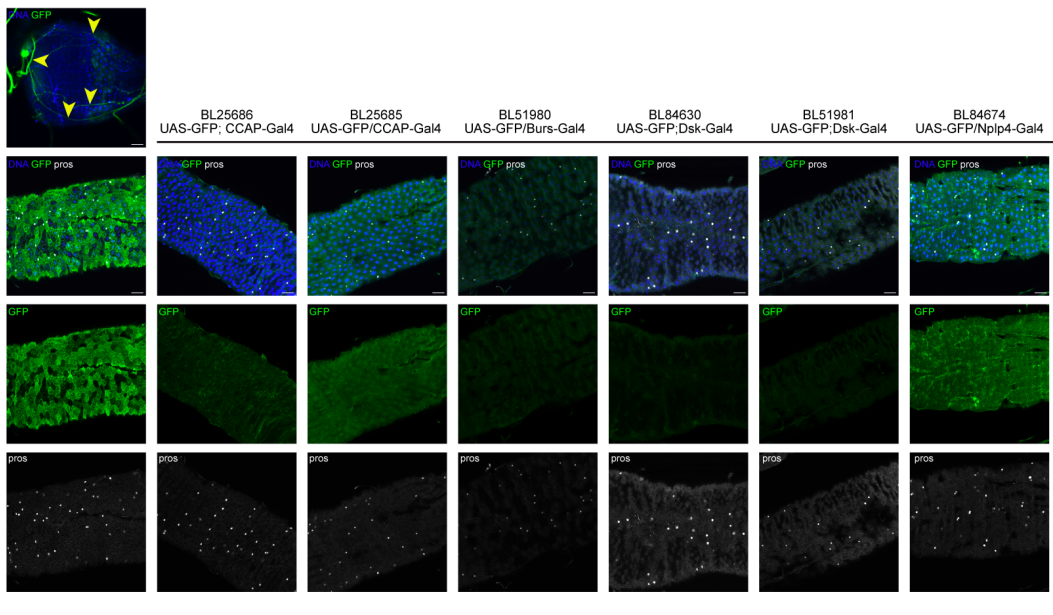

Chen J et al., Mol Cells, 2016 (PMID: 27025390)

A

BL91402xBL91403
R57F07-p65(AD)/UAS-DSCP-6xEGFP;UAS-DSCP-6xEGFPP/R57F07-Gal4(DBD)

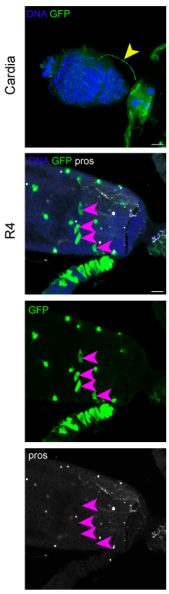

B

DBD drivers selected based on no brain/proventriculus expression and >=1 expression in all gut segments
https://bdsc.indiana.edu/stocks/gal4/midgut_EEs.html

Stk #	Split-GAL4	Ref	PV	R1A	R1B	R2A	R2B	R2C	R3	R4A	R4B	R4C	R5A	R5B	HG	Brain
68537	P{R33A12-GAL4.DBD}attP2	EE2	No	1	1	1	2	2	1	1	1	2	2	1	No	0
69158	P{R61H08-GAL4.DBD}attP2	EE2	No	1	1	1	1	1	2	1	2	2	1	1	No	0

BL91402xBL68537
R57F07-p65(AD);UAS-DSCP-6xEGFP/R33A12-GAL4(DBD)

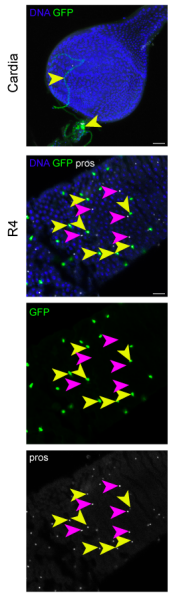

BL91402x69158
R57F07-p65(AD);UAS-DSCP-6xEGFP/R61H08-GAL4(DBD)

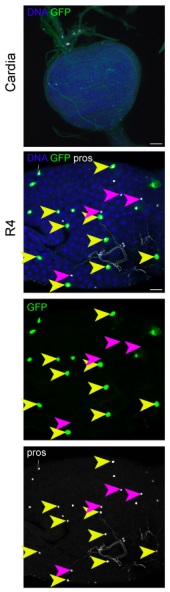

BL91402x69158
R57F07-p65(AD);UAS-DSCP-6xEGFP/R61H08-GAL4(DBD)

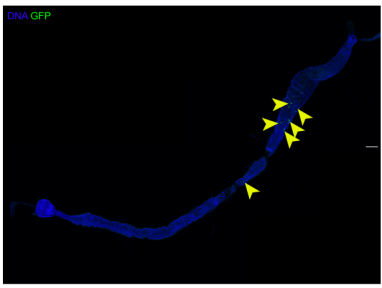

C

BL91402x60318
R57F07-p65(AD);UAS-DSCP-6xEGFP/ChAT-Gal4(DBD)

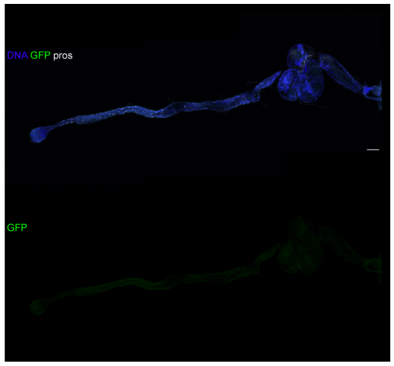

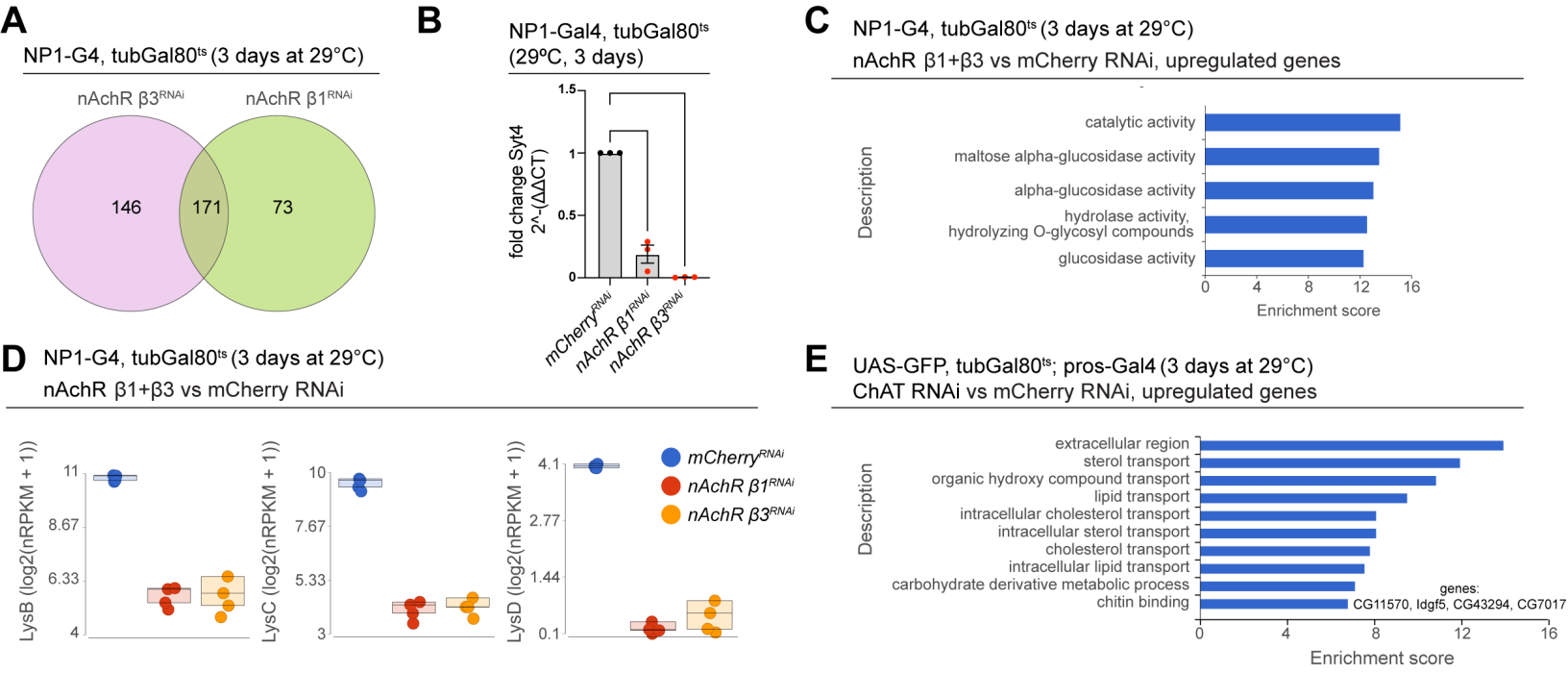
A
NP1-G4, tubGal80ts (3 days at 29°C)
nAchR β3RNAi
nAchR β1RNAi
146
171
73
B
NP1-Gal4, tubGal80ts
(29ºC, 3 days)
fold change Syt4
2^-(ΔΔCT)
1.5
1
0.5
0
mCherryRNAi
nAchR β1RNAi
nAchR β3RNAi
C
NP1-G4, tubGal80ts (3 days at 29°C)
nAchR β1+β3 vs mCherry RNAi, upregulated genes
Description
catalytic activity
maltose alpha-glucosidase activity
alpha-glucosidase activity
hydrolase activity,
hydrolyzing O-glycosyl compounds
glucosidase activity
0
4
8
12
16
Enrichment score
D
NP1-G4, tubGal80ts (3 days at 29°C)
nAchR β1+β3 vs mCherry RNAi
LysB (log2(nRPKM + 1))
11
8.67
6.33
4
LysC (log2(nRPKM + 1))
10
7.67
5.33
3
LysD (log2(nRPKM + 1))
4.1
2.77
1.44
0.1
mCherryRNAi
nAchR β1RNAi
nAchR β3RNAi
E
UAS-GFP, tubGal80ts; pros-Gal4 (3 days at 29°C)
ChAT RNAi vs mCherry RNAi, upregulated genes
Description
extracellular region
sterol transport
organic hydroxy compound transport
lipid transport
intracellular cholesterol transport
intracellular sterol transport
cholesterol transport
intracellular lipid transport
carbohydrate derivative metabolic process
chitin binding
genes:
CG11570, Idgf5, CG43294, CG7017
0
4
8
12
16
Enrichment score
F
NP1-G4, tubGal80ts (3 days at 29°C)
nAchR β1+β3 vs mCherry RNAi, top 20 upregulated genes
Z-score
-2
0
2
mCherryRNAi
nAchR β1RNAi
nAchR β3RNAi
mCherryRNAi
nAchR β3RNAi
nAchR β1RNAi
tobi
CG15263
Amyrel
CG34040
CG14744
PPO2
Ugt37a1
CG31380
phr
FucTC
CG31810
CR45822
Ptth
CG8358
CR44430
CR45670
CG11570
CG3345
mthl8
CR44628
G
UAS-GFP, tubGal80ts; pros-Gal4 (3 days at 29°C)
ChAT RNAi vs mCherry RNAi, top 20 upregulated genes
Z-score
-1.5
0
1.5
mCherryRNAi
ChATRNAi
mCherryRNAi
ChATRNAi
CG2233
Spn88Eb
v
Npc2h
CG12116
CG15068
CR44430
CR45822
phr
Twdlalpha
CG9021
Ect3
CG34291
CG11570
shd
CG14528
CG32568
CG9465
CG43294
CG7017

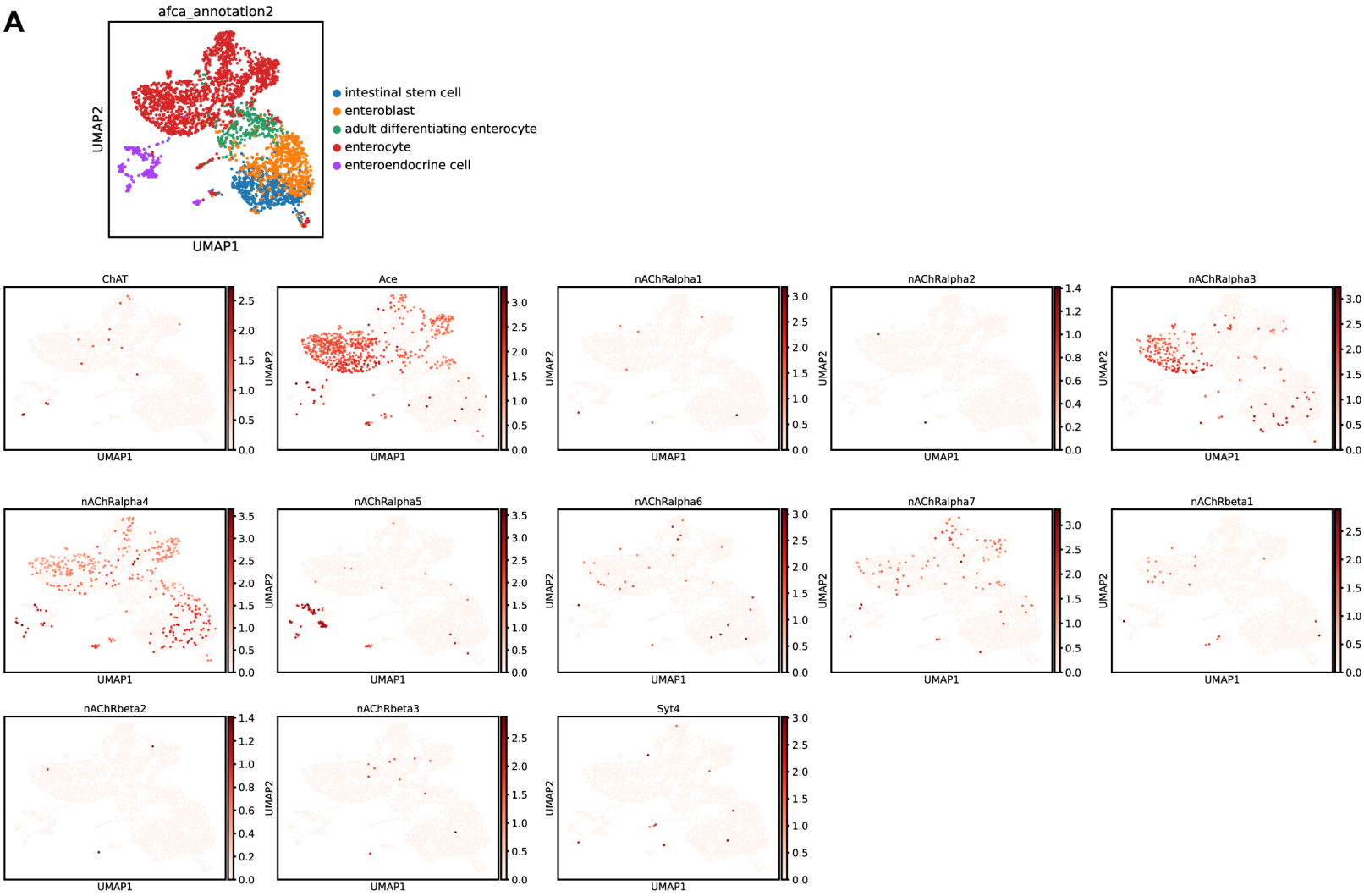
A
afca_annotation2
intestinal stem cell
enteroblast
adult differentiating enterocyte
enterocyte
enteroendocrine cell
UMAP1
UMAP2
ChAT
Ace
nAChRalpha1
nAChRalpha2
nAChRalpha3
nAChRalpha4
nAChRalpha5
nAChRalpha6
nAChRalpha7
nAChRbeta1
nAChRbeta2
nAChRbeta3
Syt4

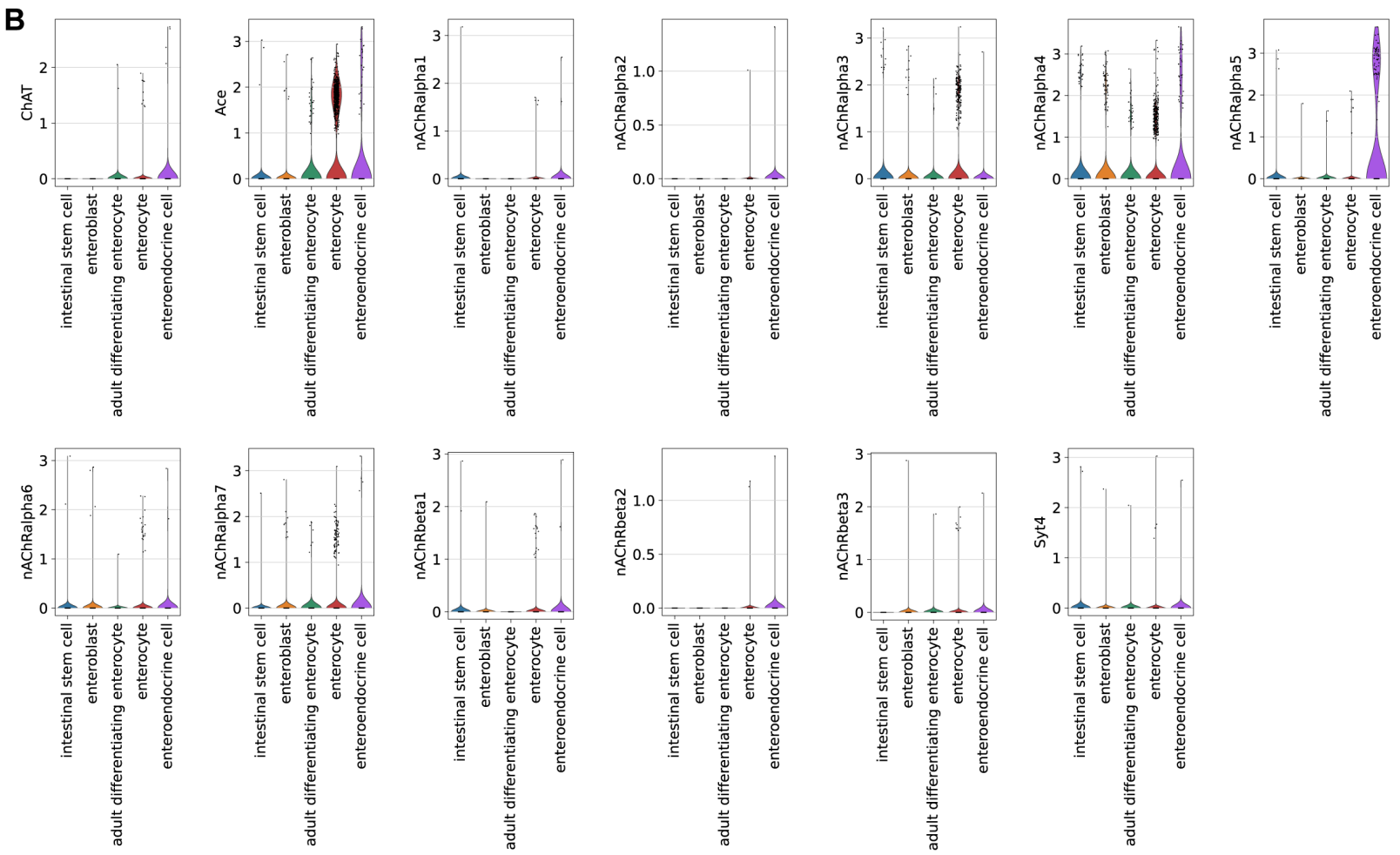
B
ChAT
Ace
nAChRalpha1
nAChRalpha2
nAChRalpha3
nAChRalpha4
nAChRalpha5
nAChRalpha6
nAChRalpha7
nAChRbeta1
nAChRbeta2
nAChRbeta3
Syt4
intestinal stem cell
enteroblast
adult differentiating enterocyte
enterocyte
enteroendocrine cell

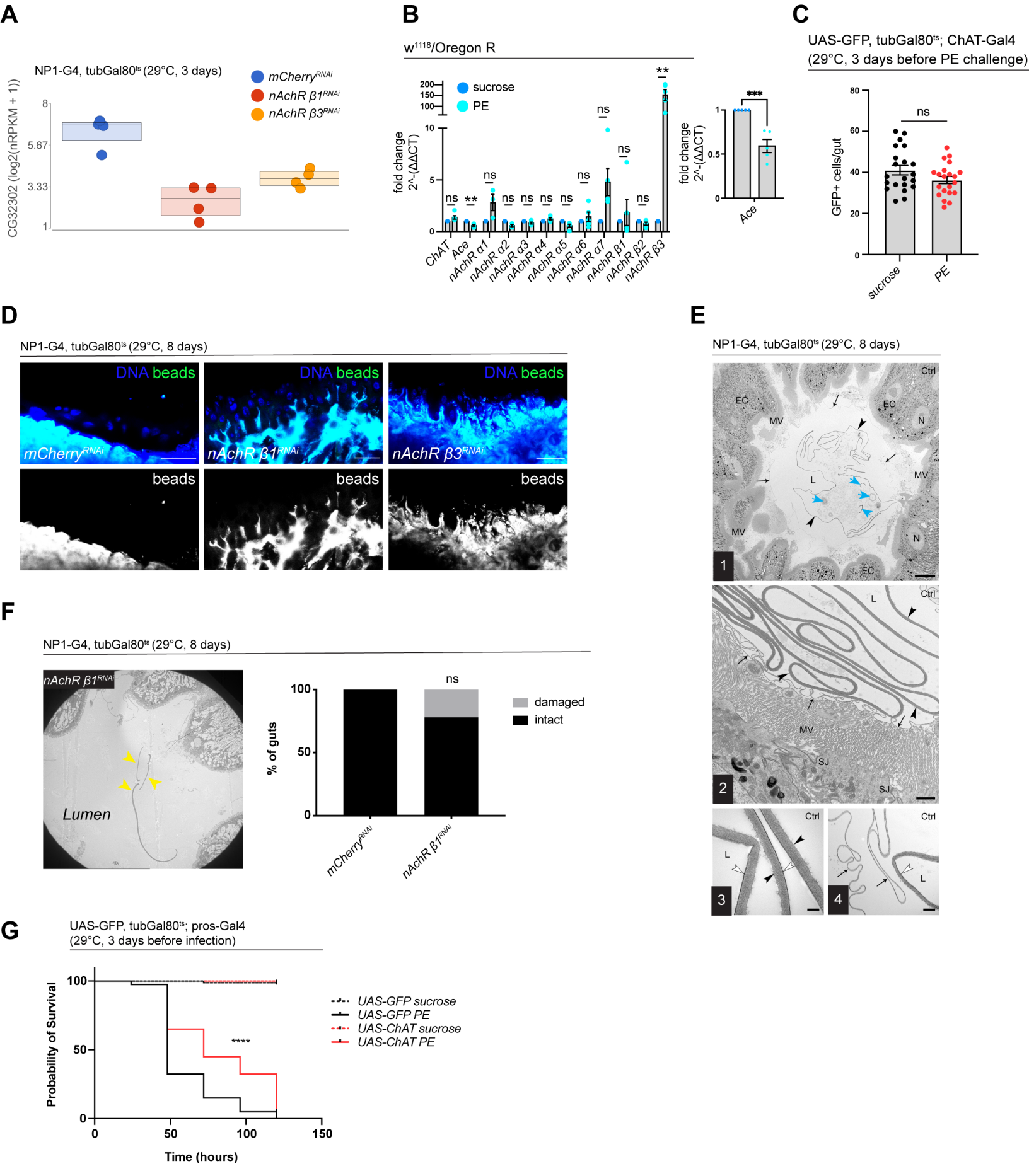
A
NP1-G4, tubGal80ts (29°C, 3 days)
mCherryRNAi
nAchR β1RNAi
nAchR β3RNAi
CG32302 (log2(nRPKM + 1))
8
5.67
3.33
1
B
w1118/Oregon R
sucrose
PE
fold change 2^-(ΔΔCT)
ChAT
Ace
nAchR α1
nAchR α2
nAchR α3
nAchR α4
nAchR α5
nAchR α6
nAchR α7
nAchR β1
nAchR β2
nAchR β3
ns
**
***
C
UAS-GFP, tubGal80ts; ChAT-Gal4
(29°C, 3 days before PE challenge)
GFP+ cells/gut
sucrose
PE
D
NP1-G4, tubGal80ts (29°C, 8 days)
DNA beads
beads
mCherryRNAi
nAchR β1RNAi
nAchR β3RNAi
E
NP1-G4, tubGal80ts (29°C, 8 days)
Ctrl
EC
MV
N
L
SJ
1
2
3
4
F
NP1-G4, tubGal80ts (29°C, 8 days)
nAchR β1RNAi
Lumen
% of guts
damaged
intact
G
UAS-GFP, tubGal80ts; pros-Gal4
(29°C, 3 days before infection)
Probability of Survival
Time (hours)
UAS-GFP sucrose
UAS-GFP PE
UAS-ChAT sucrose
UAS-ChAT PE
****

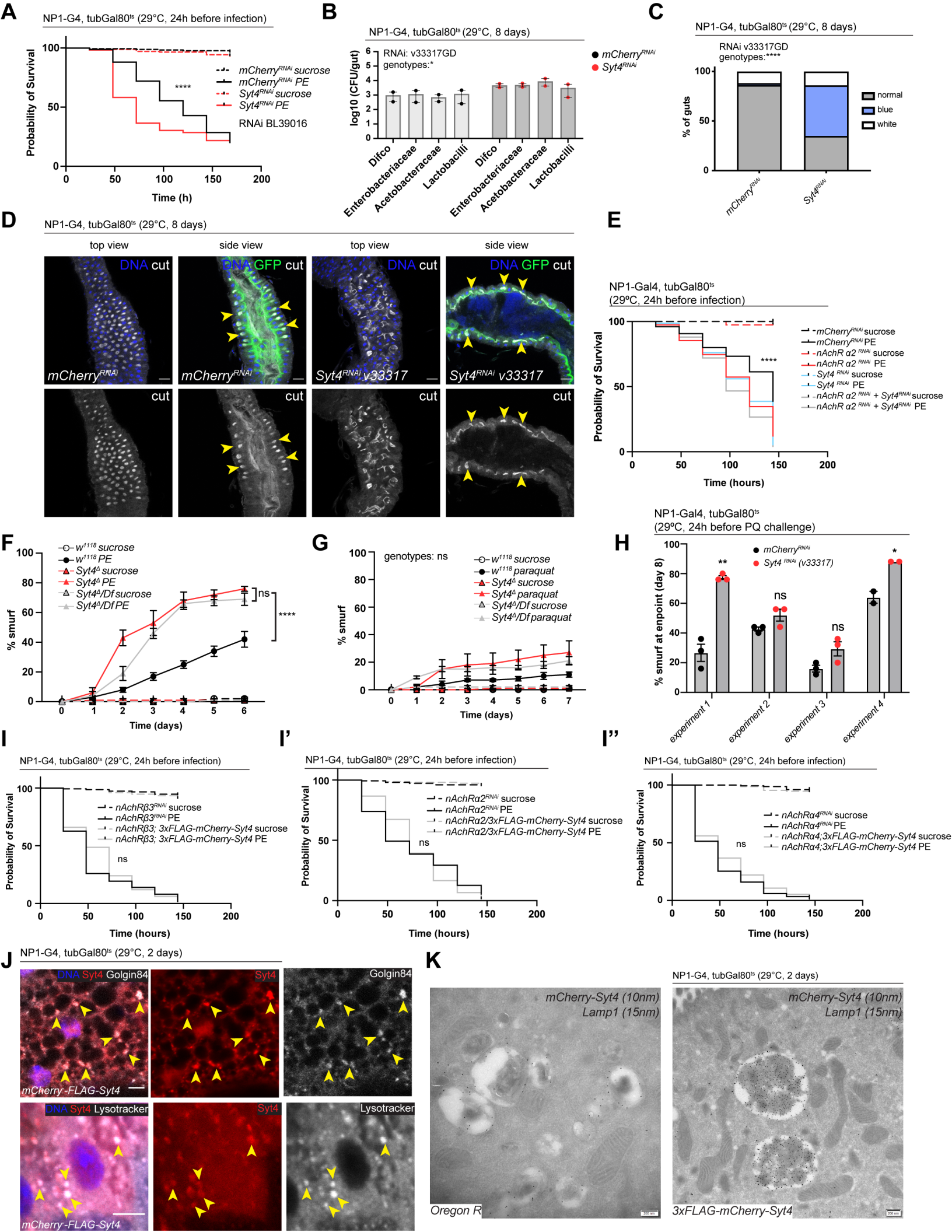
A
NP1-G4, tubGal80ts (29°C, 24h before infection)
Probability of Survival
Time (h)
mCherryRNAi sucrose
mCherryRNAi PE
Syt4RNAi sucrose
Syt4RNAi PE
RNAi BL39016
****
B
NP1-G4, tubGal80ts (29°C, 8 days)
RNAi: v33317GD
genotypes:*
log10 (CFU/gut)
mCherryRNAi
Syt4RNAi
Difco
Enterobacteriaceae
Acetobacteraceae
Lactobacilli
C
NP1-G4, tubGal80ts (29°C, 8 days)
RNAi v33317GD
genotypes:****
% of guts
normal
blue
white
D
NP1-G4, tubGal80ts (29°C, 8 days)
top view
side view
DNA cut
DNA GFP cut
cut
E
NP1-Gal4, tubGal80ts
(29ºC, 24h before infection)
Probability of Survival
Time (hours)
nAchR α2 RNAi sucrose
nAchR α2 RNAi PE
Syt4 RNAi sucrose
Syt4 RNAi PE
nAchR α2 RNAi + Syt4RNAi sucrose
nAchR α2 RNAi + Syt4RNAi PE
F
w1118 sucrose
w1118 PE
Syt4Δ sucrose
Syt4Δ PE
Syt4Δ/Df sucrose
Syt4Δ/Df PE
% smurf
Time (days)
ns
****
G
genotypes: ns
w1118 paraquat
Syt4Δ paraquat
Syt4Δ/Df paraquat
H
NP1-Gal4, tubGal80ts
(29ºC, 24h before PQ challenge)
% smurf at enpoint (day 8)
Syt4 RNAi (v33317)
experiment 1
experiment 2
experiment 3
experiment 4
I
NP1-G4, tubGal80ts (29°C, 24h before infection)
nAchRβ3RNAi sucrose
nAchRβ3RNAi PE
nAchRβ3; 3xFLAG-mCherry-Syt4 sucrose
nAchRβ3; 3xFLAG-mCherry-Syt4 PE
I'
nAchRα2RNAi sucrose
nAchRα2RNAi PE
nAchRα2/3xFLAG-mCherry-Syt4 sucrose
nAchRα2/3xFLAG-mCherry-Syt4 PE
I''
nAchRα4RNAi sucrose
nAchRα4RNAi PE
nAchRα4;3xFLAG-mCherry-Syt4 sucrose
nAchRα4;3xFLAG-mCherry-Syt4 PE
J
NP1-G4, tubGal80ts (29°C, 2 days)
DNA Syt4 Golgin84
Syt4
Golgin84
mCherry-FLAG-Syt4
DNA Syt4 Lysotracker
Lysotracker
K
NP1-G4, tubGal80ts (29°C, 2 days)
mCherry-Syt4 (10nm)
Lamp1 (15nm)
Oregon R
3xFLAG-mCherry-Syt4